(2)

WRDC-TR-90-3046

AD-A225 658

DESIGN OF A MODULAR TEST LOOP FOR STUDY OF TWO-PHASE FLOW AND HEAT TRANSFER IN LOW AND HIGH ACCELERATIONS

Davood Abdollahian

S. Levy Incorporated
3425 S. Bascom Avenue
Capmbell, CA 95008-7006

July 1990

Final Report for Period September 1989 - April 1990

Approved for Public Release; Distribution is Unlimited

FLIGHT DYNAMICS LABORATORY
WRIGHT RESEARCH AND DEVELOPMENT CENTER
AIR FORCE SYSTEMS COMMAND
WRIGHT-PATTERSON AIR FORCE BASE, OHIO 45433-6553

90 08 . 127

DISCLAIMER NOTICE

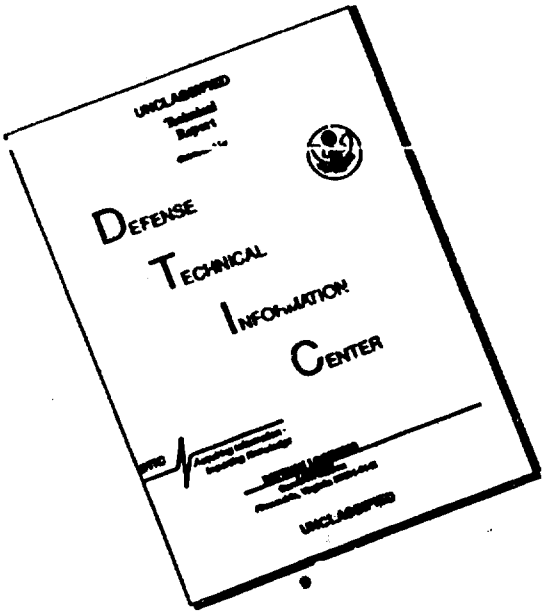

THIS DOCUMENT IS BEST QUALITY AVAILABLE. THE COPY FURNISHED TO DTIC CONTAINED A SIGNIFICANT NUMBER OF PAGES WHICH DO NOT REPRODUCE LEGIBLY.

NOTICE

When Government drawings, specifications, or other data are used for any purpose other than in connection with a definitely Government-related procurement, the United States Government incurs no responsibility or any obligation whatsoever. The fact that the government may have formulated or in any way supplied the said drawings, specifications, or other data, is not to be regarded by implication, or otherwise in any manner construed, as licensing the holder, or any other person or corporation; or as conveying any rights or permission to manufacture, use, or sell any patented invention that may in any way be related thereto.

This report is releasable to the National Technical Information Service (NTIS). At NTIS, it will be available to the general public, including foreign nations.

This technical report has been reviewed and is approved for publication.

William L. Haskin

WILLIAM L. HASKIN
Project Engineer

George A. Kline

GEORGE A. KLINE
Technical Manager

FOR THE COMMANDER

Richard E. Colclough, Jr.

RICHARD E. COLCLOUGH, Jr., Chief
Vehicle Subsystems Division
Flight Dynamics Laboratory

If your address has changed, if you wish to be removed from our mailing list, or if the addressee is no longer employed by your organization please notify WRDC/FIVE, WPAFB, OH 45433-6553 to help us maintain a current mailing list.

Copies of this report should not be returned unless return is required by security considerations, contractual obligations, or notice on a specific document.

UNCLASSIFIED
SECURITY CLASSIFICATION OF THIS PAGE

REPORT DOCUMENTATION PAGE

Form Approved
OMB No. 0704-0188

1a REPORT SECURITY CLASSIFICATION UNCLASSIFIED	1b RESTRICTIVE MARKINGS
2a SECURITY CLASSIFICATION AUTHORITY	3 DISTRIBUTION/AVAILABILITY OF REPORT APPROVAL FOR PUBLIC RELEASE: DISTRIBUTION IS UNLIMITED
2b DECLASSIFICATION/DOWNGRADING SCHEDULE	
4 PERFORMING ORGANIZATION REPORT NUMBER(S) SLI-9008	5 MONITORING ORGANIZATION REPORT NUMBER(S) WRDC-TR-90-3046
6a NAME OF PERFORMING ORGANIZATION S. LEVY INCORPORATED 6b OFFICE SYMBOL (If applicable)	7a NAME OF MONITORING ORGANIZATION FLIGHT DYNAMICS LABORATORY (WRDC/FIVE) WRIGHT RESEARCH & DEVELOPMENT CENTER (AFSC)
6c ADDRESS (City, State, and ZIP Code) 3667 S. BASCOM AVENUE CAMPBELL, CA 95008-7006	7b ADDRESS (City, State, and ZIP Code) WRIGHT-PATTERSON AFB, OHIO 45433-6553
8a NAME OF FUNDING/SPONSORING ORGANIZATION 8b OFFICE SYMBOL (If applicable)	9 PROCUREMENT INSTRUMENT IDENTIFICATION NUMBER F33615-89-C-3403
8c ADDRESS (City, State, and ZIP Code)	10 SOURCE OF FUNDING NUMBERS PROGRAM ELEMENT NO: 65502F; PROJECT NO: 3005; TASK NO: 40; WORK UNIT ACCESSION NO: 59

11 TITLE (Include Security Classification)
DESIGN OF A MODULAR TEST LOOP FOR STUDY OF TWO-PHASE FLOW AND HEAT TRANSFER IN LOW AND HIGH ACCELERATIONS

12 PERSONAL AUTHOR(S)
DAVOOD MOOLLAHIAN

13a TYPE OF REPORT	13b TIME COVERED	14 DATE OF REPORT (Year, Month, Day)	15 PAGE COUNT
FINAL	FROM SEP 89 TO APR 90	1990 July	123

16 SUPPLEMENTARY NOTATION
THIS IS A PHASE I SMALL BUSINESS INNOVATION RESEARCH (SBIR) PROGRAM REPORT

17 COSATI CODES		
FIELD	GROUP	SUB-GROUP
20	13	
20	04	

18 SUBJECT TERMS (Continue on reverse if necessary and identify by block number)
TWO-PHASE FLOW; SPACECRAFT HEAT TRANSFER; HYDRODYNAMIC INSTABILITY; CRITICAL HEAT FLUX

19 ABSTRACT (Continue on reverse if necessary and identify by block number)

Thermal management systems utilizing two-phase heat transfer loops are being developed for application on future spacecraft operating at high power levels.

Design of these systems requires a knowledge of two-phase flow and heat transfer in microgravity and high acceleration environments. In addition to the two-phase flow parameters, several criteria including heat transfer boundaries and instability mechanisms are expected to be strongly dependent on the acceleration levels. These should be analyzed in detail and experimentally verified.

The overall objective of this program was to identify the parameters and criteria of immediate importance for design of two-phase systems and to develop the conceptual design for a modular two-phase loop which can be used to generate the necessary data.

(Continued on attached page)

20 DISTRIBUTION/AVAILABILITY OF ABSTRACT ☒ UNCLASSIFIED/UNLIMITED ☐ SAME AS RPT ☐ DTIC USERS	21 ABSTRACT SECURITY CLASSIFICATION UNCLASSIFIED
22a NAME OF RESPONSIBLE INDIVIDUAL WILLIAM F. HASKIN	22b TELEPHONE (Include Area Code) 513-255-6078 22c OFFICE SYMBOL WRDC/FIVE

DD Form 1473, JUN 86 *Previous editions are obsolete*

19. Abstract (Continued)

A survey of the existing and ongoing efforts was performed to identify the areas that need more testing, and to select the two-phase flow models which could be used in the design analysis.

A preliminary design for a baseline configuration was completed which is intended to perform the defined experiments at earth gravity and aboard an airplane in Keplerian trajectory. This effort consisted of fluid selection, design analysis, and specification of the test matrix.

TABLE OF CONTENTS

LIST OF ILLUSTRATIONS

LIST OF ILLUSTRATIONS (Continued)

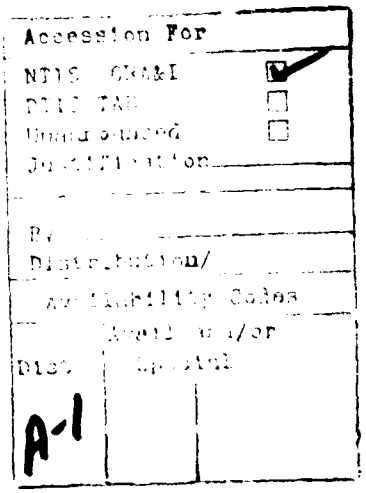

LIST OF TABLES

NOMENCLATURE

A	Cross-Sectional Area
C_o	Concentration Parameter in Drift Flux Model
C_p	Heat Capacity
D	Tube Diameter
E	Entrainment Fraction
f	Friction Coefficient
Fr	Froude Number
g	Acceleration of Gravity
g_o	Earth Gravity
G	Mass Flux
h	Heat Transfer Coefficient
h	Enthalpy
h_{LG}	Heat of Vaporization
Δh_{in}	Inlet Subcooling
j	Volume Flux, Superficial Velocity
K	Thermal Conductivity
L_T	Taylor Instability Wavelength
P_f	Perimeter
P	Pressure
Pe	Peclet Number
Pr	Prandtl Number
$\dot{q}$	Heat Flow Rate
q''	Heat Flux
r	Radial Direction

NOMENCLATURE (Continued)

Re	Reynolds Number
S	Slip Ratio
t	Time
u	Velocity in Direction
U_{gj}	Drift Velocity
x	Quality
X_{tt}	Martinelli Parameter
$\dot{W}$	Mass Flow Rate
y	Transverse Direction
Z	Axial Direction

Greek Letters

α	Void Fraction
ρ	Density
μ	Viscosity
ϕ_L^2	Two-Phase Friction Multiplier with Liquid Flowing Alone
ϕ_{Lo}^2	Two-Phase Friction Multiplier with Liquid Flowing at Total Mass Flux
σ	Stress Component
τ	Stress Component
ε	Eddy Diffusivity
δ	Film Thickness
θ	Inclination Angle
Γ	Property Index

NOMENCLATURE (Continued)

Subscripts

L,G	Liquid and Gas
TP	Two-Phase
SP	Single-Phase
NB	Nucleate Boiling
w	wall
NVG	Net Vapor Generation
CHF	Critical Heat Flux
i	Interfacial
in	Inlet
c	Core
sat	Saturated

Superscripts

*	Non-dimensionalized
	Fluctuating Component
	Mean Value

Section 1

INTRODUCTION

1.1 Background

Due to high power requirements of future spacecrafts, thermal management systems utilizing two-phase heat transfer loops have been suggested and preliminary concepts have already been developed. In comparison to a single-phase loop, the two-phase system operates at considerably smaller flow rates and maintains a tighter temperature control with still a higher heat transfer coefficient.

Design of these systems requires a knowledge of two-phase flow and heat transfer in microgravity and high acceleration environments. In addition to two phase flow parameters, several criteria including heat transfer boundaries and instability mechanisms are expected to be strongly dependent on the acceleration levels and should be analyzed in detail.

Two-phase systems are generally designed for operation under nucleate boiling regime in order to utilize the high heat transfer characteristics of two-phase flow. Operation of the system beyond the critical heat flux may lead to a sudden jump in the surface temperature due to reduction in the heat transfer coefficient (film boiling regime). This temperature is usually above the melting point of many materials and the maximum surface heat flux is also called the limit of stable burnout. In many practical situations, two-phase components fail at heat fluxes well below the limit of stable burnout. This is due to hydrodynamic instabilities which result in sudden reductions in flow and burnout at smaller heat fluxes. Knowledge of stable burnout and the onset of hydrodynamic instability are crucial for operation of any two-phase loop.

Current information on two-phase flow and heat transfer is mainly derived from terrestrial experiments. Unlike pool boiling which has been studied extensively under high and low accelerations, very little work has been

done on understanding and modeling two-phase flow. A majority of low gravity fluid mechanics and heat transfer experiments have been performed in drop towers or under simulated reduced gravity conditions. Several recent efforts have provided limited useful data from airplane trajectory tests. The recent and ongoing efforts have mainly concentrated on generating the data and developing models for two-phase pressure drop, flow regime transition, and two-phase heat transfer coefficients. At this stage, it is generally concluded that considerably more data, preferably under long duration steady-state conditions, is needed to complete and confirm the design approaches for application to low and high accelerations.

1.2 Objectives and Scope of Effort

This project was funded by the Air Force Wright Aeronautical Laboratories as a Phase I SBIR program to study two-phase flow and heat transfer at low and high accelerations. The overall objective of this program was to identify the parameters and criteria of immediate importance for design of two-phase systems and to develop the conceptual design for a modular two-phase loop which can be used to generate the necessary data. The modular loop would allow interchangability of components so that their performance can be evaluated while the basic two-phase flow data is generated.

The objectives of this program were achieved by performing a survey of the existing and ongoing efforts to identify the areas that need more testing. The parameters of interest were selected and the earth and reduced gravity two-phase flow models were reviewed to identify the correlations which could be used in the design analysis. A set of design criteria was defined which was intended to provide a final test loop that can generate as much data as possible in an efficient manner and with a minimum number of tests. The major test parameters included the onset of hydrodynamic instability and the critical heat flux. However, the test loop was instrumented to provide data for two-phase pressure drop and heat transfer. In order to have a modular test bed which can accommodate different system components with varying head and flow requirements, the test section was placed parallel to the main flow path. This arrangement, along with two other

bypass lines, was intended to provide pressure and flow regulation for different system components.

A preliminary design for a baseline configuration was completed which was intended to perform the defined experiments at earth gravity and aboard an airplane in Keplerian trajectory. This effort consisted of fluid selection, design analysis, and specification of the test matrix.

Due to difficulties in adapting the set-up to centrifuge testing, it was decided to limit the high acceleration tests to the short durations which can be achieved with airplane trajectory testing.

Section 2

PRIMARY TWO-PHASE FLOW DESIGN PARAMETERS AND METHOD OF TESTING

Two-phase flow parameters are traditionally categorized based on their direct relevance in design of nuclear and chemical systems. The degree of importance of these parameters in design of spacecraft systems, where level of gravity plays an important role, may be altered. Major two-phase flow parameters and criteria of interest are briefly described in this section.

Two-Phase Friction Multiplier

Frictional pressure loss in a single-phase flow is generally expressed in terms of the dynamic head. In a two-phase system the pressure drop can be much larger than the corresponding single-phase flow. This pressure drop is usually expressed in terms of the equivalent single-phase loss and an empirical multiplier, ϕ^2_{Lo} , which is a function flow quality and system pressure.

$$-\left(\frac{dP}{dZ}\right) = \frac{\tau_w P_f}{A} = \left(\frac{dP}{dZ}\right)_{SP} \phi^2_{Lo}$$

$$\left(\frac{dP}{dZ}\right)_{SP} = \left[\frac{2f\ G^2}{D\ \rho_L}\right]$$

f is the single-phase friction factor and D is the channel diameter. The relations for the two-phase friction multiplier in reduced gravities are needed for design of the spacecraft cooling systems. However, the models developed for predicting this parameter are generally empirical and for the given pressure, mass flow rate, and quality they are not expected to be valid for low or high gravity levels.

Forced Convective Heat Transfer Coefficients

The convective boiling heat transfer coefficient for a two-phase system is often so large that the overall rate of heat transfer is governed by other parts of the system. However, design of a boiling/condensing two-phase cycle and determination of the thermal performance of such a system requires a knowledge of convective boiling heat transfer coefficients. Like other two-phase flow parameters, the models developed under the earth gravity condition are empirical and their applicability to different gravity levels should be investigated.

Two-Phase Heat Transfer Boundaries

Since dramatic changes in heat transfer coefficients occur upon changes in two-phase heat transfer modes, knowledge of the boundaries is of great importance in design of boiling/condensing systems. When the heat input to a single-phase flow of a liquid is increased, the heat transfer coefficient makes a sudden increase at the incipience of boiling or the Net Vapor Generation (NVG) point. If the heat flux exceeds a critical value (Critical Heat Flux), a dramatic drop in heat transfer coefficient occurs which may lead to the failure of the system. Critical Heat Flux (CHF) is gravity dependent and is an important parameter in design of two-phase cycles.

Flow Regime Map

One of the most important criteria in two-phase flow is the transition between different flow regimes. Since the phases in a gas/liquid flow can distribute in a variety of configurations and the two-phase flow parameters are generally flow pattern dependent, the majority of empirical models are developed for specific flow regimes. Applicability of these models to other flow patterns is questionable unless a phenomenological approach is taken which accounts for flow regime transition. Even the practical forms of the governing equations for two-phase flow are flow regime dependent and the general forms will contain many parameters which are not known in detail. From the design point of view, the flow regime map is needed to operate the system under the lowest loss condition, with the highest heat

transfer rate, and to avoid flow regimes which cause instabilities in the system.

Void-Quality Relationship

The mixture momentum equation for separated flow can be written in the following form for steady state conditions.

$$-\left(\frac{dP}{dZ}\right) = \frac{\tau_w P_f}{A} + \frac{1}{A}\frac{d}{dZ}\left[\rho_L A (1-\alpha) u_L^2 + \rho_G A \alpha u_G^2\right] + \bar{\rho} g \sin\theta$$

The above equation shows that the total pressure drop which governs the pumping power required in any system consists of frictional, inertia, and gravity components. In a diabatic system, the quality can generally be determined from the heat input to the system but the void fraction which is needed for the overall pressure drop is not directly known. A relation between the flow quality and void fraction is usually used to specify the average void fraction. These relations are flow regime and, therefore, gravity dependent.

In addition to the above parameters, there are other criteria which are of secondary importance for the conventional two-phase systems operating at earth gravity. Among them, hydrodynamic instability is believed to be quite important for spacecraft applications due to the expected variations in the gravity level and use of parallel components with two-phase flow. Hydrodynamic instability and the mechanisms which lead to unstable behavior are discussed below.

2.1 Hydrodynamic Instability

Two-phase systems are generally designed for operation under nucleate boiling regime in order to utilize the high heat transfer characteristics of two-phase flow. For a heat flux controlled system, there is a local maximum for the heat flux (Critical Heat Flux), beyond which there will be a jump in the surface temperature due to reduction in the heat transfer coefficient (film boiling regime). This maximum heat flux is called the

limit of stable burnout since the new temperature is usually above the melting point of many materials. In many practical situations systems fail at heat fluxes well below that predicted for stable burnout. This is due to sudden reductions in the flow rate caused by small disturbances in the pressure or flow. This unstable condition is called hydrodynamic instability. Knowledge of stable burnout and conditions which cause hydrodynamic instability are crucial for operation of any two-phase loop.

There are a number of mechanisms which lead to hydrodynamic instability. Some of these mechanisms are not important for the systems designed for operation at earth gravity, but are believed to be very important under reduced gravity operation. In order to explain this phenomenon, a brief description of some of the categories of hydrodynamic instability is given below and the mechanisms which are believed to be important are discussed in more detail.

Nucleation Instability

Nucleation or flashing instability is caused by sudden vaporization of the liquid phase with a rapid increase in the specific volume of the mixture. The wall superheat required to initiate bubble nucleation can be quite large for clean surfaces. Under these conditions the bubbles will grow violently and eject liquid from the surface. This process will cool the remaining liquid at the heater surface until sufficient superheat is built up to start the process over.

Flow Pattern Instability

This type of instability is caused by changes in two-phase flow regimes or operation under a particular flow regime (slug flow) which result in pressure and flow oscillations. Under certain conditions the oscillations during slug flow may lead to premature burnout. The most difficult aspect of this type of instability is predicting the onset of unstable behavior.

Instabilities in Forced Convection Systems

Systems operating under a forced convective mode of heat transfer are subject to both nucleation and flow pattern instabilities. These mechanisms, however, have been shown to be of secondary importance at earth gravity conditions. Instabilities resulting from the interaction of the system components and the characteristic of two-phase flow are believed to be far more important and are discussed below.

Excursive Instability-

Excursive or Ledinegg instability is the simplest form of hydrodynamic instability in forced convective systems. It occurs under operating conditions which result in an increase in two-phase pressure drop with decreasing flow rate. For an imposed pressure under such conditions, operation at more than one flow rate is possible. Small disturbances may lead to a shift from one flow rate to another (usually lower) in a non-recurring manner and burnout may occur.

Pressure drop-flow rate characteristics of two-phase channels occasionally follow an "S" shaped behavior as shown in Figure 2.1 Operation in the negative slope part of this system may lead to excursive instability. If a dynamic feedback mechanism exists, it can also lead to an oscillatory behavior. In the absence of such feedback mechanism, static equations can be used for a simple analytical treatment. Physical interpretation of the results of such an analysis is that, if the slope of the pressure drop-flow rate characteristic is more negative than the imposed external supply system, an oscillation will occur. For example, in a constant head supply system (zero slope) as shown in Figure 2.1, operation at points 1 and 3 would be stable while operation at point 2 would be unstable (slope of the system characteristic is more negative than supply slope). Physically, if the flow rate at point 2 is slightly decreased along (A), the external system is supplying less pressure drop than that which is required to maintain the flow. The flow rate will be decreased until point 3 is reached. The new operating point may be so low that burnout could occur. With a nearly constant flow delivery system (slope of $-\infty$) no excursion is

possible. Most external supply systems fall in between the two extremes mentioned above and have a characteristic as shown by (D). With such a system, point 9 is stable while operation at point 8 is unstable. It should be noted that a positive displacement pump can be selected which will provide a nearly constant flow rate for a good portion of the expected pressure drop.

Oscillatory Instability -

Oscillatory instability may result if an energy storage mechanism exists in a two-phase forced convective loop to provide the necessary feedback. The simplest form of such an energy storage is a compressible volume just upstream or within the heated length, Figure 2.2. Operation of this system in the negative slope region (point P) is unstable and an initial excursion will result in the reduction of flow along PA. Since the flow rate supplied by the pump in not initially affected, a flow imbalance and storage of mass in the compressible volume will result. This will cause an increase in ΔP along AB and a second excursion at B along BC. This excursion will result in a net evacuation of mass, ΔP reduction along CD and excursion along DE. The system will then oscillate along BCDE, but with many fluids, burnout may occur along EB.

Parallel Channel Instabilities -

When several two-phase channels are used in parallel, the variations in the flow rate through one channel do not affect the overall pressure drop. This situation is similar to imposing a constant pressure drop across a single channel which is prone to excursion instability. In such cases, severe maldistribution of flow could occur which would lead to burnout.

Density Wave Instability -

The most common form of instability encountered in industrial systems at earth gravity is density wave oscillation. This mechanism is due to multiple feedback between the flow rate, vapor generation rate, and ΔP within the boiling channel. Small perturbations in the flow will result in

pressure fluctuations in the single-phase portion of the channel. This in turn will result in void and therefore pressure fluctuations of the opposite sign in the two-phase region. With the right timing, the perturbations may acquire appropriate phases and become self sustained.

2.2 Test Parameters

It is believed that excursion and oscillatory instabilities which result from the characteristics of the two-phase systems are particularly important at reduced gravities. In addition, these instabilities may severely affect the operation of boiling a system at high accelerations if the flow is in the direction of the acceleration.

Pressure-flow characteristic data from a Freon 11 loop is shown in Figure 2.3. Exit qualities are shown on the abcissa and it can be seen that negative slope region actually starts when the bulk of the liquid is still subcooled. Apparently, voids generated at the wall during the subcooled boiling process will cause the pressure drop to increase with decreasing flow rate. When the flow becomes highly voided, further reduction in flow will cause a decrease in pressure drop with flow rate and eventually the fluid becomes single-phase vapor. For the particular system shown in Figure 2.3 pressure oscillations with a period of approximately 40 to 50 seconds were observed for exit qualities in the range of 0.02 to 0.08. These oscillations died out when the flow was decreased and quality increased further. At a flow rate of 0.42 lb/min density wave oscillations with a period of 3 to 4 seconds were initiated.

For a given heat flux, the maximum and minimum of the pressure drop-flow rate characteristic depend on the particular system. A boiling channel with vertical upward flow can operate into the negative slope region before becoming unstable. However, the same channel with downward flow will become unstable at the onset of subcooled void generation which is very close to minimum point. The reason is that for upward flow, vapor generated initially at the exit will be swept out, while in downward flow it will be swept upstream into the channel which will increase the pressure drop (more negative slope) and start oscillations. Therefore, the onset of

oscillatory instability in downward flow will correspond to the minimum in the pressure drop-flow characteristic, while for vertical upward flow (without a compressible volume) it moves up in the negative slope region. High accelerations ($g > g_0$) in the direction of the flow would even be more severe than downward flow since the bubbles will be swept upstream with higher velocities. On the other hand, higher accelerations in the direction opposite to the flow will be stabilizing.

Generally, systems should be designed to avoid operation in the negative slope region completely. This is particularly important when several channels with multivalued characteristics operate in parallel. Due to the imposed constant pressure across the channels, severe flow maldistribution may result which could lead to unstable behavior and burnout. At earth gravity, this situation is usually avoided by orificing the flow at the entrance so that single-phase pressure drop is comparable to two-phase pressure drop. As shown in Figure 2.4, orificing will shift the minimum to lower flow rates and lower negative slopes, therefore stabilizing the system. Two-phase systems for spacecraft applications probably cannot afford to have such a large pressure drop (orifice or throttling valve) in the loop to stabilize the flow.

For a given flow rate, the negative slope region depends on the void distribution and the two-phase pressure drop. It is known that for the same conditions, two-phase pressure drops under reduced gravities are considerably larger than at earth gravity. This would mean a steeper negative slope which could result in burnout at lower flow rates or for a given flow rate at a lower heat flux.

When a two-phase boiling system is expected to undergo high accelerations, it should be designed such that the boiling channels are perpendicular to the axis of acceleration. This will reduce the possibility of excursion instability and burnout.

Based on the above discussions it can be concluded that knowledge of pressure drop-flow characteristics of two-phase systems under high and low accelerations is of particular importance for design of any two-phase

boiling system. The experimental loop designed in this program will be aimed at generating the pressure drop-flow behavior and burnout (critical heat flux) data. In addition to the above primary parameters, data on pressure drop and two-phase heat transfer coefficients will also be generated.

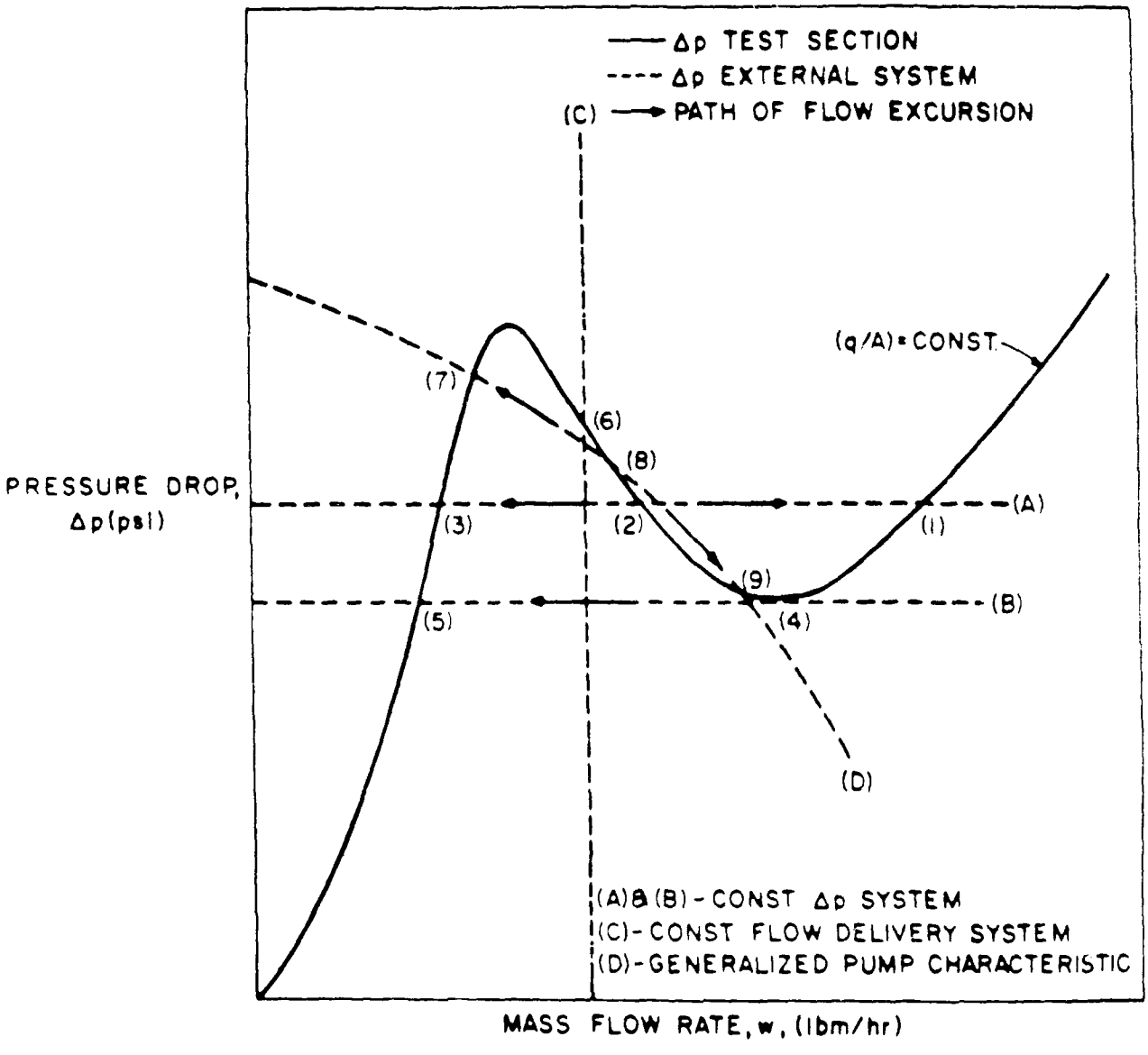

FIGURE 2.1 GRAPHICAL INTERPRETATION OF EXCURSIVE INSTABILITY

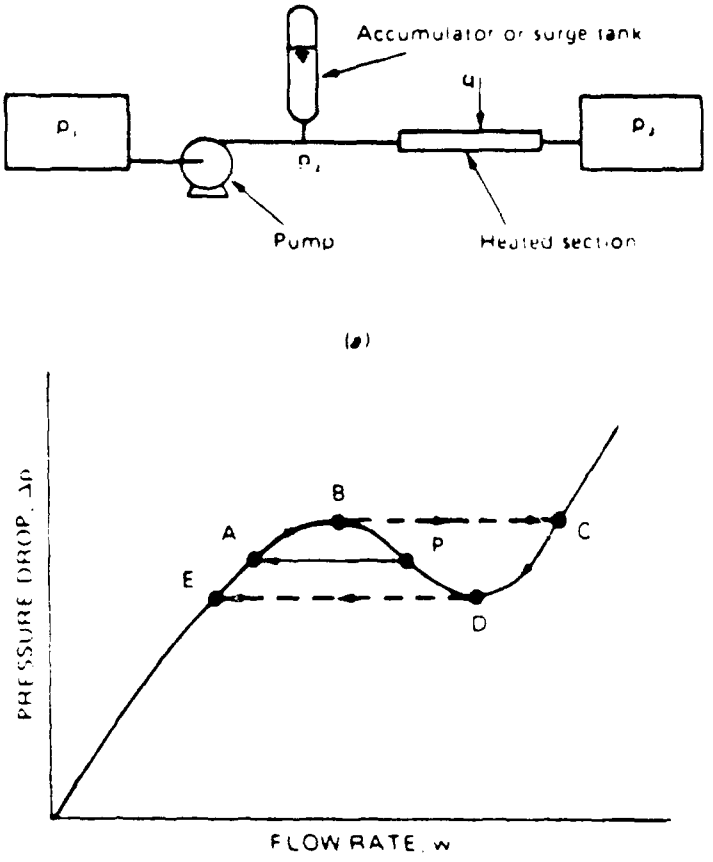

Figure 2.2 - Oscillatory Instability

From: Stenning, A. H., and Veziroglu, T. N., "Flow Oscillation Modes in Forced Convection Boiling," Proc. 1965 Heat Transfer and Fluid Mechanics Institute, pp. 301-316, Stanford University Press, 1965.

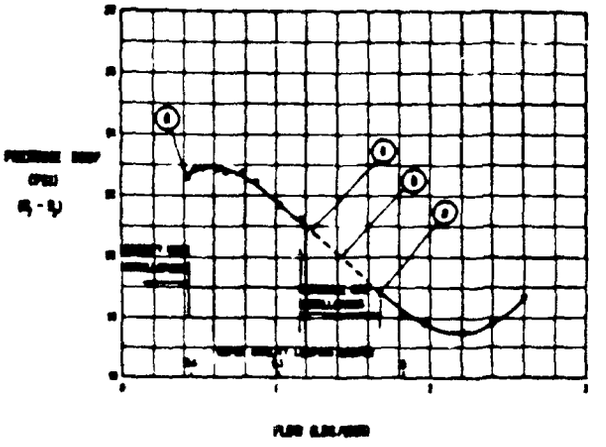

Figure 2.3 - Pressure Drop vs. Flow Rate for 344 Watts Heat Input.

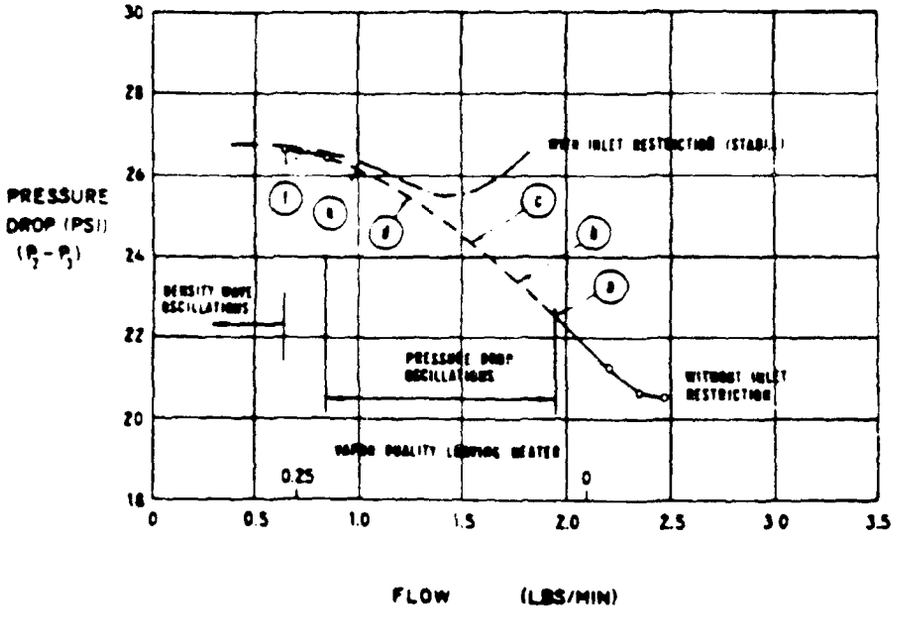

Figure 2.4 - Pressure Drop vs. Flow Rate for 389 Watts Heat Input.

Section 3

REVIEW OF SELECTED EFFORTS IN REDUCED GRAVITY TWO-PHASE FLOW

Several literature surveys on the subject of reduced gravity two-phase flow have been recently published, (1) (2), which covered experimental and analytical efforts prior to 1987. In Ref. (1), the results of an extensive literature review performed by our organization have been reported. This included evaluation of the existing correlations and data, and comparison of the predictions with limited available reduced gravity data.

In this section, results of selected experimental and analytical studies will be discussed and recent efforts which have not been covered in the published surveys will be briefly described.

3.1 Results of Selected Experimental Efforts

Prior to 1980, very little work had been done on understanding and modeling two-phase flow in low and high accelerations. A majority of the efforts provided qualitative information on two-phase flow behavior under reduced gravity conditions. No quantitative data was reported and basically no experiments were performed at high accelerations. Recent studies initiated by the Air Force and NASA have generated limited useful information.

A survey of existing literature resulted in the general conclusion that considerably more data is needed to understand the two-phase flow behavior and to predict the important parameters at different gravity levels. However, several of the experimental programs provided valuable data which will be discussed in more detail in this section.

Heppner et al., Ref. (3)

This is one of the major two-phase flow studies which was aimed at flow regime map identification in zero gravity. The tests were performed with air/water in a transparent test section with L/D=20. The test variables consisted of the total flow rate and the mass quality. A high speed camera

was used to record the flow regimes during the experiments. The test section consisted of a rigid plastic block with a 2.5 inch square cross section. A cylindrical flow passage with a diameter of 1 inch was bored along the length of the block. Water was introduced through four peripheral ports at a location 3 inches from the entrance. Static pressures were measured at three axial locations along the test section. Experiments were performed at earth gravity and aboard the KC-135 airplane. Data was recorded during the 2 g and 0 g (10^{-2} g_0) accelerations.

The measured pressure drops show a significant increase in comparison to equivalent conditions tested at 1 g. Since the system pressure and temperature were not reported and the length of the section over which the pressure drop is measured is not specified, this data has little practical application for modeling or design purposes. The major outcome of these tests was a series of flow regime records which were compared to the maps developed by Baker (4) and Quandt (5). The observed flow regimes were not characteristic of the regimes identified by Baker and often were a combination of two or more regimes. This could be due to method of interpretation of flow regimes or due to short length of the test section. It was concluded that the gravity level affects the flow patterns and Quandt's hypothesis of flow regime transition based on Froude number (which brings in the effect of gravity) is valid.

University of Houston Study, (6)

This is the most significant study published on the subject of two-phase flow regime transition at reduced gravities. The experiments were carried out in a NASA drop tower and aboard the NASA Learjet.

The drop tower loop consisted of a 3/8 inch diameter transparent test section with a length of 18 inches. Air was introduced into the water line at four peripheral ports. Air flow rate was set by a calibrated valve and the water flow rate was set by the pump speed. The loop was not equipped with flowmeters and it was assumed that the flow rates did not change

during the free fall. However, post-test analysis showed that for certain runs the speed of the pump changed during the drop.

The Learjet loop consisted of a 0.5 inch diameter, 42 inch long test section. Air flow was monitored by a set of orifices and water flow rate was measured by a turbine meter. Color films of the flow were taken at 400 frames/s through the transparent test section. The films provided information on the flow regimes, velocities of the slugs, and sizes of bubbles and slugs. The data acquisition was limited to periods when the measured accelerations in any of the three principal coordinates was less than $\pm 0.02\ g_0$. Following the learjet tests, a series of experiments at the same gas and liquid velocities were performed at 1 g condition.

The observed flow regimes consisted of dispersed, bubbly, slug, and annular regimes. Evaluation of the films has shown that unlike the 1 g condition, the bubbles carried in the liquid slug travel at exactly the same velocity as the front of the slug. During the bubbly flow, the local slip between gas and liquid is negligible and the phases are in local homogeneous condition. Based on a preliminary analysis, a model for the bubbly/slug and slug/annular flow pattern transitions has been developed.

This flow regime transition and the comparison with data is reproduced from Ref. (6) and shown in Figure 3.1.

Pressure drop data from these tests were not considered to be reliable and have not been released. In addition to flow regime map determination, this program included modeling of slug flow and interfacial shear which have not been reported yet.

Sunstrand Study, (7)

This program was aimed at studying the performance of a two-phase thermal management system with prototypical components. However, data on two-phase flow regime and pressure drop was also generated.

The schematic of the test loop is shown in Figure 3.2. Nearly saturated Freon 114 is pumped to a swirl flow evaporator where two-phase flow with the desired quality is generated and passed to the adiabatic test section. The test section consisted of two transparent portions; a curved section with 180 degree bend, and a six foot long 0.623 diameter straight section. The exiting two-phase mixture is passed to the Rotary Fluid Management Device (RFMD) where the phases were separated. The vapor enters a shear flow condenser with a clear cover and the exiting subcooled liquid is returned to the RFMD. The test section was instrumented with pressure transducers and observation and photography of the flow regime was made at the straight section. Tests were performed at earth gravity and aboard NASA KC-135 at reduced gravities. A total of 54 parabolae were flown where the flow rate was kept essentially constant and quality was varied. Some variation in the flow rate was observed during the tests but average values were reported.

For the flow rate and the range of qualities tested, only two flow regimes were observed in these experiments. For qualities below 10% the flow regime was slug and for qualities above 15% annular pattern was observed. At high qualities the flow became annular-mist. The observed flow patterns were compared with several flow regime maps and good agreement was obtained with Baker (4) and Taitel & Dukler (8) maps. However, the slug/annular transition in Dukler's reduced gravity map apparently did not have a solution for R-114. It should be noted that a very limited number of data points were generated on flow regimes. Generally, a conclusion regarding the applicability of a flow map cannot be made based on so few points.

The major outcome of this program was the pressure drop data which was measured along the straight and curved sections at reduced and earth gravity conditions. The data for the straight section is shown in Figure 3.3. It can be seen that the reduced gravity pressure drop is generally 100% to 150% higher than the equivalent 1 g data. Due to limitations in pressure transducer accuracy most of the reliable pressure drop data are for annular flow regime. A number of models for the two-phase pressure drop

were compared with this data; this will be discussed in the following sections.

Simulation Tests

A series of experimental efforts have been performed which were aimed at simulating two-phase flow behavior by using two nearly equal density liquids. Since the data from these experiments does not represent the exact gas/liquid flow behavior, it should only be used in development of the phenomenological models which incorporate the effect of actual density differences. This means that purely empirical fits to the data will have little practical application.

Among this type of experiments, the S. Levy Incorporated/University of California study (9) was aimed at generating data for two-phase friction multiplier and void-quality relations under simulated bubbly and annular flow patterns. The major test parameters were the void fraction and the pressure drop along the test section. The test variables included the total mass flow rate, relative phase content (quality), and the fluid properties. Distilled water was used as the fluid which simulated the gas phase and Dimethyl silicone fluid L-45 or Dowtherm LF heat transfer fluid (DT-LF) represented the liquid phase.

The experimental results showed that for bubbly flow the pressure drop and void-quality relation could be closely predicted by the Homogeneous Equilibrium Model (HEM). However, it was concluded that such a result was due to equal densities of the fluids rather than an inherent condition in the absence of gravity. This type of simulation can only provide qualitative information for the annular flow regime. This is due to the fact that the liquid representing the gas phase travels at a velocity which is not greatly different from the velocity of the other phase. However, in a gas/liquid annular flow, the phases travel at considerably different velocities due to density differences.

The experiments performed by AETA/University of New Hampshire/Dartmouth, (10) were aimed at studying the flow regime transition by using equal

density liquids. The experimental setup consisted of a 1 inch diameter, 21 foot long pyrex glass tube with two entrance ports for mixing of immiscible liquids. Water was used to simulate the gas phase in these experiments and four liquids were selected to represent the "liquid" phase. Therefore a wide range of viscosity ratios and relative surface tensions were tested. The test variables consisted of the total flow rate, mean phase content, and fluid properties. The major test parameter was the flow pattern which was monitored at a location 75 diameters from the entrance to ensure fully developed flow condition.

The observed flow regimes consisted of bubbly, slug, and a thin film annular flow (drop flow). It was also concluded that the laminar to turbulent flow transition and viscosity changes made little difference on the transition lines. Authors have expressed concern regarding the applicability of this data to reduced gravity conditions.

High g Studies

As mentioned earlier, there has been essentially no studies reported in the open literature on the subject of two-phase flow in high accelerations. However, there is a multitude of efforts on heat transfer augmentation through centrifugal forces within the flow. This is accomplished by inlet vortex generators which can produce accelerations in excess of 100,000 g, and insertion of twisted tapes within the tubes. Although these techniques produce a large acceleration within the flow field, they do not simulate true high g situations.

Detailed surveys of heat transfer augmentative techniques are given in Refs. (11) and (12). Existing studies have covered single-phase, as well as subcooled and bulk boiling conditions. Among them the work of Gambill et al (13) on subcooled boiling and Blat and Adt (14) on bulk boiling should be noted. The results of these studies on boiling heat transfer are inconclusive and in poor agreement. However, it is generally accepted that considerably larger critical heat flux is attainable in swirl flows than can be achieved in equivalent axial flow conditions. In the study reported

by Lopina et al. (12) it is concluded that single-phase heat transfers can be improved by as much as 85% by tape generated swirl flow, while subcooled boiling did not show significant improvements over straight flows.

For convective boiling, the centrifugal force acting on the liquid is larger than bubbles and this results in a net migration of bubbles to the center of the tube and liquid to the wall. This type of flow cannot simulate high g situations occurring in the space applications where g could be in the direction of flow or even perpendicular to it. As mentioned earlier, the direction of g can stabilize or enhance hydrodynamic instabilities.

In a different type of experiment, the set-up was placed in a centrifuge to generate high accelerations. This technique is suitable for study of hydrodynamic instability and critical heat flux. The loop can be placed with the flow in the direction, opposite, or perpendicular to the gravity field. Lienhard (15) has used the University of Kentucky centrifuge to generate data on pool boiling critical and minimum heat fluxes. One of the major findings of this study was that peak and minimum heat fluxes in pool boiling do not always depend on $g^{1/4}$ as previously believed. Instead, there is a secondary dependence on gravity which can change the overall gravity dependence significantly. Based on the evaluation of data on spheres, the secondary effect was shown to be important for minimum heat flux only. No flow boiling data has been found with this type of high g simulation.

3.2 Recent Experimental Studies

In addition to the studies which have been reported in the open literature, several experimental programs are presently underway and are expected to produce valuable information on the subject of two-phase flow at reduced gravities.

Foster-Miller, Inc. (16)

The schematic of this experimental loop is shown in Figure 3.4. The test program will include a series of ground tests and airplane trajectory

tests. The main parameters to be measured include: two-phase friction pressure drop, two-phase heat transfer coefficient, and flow regimes by high speed digital image recording. The main feature of this loop is the Foster-Miller two-phase pump which can accept a mixture of vapor and liquid with any quality, separate the phases, and pump them separately. Therefore, by adjusting the flow rates, the quality of the two-phase mixture entering the adiabatic test section can be controlled. A high speed image recorder will be used for recording the flow regimes in the adiabatic section. In addition, the pressure drop across this section will be used to provide two-phase pressure drop information. For the ground tests, two succeeding glass sections, one configured for upflow and one for downflow, will be used. For airplane trajectory tests a single horizontal section will be employed.

Two-phase flow will enter the condenser and then the evaporator. The condenser consists of three tube-in-tube heat exchangers in series. The evaporator consists of three glass sections with sputtered gold films which are heated by DC power. The condenser and evaporator are instrumented to provide data on the average heat transfer coefficient. The vapor quality entering the adiabatic section and the condenser is known (assuming no condensation takes place in the lines). Since no void fraction or quality measurement at the condenser exit is performed, the evaporator results will be useful only if the vapor is condensed completely and single-phase liquid enters the evaporator.

Creare, Inc. (17)

This program consists of a series of ground and airplane trajectory tests with a two-phase loop using R-22 as the working fluid. The test section consists of three 1/4 inch diameter sections separated by a 2 inch transparent section for visualization purposes. Up to 500 Watt power can be supplied to every section of test tube for boiling the fluid. A one meter long adiabatic section is also provided for flow visualization and pressure drop measurement. A positive displacement pump is used and a bladder type accumulator is provided for surge protection or pulsation damping depending

on the location of the accumulator. A two meter long section which consists of six 30 centimeter diameter sections is used as the condenser. The measurements include: surface and fluid temperatures, heat input to the evaporator, and pressure drops across different sections of the loop. In addition, a high speed digital imaging system is used for recording the flow regimes in the transparent sections. No void fraction measurement is performed and the quality is obtained from a heat balance on the system. The main two-phase flow parameters which will be obtained from this study include: two-phase pressure drop, heat transfer coefficient, and two-phase flow regime information. In addition, data on the transient response of the system to power surges or drops will be generated. Heat transfer coefficient is obtained from the total power to the test section and the measured wall temperature.

Kirtland AFB Program (18)

In order to study two-phase flow parameters under long duration reduced gravity environment, a set of tests aboard a rocket will be performed. The loop is being developed internally at Kirtland AFB and was scheduled for delivery to Sandia Lab. by April 1, 1990. No information on the details of the loop has been released.

NASA GSFC Space Station Advanced Development Flight Experiments (19)

TEMP 2A-3 Flight experiment is mainly intended to demonstrate the operation of a mechanically pumped two-phase heat acquisition and rejection loop. This loop is designed for integration within the space shuttle cargo bay and the scheduled flight date is June 1991. In addition to the above main objective, the test loop will be used to evaluate a propulsion type fluid management reservoir and a two-phase cold plate design. The test loop is also instrumented to provide two-phase heat transfer data in a spiral boiling section and pressure drop data in a 1/16 inch diameter tube. The working fluid is ammonia and the test schematic is shown in Figure 3.5. According to NASA, since two-phase flow measurements are secondary to the main objectives, parametric data for the desired variables is not expected

within the planned test matrix. However, it is possible that the set-up will be flown at a later date for the purpose of generating two-phase flow information. Due to size limitations of the boiling and pressure drop measurement sections (1/16 inch), only qualitative two-phase flow data is expected.

3.3 Selected Analytical Models

As previously discussed, there are very few analytical models for the two-phase flow parameters which were derived specifically for the reduced gravity condition. In addition, there has been no interest in formulating models applicable to high accelerations. This is due to the fact that until recently, there was no industrial application for two-phase flow under high g conditions. If the models developed for earth gravity were based on physical principals, it would be possible to isolate the gravity effect. However, the majority of two-phase flow models are either purely empirical or contain some empirical parameters which will limit their applicability outside the range of data. Since each empirical model predicts a certain set of experimental data, it will not be surprising to find an earth gravity model which predicts the available low or high g conditions.

Due to the lack of analytical models for high gravity conditions, the review of models in this section will be limited to the few existing correlations developed for reduced gravities. In addition, several physically based models which may be applied to other gravity levels will be discussed.

3.3.1 Two-Phase Flow Regime Map

Traditionally, flow regime maps have been used to chart the boundaries of the various flow patterns. The usual approach has been to perform a series of tests for a range of flow parameters, visually identify the flow regimes, and map the data with the specified transition lines on a two-dimensional plot. There are two major disadvantages with this approach, namely, the lack of precision in describing the visual observations, and the lack of a theoretical basis for the coordinate selection. This has

resulted in different and sometimes conflicting flow classifications. Extrapolation of these correlations to different gravity levels is highly questionable.

There are several models which have taken a physical approach for arriving at transition criteria. Among these models are the work of Dukler and co-workers, (8) (20), and the study of Mishima and Ishii (21).

Before discussing the flow transition models, it should be noted that the films taken from reduced gravity tests have shown that the flow pattern resembles the vertical upflow at earth gravity with the exception that the churn-turbulent flow was not observed. Therefore, the flow patterns are bubbly, slug, and annular. The analysis of flow regime transition for horizontal flow usually starts from a stratified flow condition and the mechanisms by which a change from stratified flow is expected are investigated. Since a stratified flow configuration is not expected under reduced gravity conditions, it seems more appropriate to extend the vertical flow transition criteria to reduced g conditions. On the other hand, stratified flow would be the dominant regime at higher accelerations and the transition mechanisms developed for horizontal flow should be considered.

The transition criteria for the vertical upward gas/liquid flow from the above models are:

Bubbly/slug transition:

This transition is based on coalescence of bubbles that create the slugs. Typically this transition for earth gravity occurs at void fractions between 0.1 and 0.3. The criteria derived in the transition models is based on the maximum allowable packing of bubbles beyond which the coalescence begins to increase sharply. Ref. (20) assumes a cubic packing with the spacing equal to half the radius and arrives at $\alpha = 0.25$. Ref. (21) uses planar packing with bubbles spaced two diameters apart and arrives at $\alpha = 0.3$.

To derive a relation in terms of the phase velocities, a drift flux model is used and the final equation for transition becomes

$$\text{Ref.} \qquad J_L = 3.0\, J_G - 1.15 \left[\frac{g\,(\rho_L-\rho_G)\,\sigma}{\rho_L^2} \right]^{1/4} \tag{3.1}$$

$$\text{Ref.} \qquad J_L = 2.33\, J_G - 1.15 \left[\frac{g\,(\rho_L-\rho_G)\,\sigma}{\rho_L^2} \right]^{1/4} \tag{3.2}$$

In the model developed in Ref. (6) specifically for the reduced gravity condition, the transition void is obtained from the average of maximum packing values for spheres, 0.5, and ellipsoids, 0.4. A void fraction of 0.45 is used but instead of drift flux approach, homogeneous flow is assumed to arrive at

$$J_L = 1.22\, j_G \tag{3.3}$$

The void fraction criteria used seems to be very high and it was basically adopted to fit the only existing set of reduced gravity data, Figure 3.1. The same criterion as equation (3.3) can be obtained with lower transition void fraction by assuming local homogeneous flow and using drift-flux formulation.

Slug/annular transition:

Three different mechanisms have been suggested for this transition. Ref. (20) suggests that annular flow occurs when the gas velocity is large enough to lift all the entrained droplets generated from the shattered waves on the film. The following equation is arrived at:

$$J_G = 3.1\, \frac{[\sigma g\,(\rho_L-\rho_G)]^{1/4}}{\rho_G^{1/2}} \tag{3.4}$$

Ref. (21) suggests that for small diameter tubes, the criterion for annular flow is based on the assumption that gas velocity should be large enough to reverse the direction of the falling film. The following equation is derived

$$J_G = (\alpha - 0.1) \left[\frac{gD\ (\rho_L - \rho_G)}{\rho_G} \right]^{1/4} \tag{3.5}$$

For large diameter tubes, a criteria based on the gas velocity to shatter the liquid slugs is suggested as follows

$$J_G = \left[\frac{\sigma\ g\ (\rho_L - \rho_G)}{\rho_G^2} \right]^{1/4} N_\mu^{-0.2} \tag{3.6}$$

where

$$N_\mu = \frac{\mu_L}{\left[\rho_L\ \sigma \sqrt{\frac{\sigma}{g\ (\rho_L - \rho_G)}} \right]^{1/2}} \tag{3.7}$$

The criterion developed in Ref. (6) for reduced gravities is based on equating the void fractions for slug and annular flow. A relation for the slug flow void fraction is developed using the reduced gravity films and the measurements for the bubble velocity relative to the velocity of center of volume. The following relation is obtained

$$\frac{J_G}{J_L + J_G} = 1.2\ \alpha \tag{3.8}$$

A force balance on the smooth annular film results in

$$\frac{\alpha^{5/2}}{(1-\alpha)^2} = \left(\frac{f_i}{f_w}\right) \left(\frac{\rho_G}{\rho_L}\right) \left(\frac{J_G}{J_L}\right)^2 \tag{3.9}$$

where f_i and f_w are the interfacial and wall friction factors.

Equations (3.8) and (3.9) are solved simultaneously to arrive at a relation for superficial velocities. The result for the air/water flow is shown in Figure 3.1. Although, this criterion does not contain a gravity term, it is superior to the other two relations since it is derived to fit the data at reduced gravities. Equations (3.5) and (3.6) result in constant J_G for annular flow transition.

Sunstrand data has been compared to the model of Ref. (6) and it is claimed that Equations (3.8) and (3.9) do not have a solution for R-114. It is suggested that a value of 1.06 be used as the constant in Equation (3.8) to fit the data. Figure 3.6 shows this comparison and the criterion of Equation (3.4).

3.3.2 Two-Phase Pressure Drop

Estimation of pressure drop and void fraction are the two main concerns in design and analysis of any system operating with a two-phase flow. A larger number of publications on this subject have appeared in the literature over the last fifty years. However, there is still no completely satisfactory procedure for evaluating the two-phase pressure drop under all conditions. Although the influence of the main parameters affecting the pressure drop and void fraction can be modeled accurately, the effect of some secondary parameters cannot be accounted for. The majority of commonly used models are empirical and account for the effect of the main parameters within the range of their applicability. These models do a good job of predicting the pressure drop if they are properly used for the geometries and flow conditions that they are intended for. Most of the empirical models do not differentiate between different flow regimes, boiling or adiabatic conditions, and the test section orientation. There are, however, some flow regime dependent pressure drop models but it would be more difficult to apply them since they require a knowledge of flow regime boundaries and transition criteria.

The two-phase frictional pressure drop is usually expressed in terms of the corresponding single-phase gradient by using a two-phase multiplier. The multiplier is defined as

$$\phi_L^2 = \frac{\left(\frac{dP}{dZ}\right)_{\text{two-phase}}}{\left(\frac{dP}{dZ}\right)_{\text{single-phase}}} \tag{3.10}$$

There are a variety of models for the two-phase friction multiplier, and for every set of data at low or high gravity levels one can find an empirical model developed for 1 g which will result in satisfactory agreement. Unfortunately, there is not a sufficient amount of data at different gravities to qualify any of these models. In this section some of the commonly used models will be discussed and comparison with the limited available data will be presented.

Empirical Models

The most widely used two-phase pressure drop correlations are Martinelli, et al. models (22), (23) which are discussed in every classical text on this subject. These models were developed for adiabatic (air/water) and convective boiling of water, respectively. Two correlations used frequently in nuclear industry are Thom (24) for steam-water flow and Baroczy (25) which have used a broader range of data. The Baroczy correlation has incorporated the data from different fluids and accounts for the effect of mass flow rate and fluid properties on the two-phase multiplier. This correlation is presented graphically which makes its use rather difficult.

More recent correlatiions for two-phase friction multiplier have been based on a larger data base and are applicable to a wider range of conditions. Among them, Chisholm and Friedel models are discussed below.

Chisholm correlation, (26):

This correlation was developed in an attempt to generate an analytical basis for the Lockhart-Martinelli correlation. Later, the variation of parameters with property index Γ was added which resulted in a correlation that predicted Lockhart-Martinelli, Martinelli-Nelson, Thom, and Baroczy correlations. The two-phase multiplier is given by

$$\phi_L^2 = 1 + (\Gamma^2 - 1) \left\{ B\,[x\,(1-x)]^{\frac{2-n}{2}} + x^{2-n} \right\} \qquad (3.11)$$

where n is the exponent for the single-phase friction factor

$$f = \frac{C}{(Re)_L^n}$$

and its value is between 0.2 and 0.25. B is given by the following table

Γ	$G(lbm/ft^2s)$	B
≤ 9.5	≤ 102	4.8
	$102 < G < 390$	$\frac{492}{G}$
	≥ 390	$\frac{25}{G^{0.5}}$
$9.5 < \Gamma < 28$	≤ 123	$\frac{235}{\Gamma G^{.5}}$
	> 123	$\frac{21}{\Gamma}$
> 28		$\frac{6788}{\Gamma^2 G^{.5}}$

Friedel Correlation, (27):

Using a large data bank containing over 25,000 data points for pressure drop, Friedel developed the following correlation which is valid for both horizontal and vertical upflow.

$$\phi_{Lo}^2 = E + \frac{3.24\ FH}{Fr^{0.045}\ We^{0.035}}$$

$$E = (1-x)^2 + x^2 \frac{\rho_L\ f_{Go}}{\rho_G\ f_{Lo}}$$

$$F = x^{0.78}\ (1-x)^{0.24}$$

$$H = \left(\frac{\rho_L}{\rho_G}\right)^{0.91} \left(\frac{\mu_G}{\mu_L}\right)^{0.19} \left(1 - \frac{\mu_G}{\mu_L}\right)^{0.7} \qquad (3.12)$$

$$Fr = \frac{G^2}{g\ D\ \rho_{TP}^2}$$

$$We = \frac{G^2\ D}{\rho_{TP}\ \sigma}$$

$$\rho_{TP} = \left(\frac{x}{\rho_G} + \frac{1-x}{\rho_L}\right)^{-1}$$

In Ref. (7), the above and several other models were compared with the reduced and earth gravity pressure drop data. It was concluded that Friedel and HTRI (which is a proprietary correlation) resulted in best agreement with data. The HTRI model was modified to allow annular flow in the regions of high quality. For the earth gravity tests, the above correlations were not successful and the Chisholm stratified flow correlation resulted in

good agreement. This correlation does not have a physical basis and is given by the following relation:

$$\phi_L^2 = 1 + \frac{1.5}{X_{tt}} + \frac{1}{X_{tt}} \tag{3.13}$$

For high g conditions, this correlation may be applicable over a wider range of conditions. The HTRI model overpredicted the data by as much as 100% which was attributed to the flow regime used in this model.

The predictions by several empirical models were obtained for the average mass flux of Sunstrand tests and are plotted in Figures 3.7 and 3.8. Chis. Strat. refers to Chisholm stratified, HEM (mix. visc.) to HEM with the mixture viscosity. The Friedel model has a gravity dependent term and the predictions can be performed with the actual gravity level tested. However unlike the observed trend, the predictions decrease for reduced gravity levels.

Although all the above models are developed for earth gravity conditions, they result in widely different predictions. The comparisons show that the Friedel model which is developed for earth gravity results in best agreement with reduced gravity data but fails in predicting the earth gravity data. As mentioned earlier, one can always find a pressure drop model which can predict a particular set of data. Since none of these models are developed for reduced gravity conditions it is highly unlikely that they result in satisfactory agreement with data for other fluids at different ranges of flow rate.

Phenomenological Models

Hewitt's Triangular Model for Annular Flow, (28):

This is actually a phenomenological set of relationships developed for annular flow. It provides an interrelation among liquid film flow rate, film thickness, and pressure gradient in such a way that any one of the parameters can be calculated from the knowledge of the other two. The model

is complicated and requires an iterative solution. For a given mass flux, G, and quality, X, the steps taken for the applying this model consist of:

1) Assume a flow thickness δ and calculate the core void fraction from

$$\alpha_c = (1 - 2\frac{\delta}{D})^2$$

2) Given the relation for the interfacial friction factor, f_i, the interfacial shear and the pressure gradient are calculated from

$$\tau_i = \frac{1}{2} \rho_c u_c^2 f_i$$

$$u_c = \frac{G [x + (1-x) E]}{\alpha_c \rho_c}$$

$$\rho_c = \rho_G [1 + \frac{1-x}{x} E]$$

$$\frac{dP}{dZ} = \frac{-4}{D \sqrt{\alpha_c}} \tau_i$$

where E is the entrainment rate.

3) Using the relation for eddy diffusivity, ε, calculate the liquid film velocity and integrate to get film flow rate from

$$\dot{W}_L = \int_0^{\delta} \pi(D-2y) \rho_L u \, dy$$

$$\frac{du}{dy} = \frac{\tau}{\mu_\ell + \varepsilon \rho_L}$$

$$\tau = \tau_i \left(\frac{r_i}{r}\right) + \frac{1}{2} \frac{dP}{dZ} \left(\frac{r_i^2 - r^2}{r}\right)$$

Therefore, the model requires a knowledge of interfacial friction factor f_i, entrainment rate E, and a relation for the turbulent eddy diffusivity in the liquid film ε. In Ref. (9) a calculational scheme using this approach was developed for comparison with simulated reduced gravity data. This scheme was used in Ref. (1) along with Deissler's eddy diffusivity relation and Ishii & Mishima's, (29), entrainment correlation. Since no satisfactory interfacial friction model was found, an attempt was made to correlate one based on Sunstrand tests. The resulting correlation for interfacial friction factor is given by the following relation

$$f_i = f_G \left[1 + 3.74 \times 10^5 \left(\frac{\rho_L}{\rho_G}\right)^{1/2} (D^*)^{-0.778} (N_\sigma)^{-0.6} \frac{\delta}{D} \right]$$

where

$$D^* = D \sqrt{\frac{g (\rho_L - \rho_G)}{\sigma}} \quad \text{and} \quad N_\sigma = \frac{\rho_L \sigma D}{\mu_L^2}$$

The prediction by the above relation for R-114 at g_o and $g=0.01\ g_o$ is shown in Figure 3.9. This relation is used in the experimental design analysis which is covered in section 5.0.

SLI Bubbly Flow Model, (9):

This is a phenomenological model specifically derived for zero gravity fully developed bubbly flow. The model uses two-dimensional separated flow conservation equations. It is assumed that the phases are in local

homogeneous condition but cross-sectional void distribution exists which results in void peaking near the wall and an almost flat profile away from the wall. The forces acting on the bubble are the turbulent forces and a lift force which causes the bubbles to move towards the region of higher velocity. The turbulent eddy diffusivity is broken down into the component due to single-phase turbulence and the turbulence enhancement introduced by the presence of bubbles. Using the data of simulated reduced gravity tests, a correlation for the transverse component of the turbulent fluctuations is obtained. There is no explicit solution for this model and an iterative approach is used to solve six differential equations simultaneously from the wall to the center of the tube. For an assumed value of the non-dimensional tube radius, these equations result in values for G, X, α, and ϕ^2_{Lo}. Therefore, for every combination of mass flux and quality, the solution for the cross-sectional average void fraction and two-phase friction multiplier can be obtained.

In order to evaluate the predictive capability of this model, it should be compared with the true microgravity adiabatic gas/liquid data. However, bubbly flow pressure drop data is not presently available. It is interesting to note that, although this model was based on the data of equal density liquids where the pressure drop was essentially the same as predicted by the Homogeneous Equilibrium Model (HEM), when used for gas/liquid flow it predicts considerably larger pressure drop.

3.3.3 Void-Quality Relation

The average void fraction is defined as the fraction of the channel cross section occupied by the gas phase. Using a separated model for the two-phase flow, the fundamental void-quality relation is given by

$$\alpha = \frac{x}{x + S\left(\frac{\rho_G}{\rho_L}\right)(1-x)} \qquad (3.14)$$

where S is the ratio of the average gas to liquid velocity or the slip ratio

$$S = \frac{U_G}{U_L} \tag{3.15}$$

For the homogeneous model the phase velocities are equal and the slip ratio is unity. The above equation reduces to

$$\alpha = \frac{x}{x + (\frac{\rho_G}{\rho_L})\ (1-x)} \tag{3.16}$$

At earth gravity, the void fraction approaches the homogeneous value at high mass flux and high pressure but normally deviates significantly from that. If the variation of slip ratio was available, one can easily find the void fraction from equation 3.14. However, correlation of S in terms of the two-phase flow parameters has not been successful.

The next level of sophistication contains models which account for radial variation of velocity and void fraction by empirical distribution factors. Using the drift flux approach the average void fraction becomes

$$\alpha = \frac{x}{C_o \left[x + (\frac{\rho_G}{\rho_L})\ (1-x) \right] + \frac{\rho_G}{G} U_{gj}} \tag{3.17}$$

where Co is distribution parameter and U_{gj} is the average drift velocity which brings in the effect of local slip between the phases. When the phases are in local homogeneous condition $U_{gj} = 0$ and the slip ratio becomes

$$\alpha = \frac{x}{C_o \left[x + (\frac{\rho_G}{\rho_L})\ (1-x) \right]} \tag{3.18}$$

Therefore, even with local homogeneous condition the slip ratio which is the ratio of the cross-sectional average velocities could be different from unity. The values of the parameters C_o and U_{gj} depend on the particular flow regime and are generally empirically determined.

For bubbly vertical upflow with void fraction of less than 0.2, Wallis suggested

$$C_o = 1 \quad ; \quad U_{gj} = 1.53\ (1-\alpha)^2 \left[\frac{\sigma\ g\ (\rho_L-\rho_G)}{\rho_L^2} \right]^{1/4}$$

while for higher void fractions in the churn-turbulent regime a value of 1.41 is used for the constant in U_{gj} relation. For the vertical fully developed turbulent slug flow the following relations are recommended.

$$C_o = 1.2 \quad ; \quad U_{gj} = 0.35 \left[\frac{g\ (\rho_L-\rho_G)\ D}{\rho_L} \right]^{1/2}$$

For annular flow with no entrainment, from force balances on the total flow and on the gas core a relation for the two-phase friction multiplier can be obtained as follows

$$\phi_L^2 = \frac{1}{(1-\alpha)^2}\ \frac{f_{TP}}{f_L} \tag{3.19}$$

where f_{TP} is the single-phase friction coefficient for the liquid film and f_L is the friction coefficient for the liquid flowing alone in the channel. It can be shown that the Reynolds number for the above cases are identical and therefore $f_{TP} = f_L$.

$$\alpha = 1.0 - \frac{1}{\phi_L} \tag{3.20}$$

Therefore, void fraction for annular flow can be obtained using a relation for the two-phase friction multiplier.

Among the phenomenological models for the reduced gravity is the SLI bubbly flow model, (9), which found that the predicted void fractions for bubbly flow are essentially the same as homogeneous equilibrium predictions, Equation 3.16. For annular flow, the triangular approach described in the previous section can be used to obtain the void fraction given by the following relation

$$\alpha = \frac{\frac{\rho_G}{\rho_L}\left(1 - 2\frac{\delta}{D}\right)^2}{1 + E\,(1-x)/x}$$

Figure 3.10 shows the void-quality prediction from the homogeneous model, the triangular approach fitted to reduced gravity data, and the Lockhart-Martinelli correlation. There is no data presently available to verify any of these models. It is, however, expected that the triangular approach would provide a close representation for the Sunstrand data, since the observed flow regime was annular and the two-phase multiplier is developed to fit the data closely.

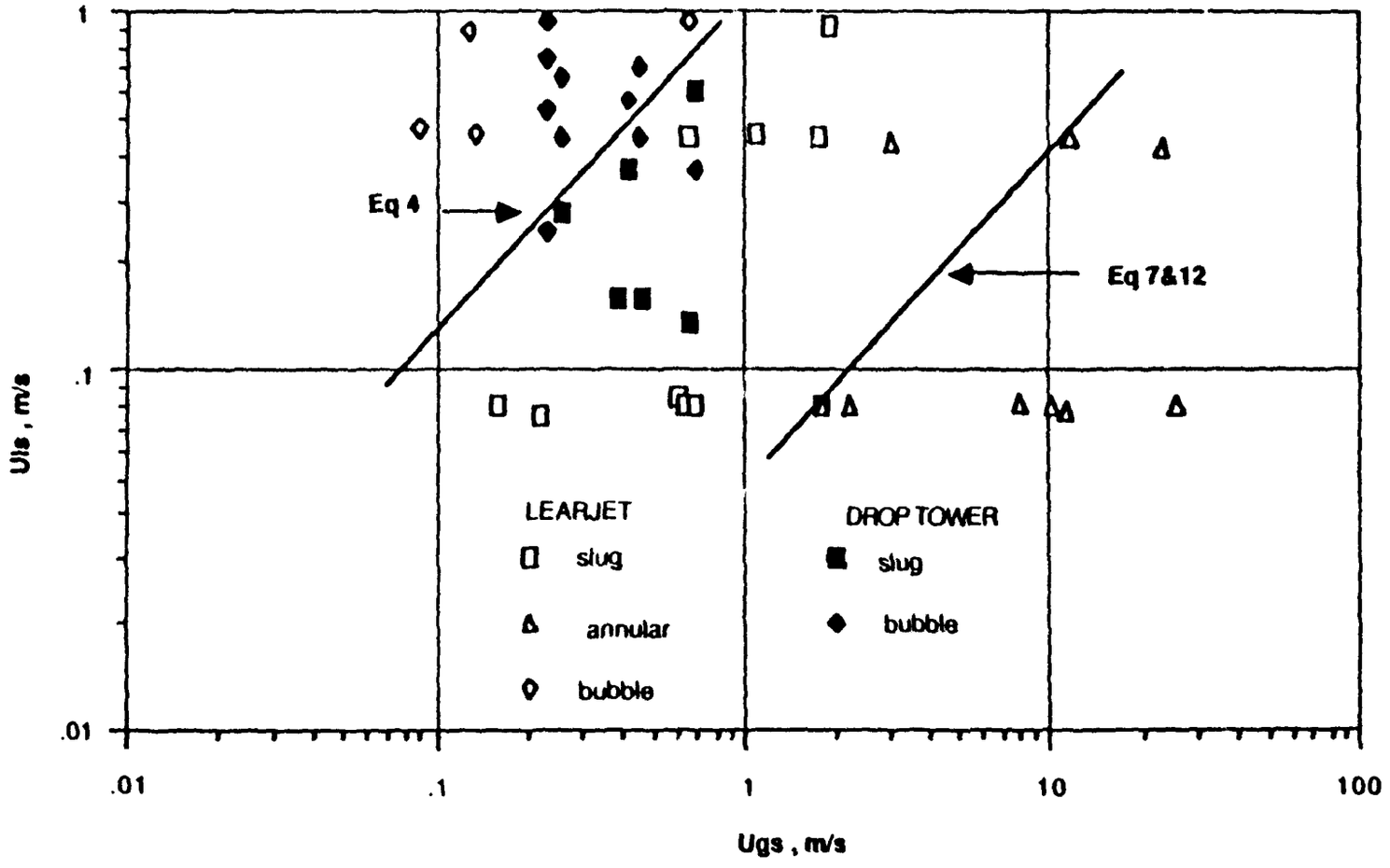

Figure 3.1 - **MICRO G FLOW PATTERN MAP**

Reproduced from Ref. (6)

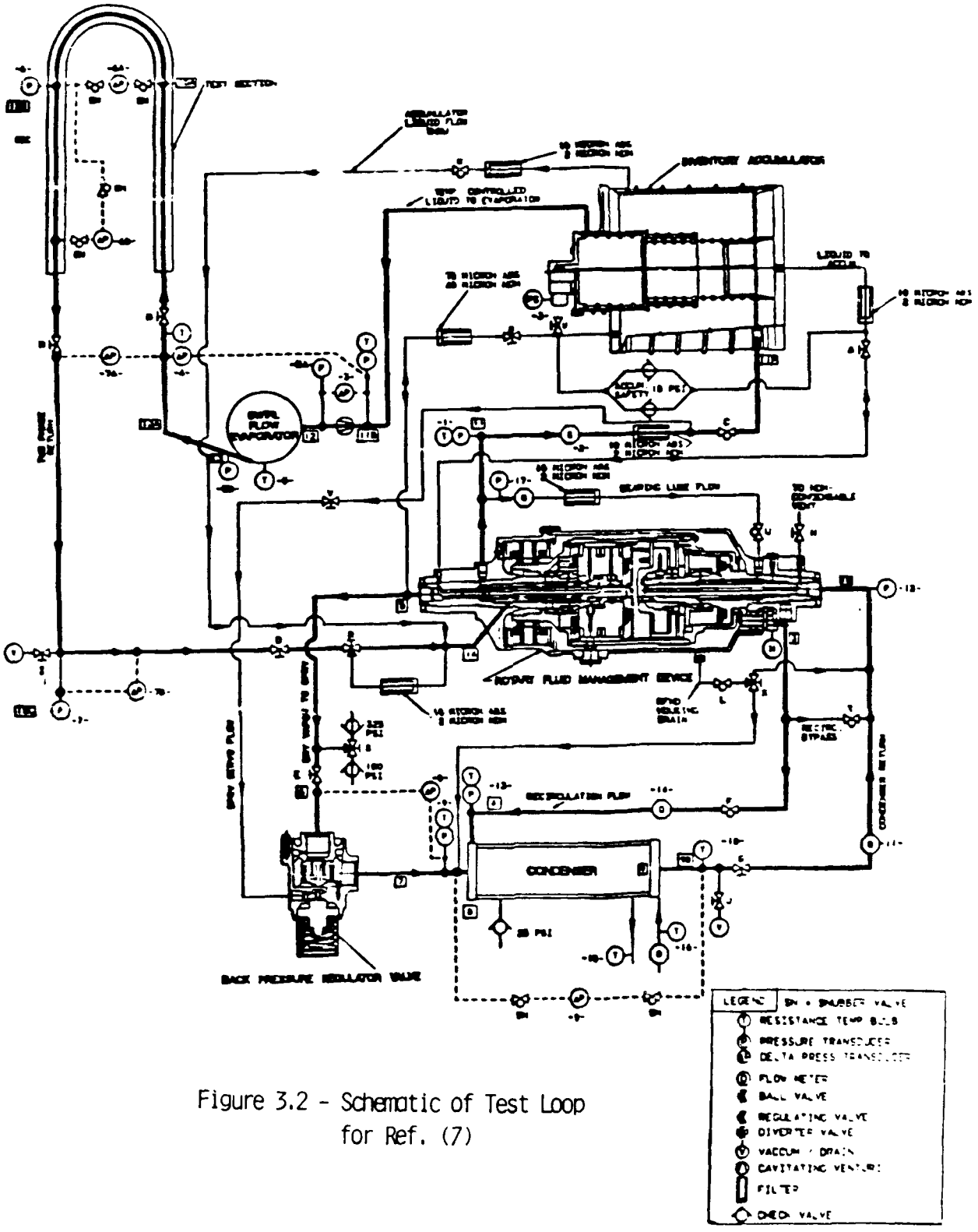

Figure 3.2 - Schematic of Test Loop
for Ref. (7)

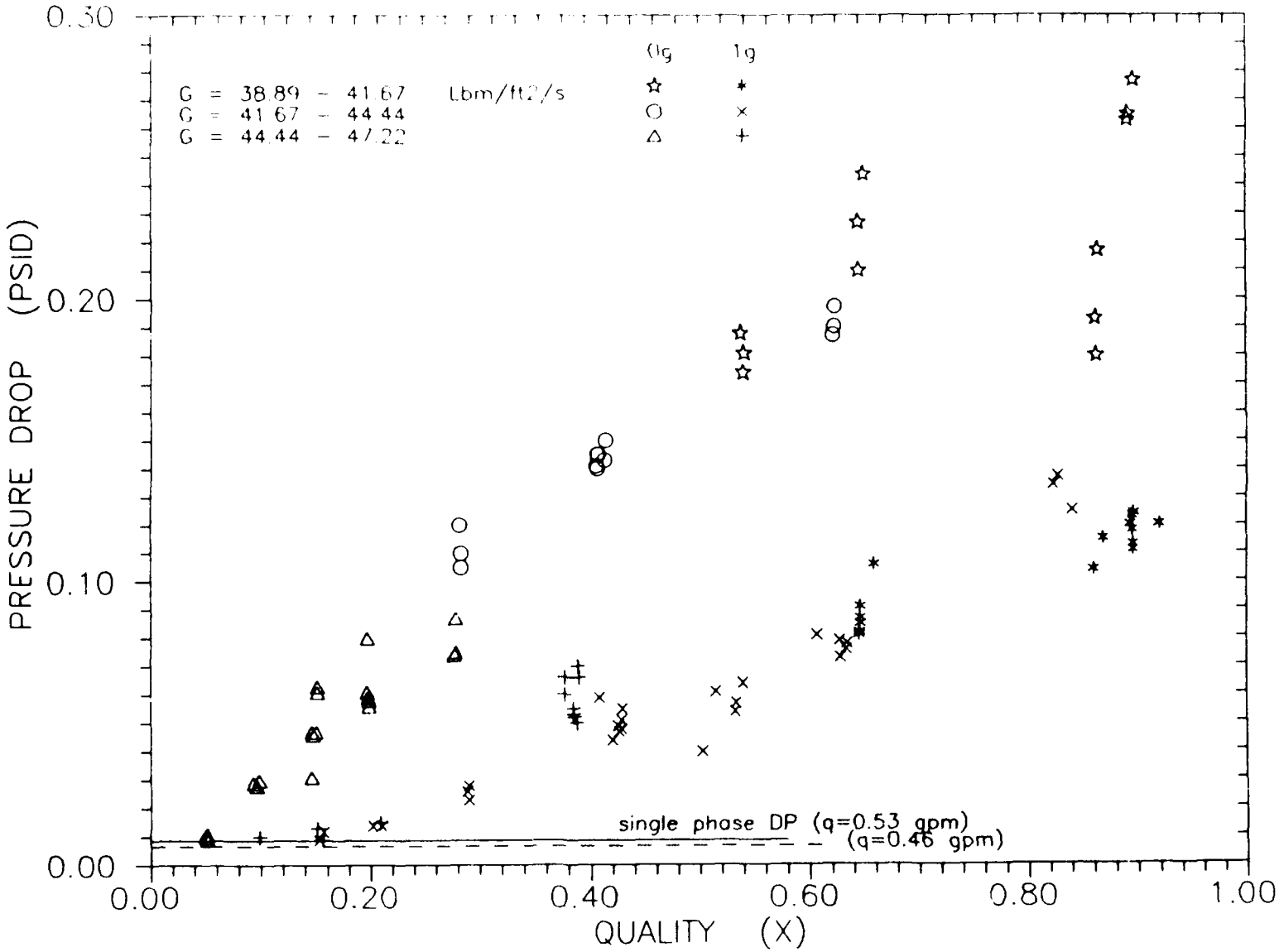

Figure 3.3 - Sunstrand Data for R-114 Under Zero g and 1 g Conditions for Several Ranges of Flow Rates.

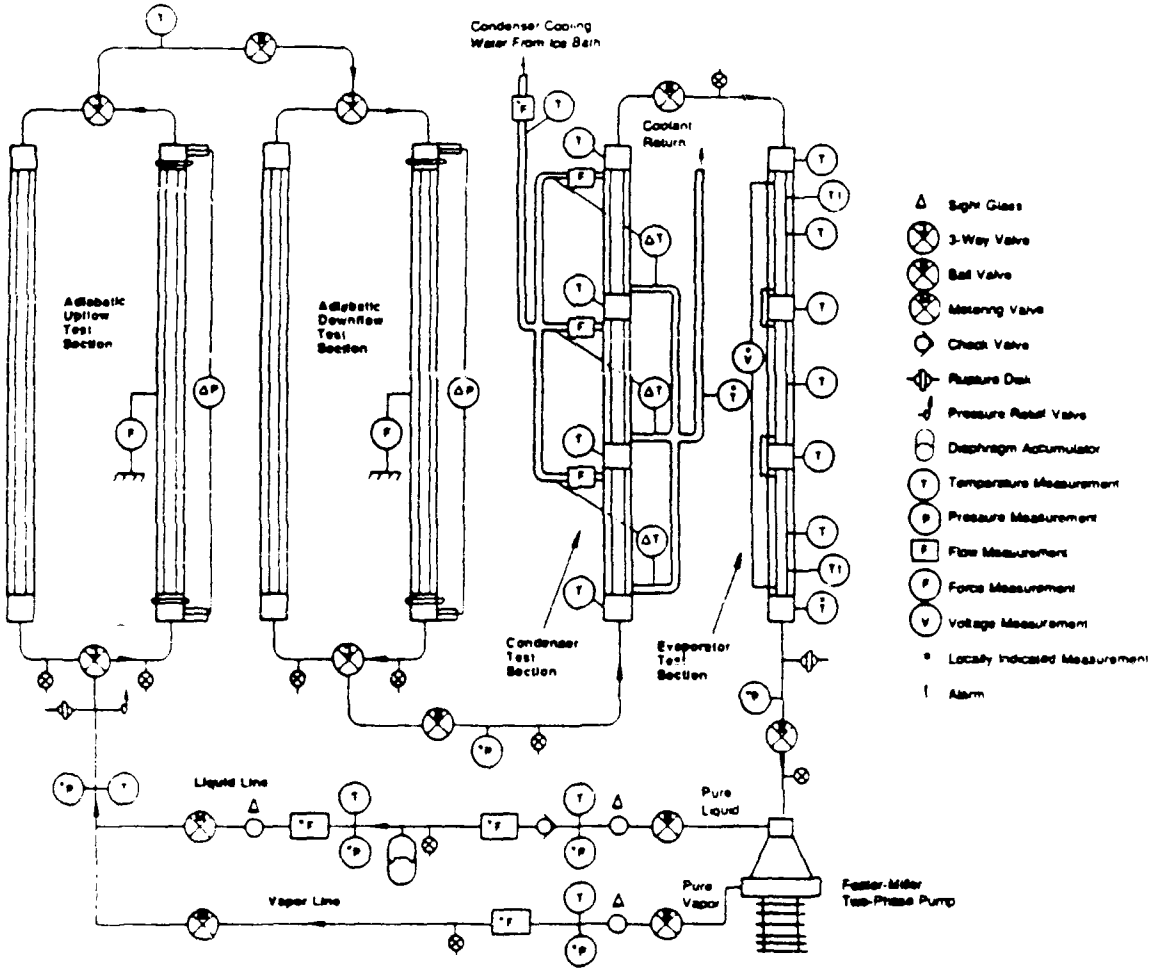

Figure 3.4 - Schematic Illustration of Free-Float Package Configuration.

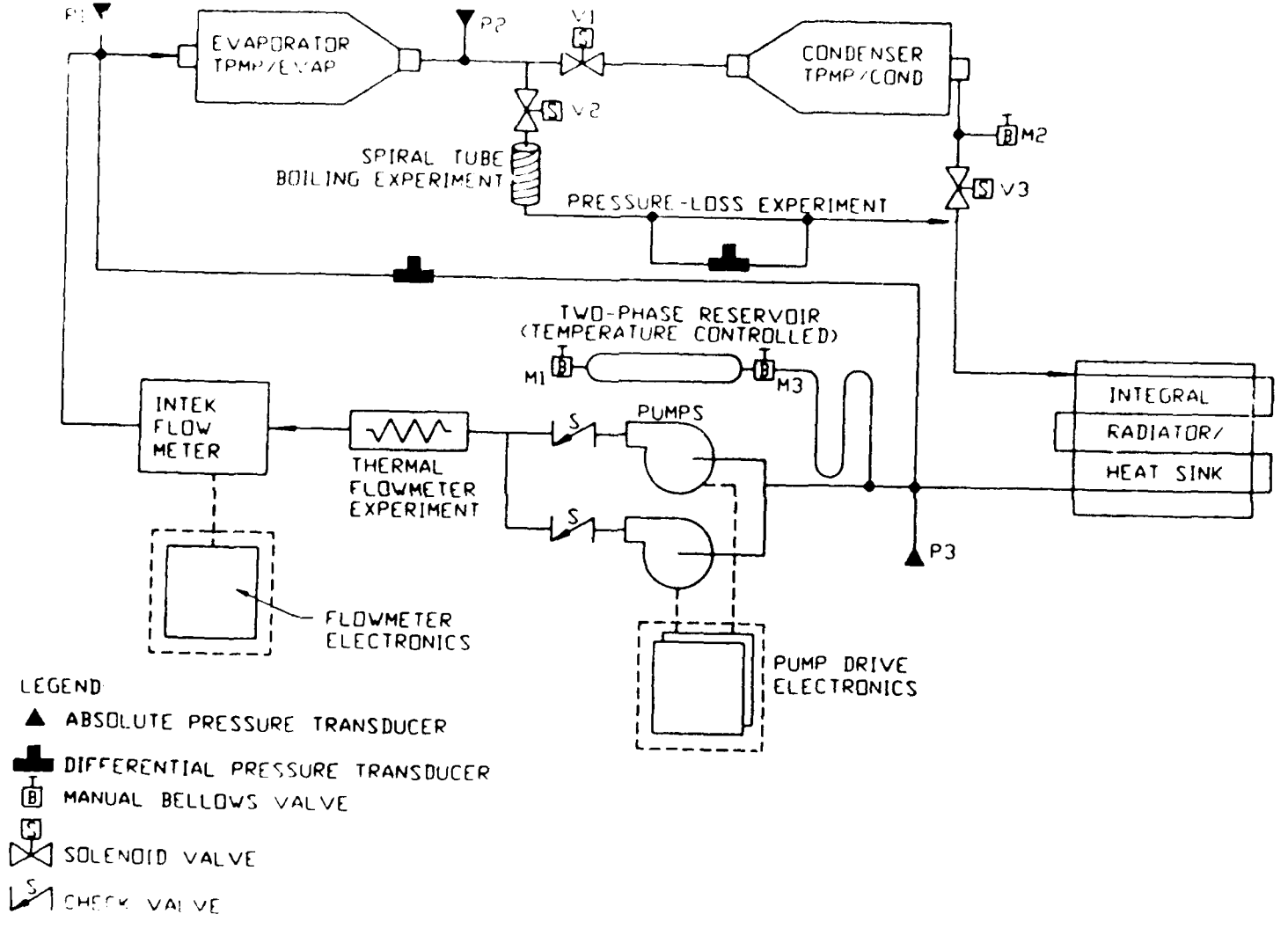

Figure 3.5 . NASA GSFC TEMP 2A-3 Test Schematic

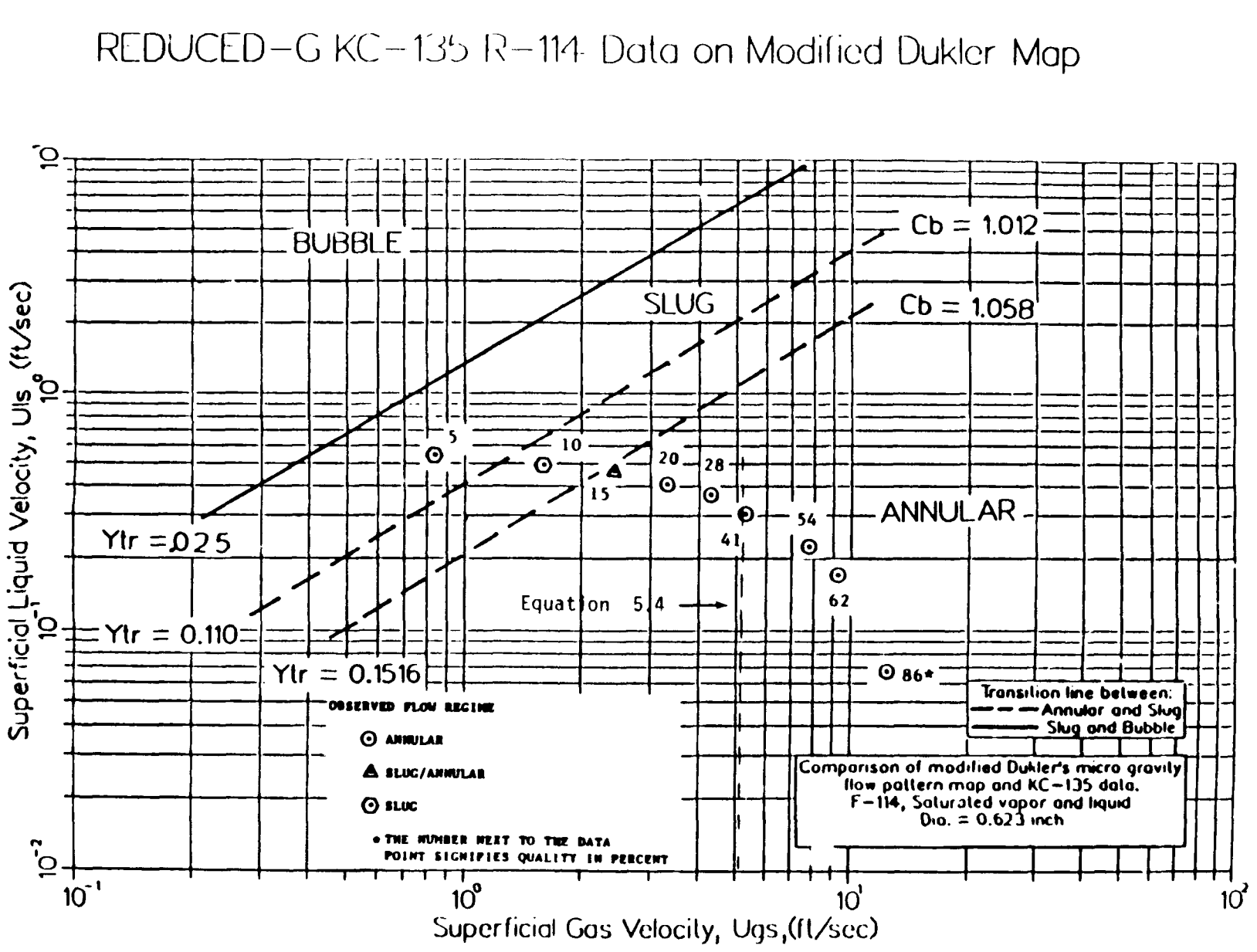

Figure 3.6 - Comparison of Flow Regime Map of Ref. (6) with Data of Ref. (7) Reproduced from Ref. (7).

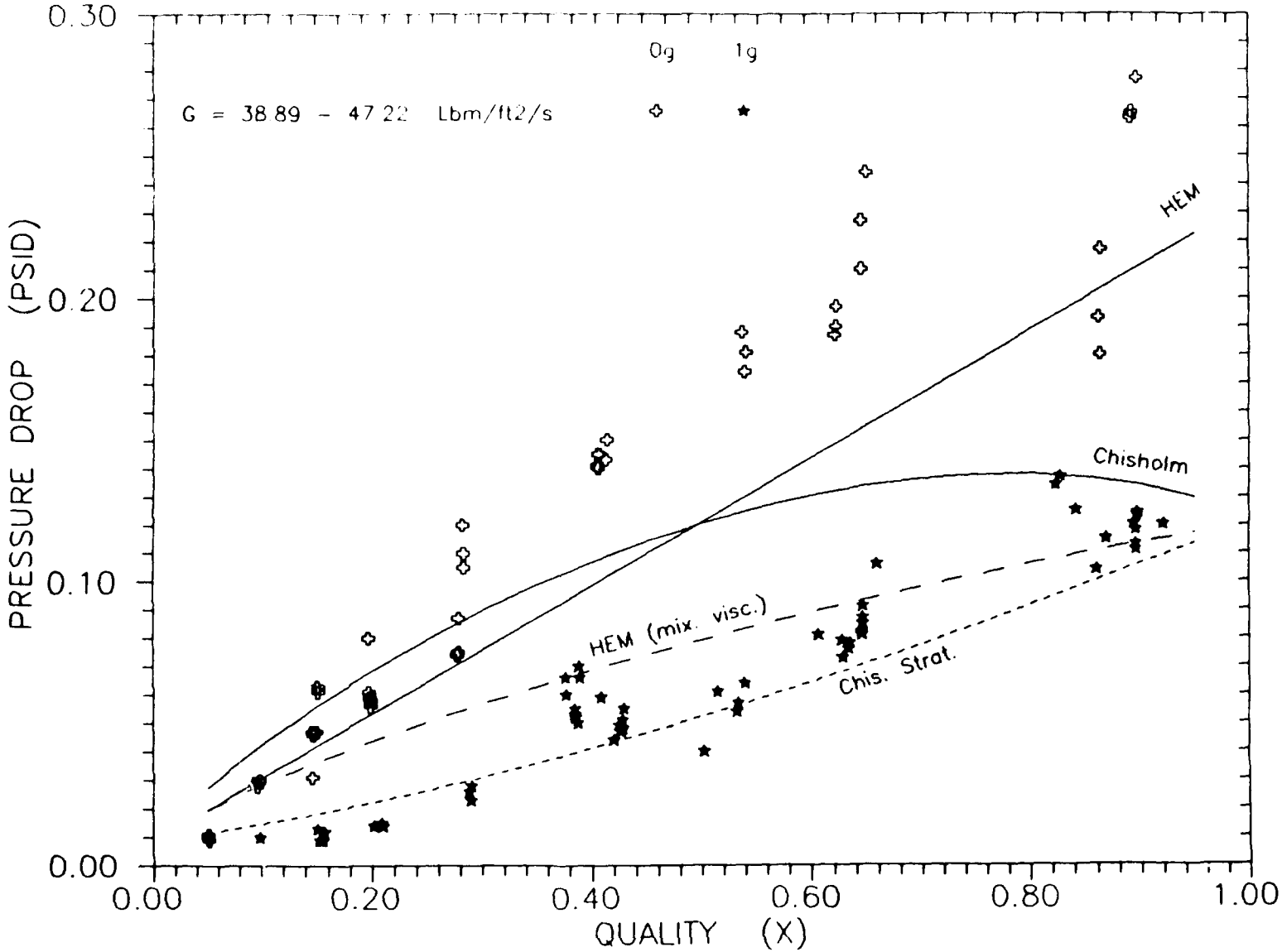

Figure 3.7 – Comparison Between Sunstrand Data and Predictions by Several Models for G = 44.45 Lbm/ft2/s.

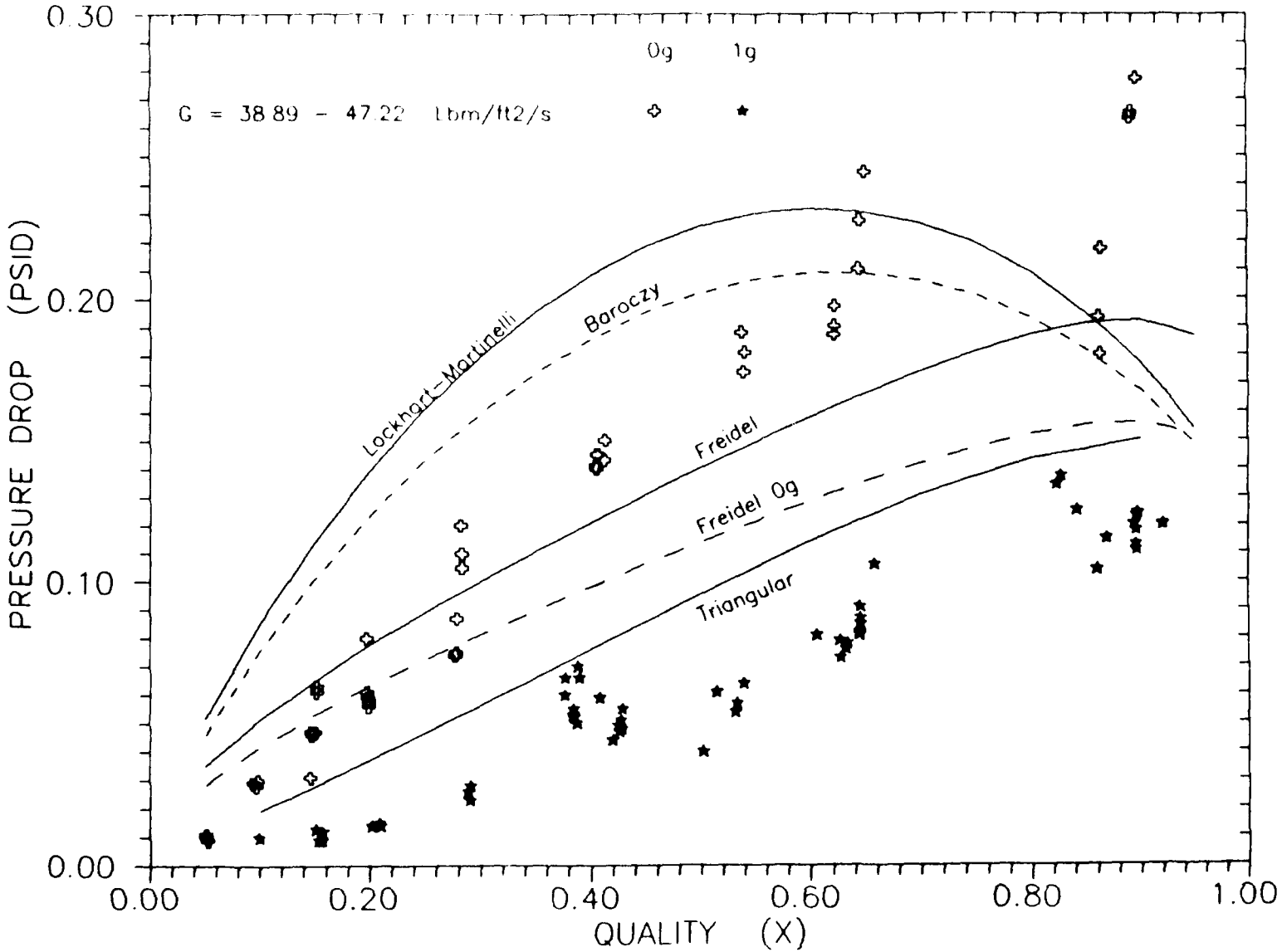

Figure 3.8 - Comparison Between Sunstrand Data and Predictions by Several Models for G = 44.45 Lbm/ft2/s.

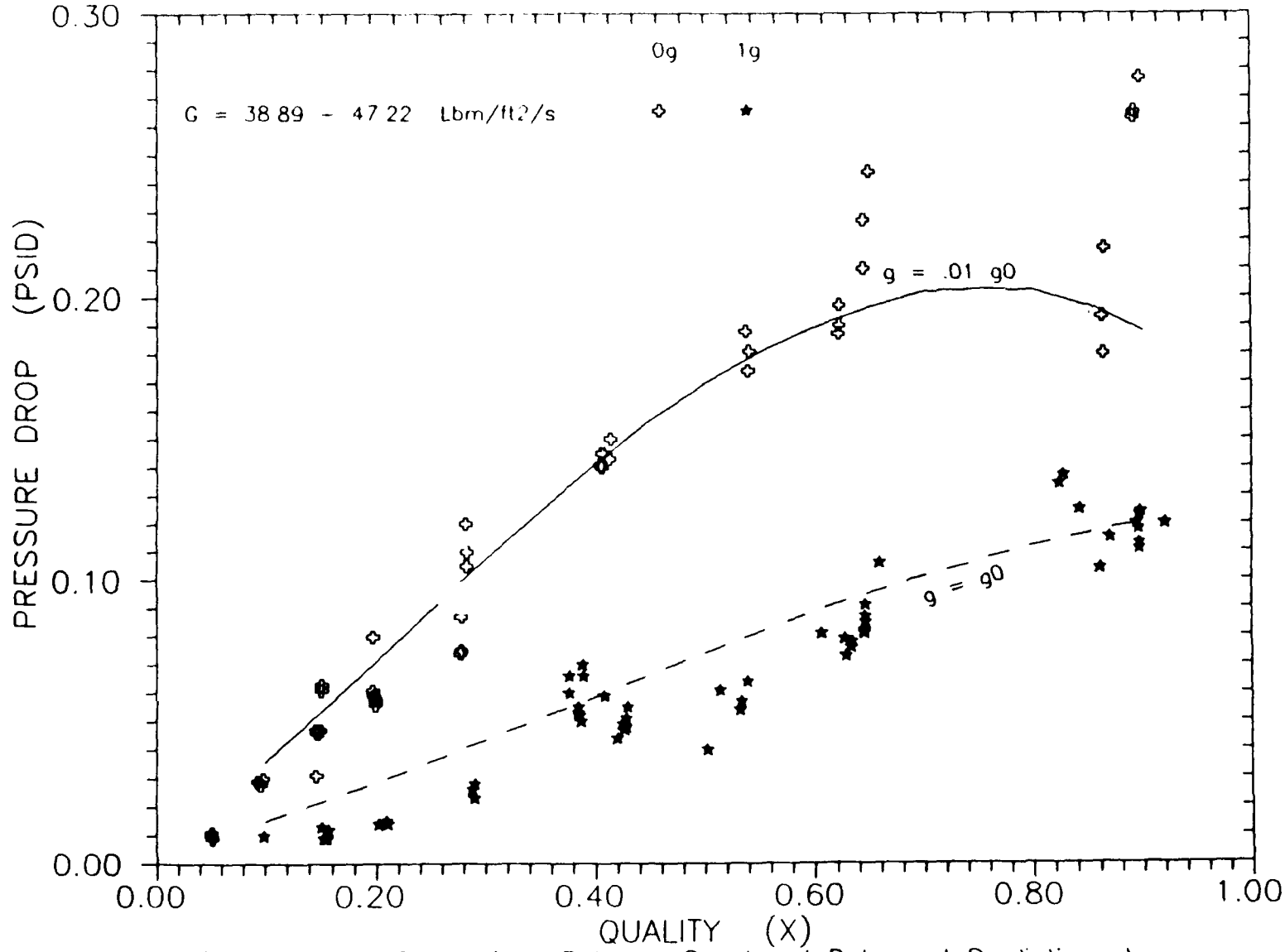

Figure 3.9 – Comparison Between Sunstrand Data and Predictions by Triangular Model of Hewitt with the New Correlation for the Interfacial Friction Relation, C = 44.44.

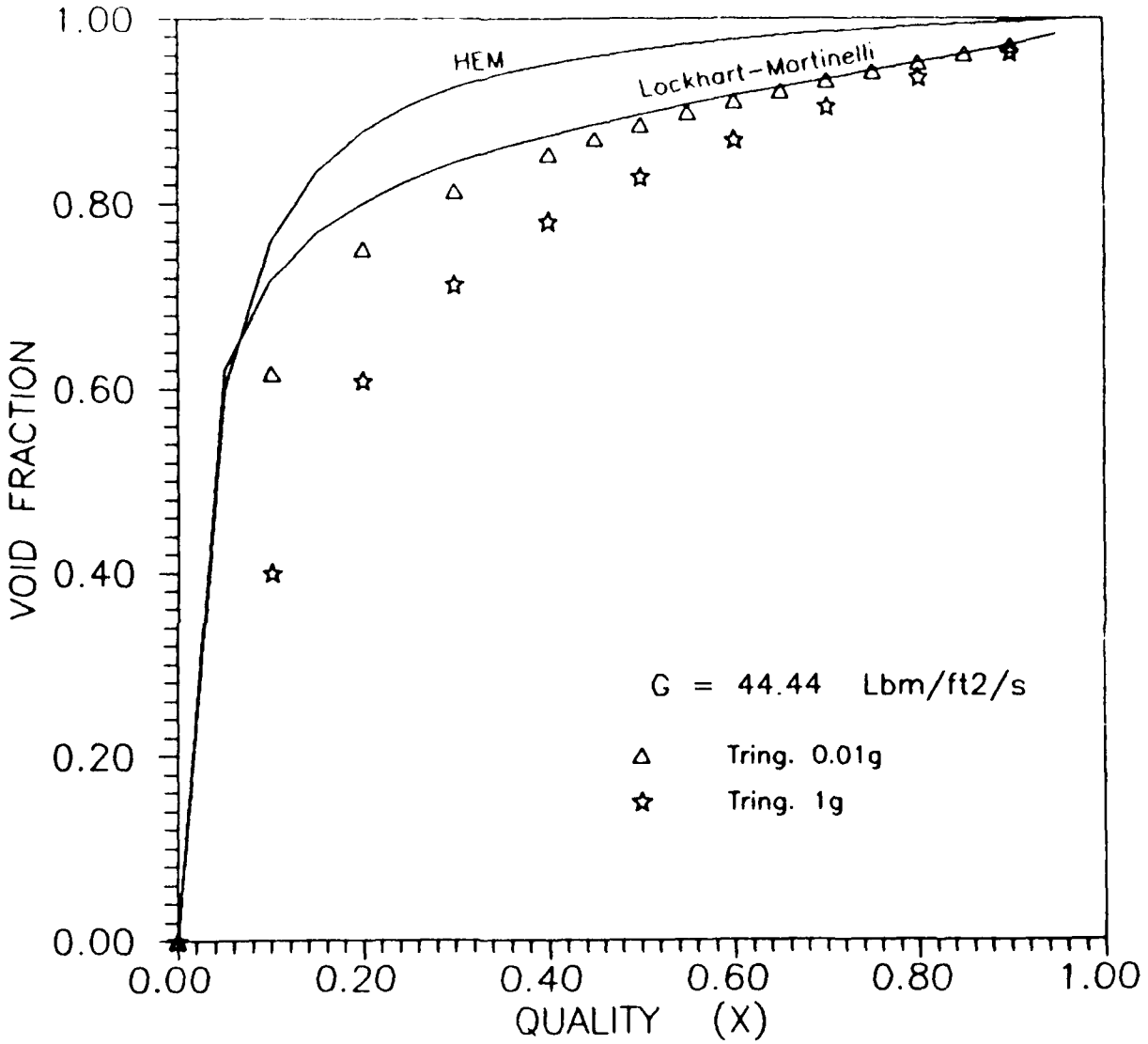

Figure 3.10 – Void–Quality Relation for Sunstrand Test Conditions using Several Models.

Section 4

TEST PLAN

One of the major objectives of the present program was to design a modular flight test bed which can be used to generate data for the two-phase flow parameters identified in this study. As mentioned earlier, the studies in progress have concentrated on two-phase heat transfer and pressure drop characteristics. Although many experiments should be performed to develop the necessary data base for analyzing a phenomenon, it was decided to focus on areas which are not presently covered by the programs in progress.

Design of a two-phase flow test loop depends on the parameters which are determined to be primary for the test objectives. The present test loop is designed to provide data on critical heat flux and onset of hydrodynamic stability.

4.1 Design Requirements

The design requirements are set forth in order to develop a test loop which will be capable of evaluating the system/component concepts in addition to generating basic reduced gravity two-phase flow data. The main requirement for the present design is modularity of the loop which will allow interchanging of the components. In addition, the test bed should consist of an adiabatic section where two-phase pressure drop data and possible flow visualization is performed. The test bed should be adaptable to airplane trajectory testing which, depending on the type of aircraft used, will impose size and power limitations on the final design. These requirements are intended to allow the system to provide as much necessary information as possible in the most efficient method and with a minimum number of flight tests.

Another design requirement, initially considered, was capability of testing at high accelerations. Designing the system for moderately high accelerations is not a major constraint. In fact the loop should be

capable of withstanding at least 4 g during the airplane trajectories anyhow. As will be discussed for the baseline configuration, designing the system to be adaptable to other methods of high g simulation, namely centrifuge, is quite difficult. It was therefore decided not to include adaptability to centrifuge testing as a design requirement.

The main emphasis in the design process is placed on developing a set-up for generating the required data for the major test parameters, namely critical heat flux and incipience of hydrodynamic instability. However, the system is designed to provide data on two-phase heat transfer and pressure drop. Provisions are also made for possible flow regime visualization and recording. In addition, the instrumentation is selected to allow possible condenser heat transfer evaluation, if it becomes necessary.

4.2 Conceptual Design

As mentioned above, the test loop is mainly designed to generate data for the critical heat flux (stable burnout) and two-phase flow instability under reduced gravity conditions. Onset of unstable behavior depends on the pressure drop-flow rate characteristic of the system. As discussed earlier, the pressure drop-flow rate characteristics of two-phase systems under reduced gravity conditions are expected to be considerably different from the earth gravity conditions. In order to avoid operation of the two-phase flow system in the negative slope region, the effect of gravity on the pressure drop-flow characteristic of a system should be determined. Generally, this type of test is performed by measuring the pressure drop across a given length of a boiling section while flow rate is reduced. For a given heat flux, tests start with a flow rate high enough that no nucleation takes place within the heated section and single-phase liquid flow exists within the entire section. As the flow rate is reduced, pressure drop decreases until a flow rate is reached where further decrease results in an increase in pressure drop (negative slope). This type of test should be performed with no compressible volume immediately upstream of the test section to avoid limit cycle, and with a refrigerant as the working fluid to avoid melt-down of the heating section in case burnout occurs.

Data on critical heat flux is usually obtained by increasing the heat flux across the heated section until a sudden surge in wall temperature occurs which marks the Departure from Nucleate Boiling (DNB). A qualitative boiling curve is shown in Figure 4.1. With a temperature controlled system, experiments can be performed to map the entire boiling curve. However, under most practical conditions, a heat flux controlled system is used. With this type of a system, increase in heat flux beyond CHF will result in switching the heat transfer regime to film boiling, along AB in Figure 4.1. Due to a significantly lower heat transfer coefficient for the film boiling regime, such a transition will result in a jump in the wall temperature which will mark CHF in experimental procedures.

As mentioned earlier, in many practical applications systems fail at heat fluxes well below that expected for stable burnout due to hydrodynamic instabilities. Therefore, in a system designed to generate data for critical heat flux, care should be taken to avoid instabilities in order to obtain stable burnout data.

A schematic of the proposed test bed is shown in Figure 4.2. It consists of a gear pump, a bladder type accumulator, a boiling and an adiabatic test section, and a shear flow type condenser. As mentioned earlier, one of the main design requirements is to develop a modular test loop which can accommodate different system components. This would require sufficient pumping head and flow to meet the requirements for different types of components and appropriate arrangement for regulating the system flow rates and pressure.

As shown in Figure 4.2, the test section path is parallel to a main line which is intended for the overall pressure and flow control. A second bypass across the condenser is provided for flow control in low flow rate tests when the quality at the condenser inlet needs to be monitored. An oversized centrifugal or a gear pump with a large bypass line can be used to provide a wide range of head-flow variations. Centrifugal pumps are better suited for high flow situations and gear pumps for high pressure head requirements. Since high pressure losses may be encountered in the

two-phase loop, a gear pump is selected for the test bed. This type of pumps provide a nearly constant flow rate irrespective of head loss. A large diameter bypass line with a regulating valve can be used to control the flow rate through the main system. In addition, a regulating valve downstream of the pump is used for pressure adjustment.

It should noted that only a conceptual design for the modular two-phase test bed is performed in the present study. The preliminary and final design of the system should be performed considering the host environment. For example, if the experiments are to be performed aboard the space shuttle, the preliminary design should include study of accommodation, power and size requirements as well as mission and safety analysis. A preliminary design for a baseline configuration is performed in the present study which can be used as proof of concept for the modular system. This design is performed for earth and airplane trajectory testing. As will be discussed later, the major parameters are such that a great deal of information can be obtained from experiments performed at earth gravity.

The test bed consists of the following major components:

Test Section

The test section will consist of a heated and an adiabatic section which are thermally isolated. The entire line will have an inside diameter of 0.25 inch. Obviously, a smaller diameter will require a shorter test section length to provide measurable pressure drop and desired quality range. However, too small a diameter will result in questionable flow regime establishment, particularly in the annular flow regime. The heated section will be stainless steel with a length to diameter ratio of at least 40. The exact length will depend on the host environment size and power limitations. Direct electrical current will be used to heat the test section. Test section surface temperature will be measured by combination of thermocouples and surface mounted RTD's placed approximately 2 inches apart. A temperature measurement close to the exit of the heated section is used as a switch to shut the power off in case of overheating. The flange

for the heated and adiabatic sections will be bolted together but insulating rings will be used for thermal and electrical isolation. An immersion thermocouple and an absolute pressure transducer will be used through the flange to measure the fluid temperature and pressure.

The adiabatic section is intended to provide pressure drop measurement in a section of the tube where the quality is known and conditions do not change. Since the fluid conditions vary along the length of the heated section, measured pressure drop will have limited use due to approximations for fluid conditions. Originally, a clear section was planned to be used for possible flow visualization. However, after evaluating the disadvantages of this approach it was decided to use an insulated stainless steel section with a small clear section at the exit. The reasons for this arrangement were:

1. The emphasis of the present study was not on flow regime identification

2. In order to have a clear observation of the flow regimes, the diameter of the visualization section should be at least 0.5 inch. This would mean that a considerably longer section is needed (L/D > 100) to allow for an established flow following the diameter change and to have a measurable pressure drop.

3. Insulating a clear section is more difficult than the stainless steel section. An evacuated PVC jacket can be used to minimize heat losses and to protect the visualization section.

The clear section at the exit of the adiabatic test section will provide qualitative information on the flow regime.

Differential pressure transducers will be used to measure the pressure drop at three locations along the adiabatic section. The pressure sensing lines will be liquid filled and purge systems will be used to assure gas ingress will not occur during pressure fluctuations.

Pump

An oversized magnetically coupled gear pump will be used to provide a wide range of head-flow variations. Magnetically coupled pumps eliminate the

seals and therefore possibility of leakage. A large diameter bypass line ($D \geq 5/8$ inch) will be used for flow control. A second bypass line with a pressure relief valve is provided for overpressure protection. A dry guard switch upstream of the pump will shut the power off in case no fluid reaches upstream piping. A variety of gear pumps for use with chemicals and corrosive environments are available.

Accumulator

Although gear pumps do not cause any pulsation in the lines, an accumulator will be used to supply the fluid for the entire life of the loop and dampen any pressure surges. If the modular loop is used to test a centrifugal pump, the accumulator will dampen pump pulsations. A bladder type accumulator with a fluid volume of nearly two times the entire volume of the loop will be used. The accumulator can store the entire fluid volume if the experimental set-up is used in a flight test which requires a dry loop during launch.

Condenser

For the condensation process of a wetting fluid, annular or wavy annular flows are the most desirable regimes of operation. Slug flow will result in instabilities for a closed system and bubbly flow would mean a low vapor flow rate and inefficient process. In earth gravity condition, the slug flow can be eliminated by increasing the vapor flow rate. For reduced gravity conditions stable flow operation can be achieved by using curved passages to provide additional body force or by using tubular strips to cause a swirling of the flow. Another recommended method is to use a tapered line which would maintain vapor shear on the condensate film and suppress the liquid wave growth.

A shear flow tube-in-tube condenser will be used in the modular design. Water will be used on the secondary side and the condenser will be instrumented as shown to provide basic data on condenser performance. It should be noted that, the measurements are not intended to provide data on condensation heat transfer.

The test loop can be used to evaluate a particular condenser design by interchanging the condensers. The power to the boiler (test section) can be varied to provide a range of qualities at the condenser inlet. Measurement of the fluid conditions at the entrance and exit of the condenser primary and secondary sides will provide the necessary information for evaluating the condenser performance.

Instrumentation

Pressure:

A total of nine absolute and three differential pressures will be measured in the proposed test loop. Among the absolute pressures, the readings from downstream of the pump and downstream of the adiabatic section will be used by the control system to stop the system operation when overpressure is detected. This will be accomplished by shutting the power to the test section heater and the pump.

Temperature:

As mentioned earlier, test section wall temperature will be measured by a combination of thermocouples and RTD's placed 2 inches apart. RRD's provide fast response and accurate temperature measurement without the need for reference junction compensation. Thin film RTD elements of 1 to 2 mm in size have a temperature rating of -50 to 600°C and can be cemented to the outside wall of the test section. Although, these types of RTD's can withstand vibration and shock, thermocouples are more rugged and a combination of the two methods will provide a reliable method for wall temperature measurement. A thermocouple measurement closest to the exit of the heated section will be used by the control system to stop the operation when accidental overheating is detected.

As shown in Figure 4-2, a total of ten fluid temperatures will be measured in the loop. Thermocouples inserted through the tube wall will be used for fluid temperature measurement. Since a narrow range of temperature variation is expected, thermisters can also be employed. However, due to

the fragile nature of thermisters, they should only be used as redundant measurement when a fast and stable response is needed.

Flow Rate:

Two turbine meters will be used for measurement of flow rate downstream of the pump and in the test section leg of the test loop. Water flow rate in the secondary side of the condenser will also be measured by a turbine flow meter. The turbine meters require at least 10 diameters of undisturbed line upstream and 5 diameters downstream of the measurement point.

Phase Content:

Flow quality at the exit of the heated section can be calculated from the known flow rate and the heat input. Due to mixing of the cold liquid from the main line, the fluid conditions at the entrance to the condenser can only be estimated. Knowledge of the mean phase content (quality) is essential for evaluating the performance of the condenser. Generally, the response of all the metering devices for a two-phase flow will depend on the mass flow rate and quality. Therefore, if the mass flow rate is known, the quality can be determined from the response of the metering system. When both parameters are unknown, the general practice has been to use void fraction measurement (by means of gamma densitometer or X-ray absorption) coupled with some flow dependent measurement.

In the present set-up, flow rate at the entrance to the condenser is known and there is no need to use a two-phase flow measurement device. A full flow drag disk will be used to calibrate for quality. Drag disks measure the force on a screen placed normal to the flow. The response of this instrument depends on the flow rate and quality. This technique has been successfully used to measure quality. So called "quality meters" are commercially available which include a combination of two-phase density and flow rate measurement. Density measurement is based on the dielectric properties of the fluid. This equipment is very expensive and has resulted in unsatisfactory results.

Void fraction measurement at the exit of the adiabatic section would have been valuable for two-phase void-quality analysis. Rotating field impedance probe and direct radioactive absorption techniques were evaluated. None of these techniques were found satisfactory for the present experiment. Since knowledge of void fraction is not needed for the major parameters under study, void fraction measurement was not incorporated in the test bed design.

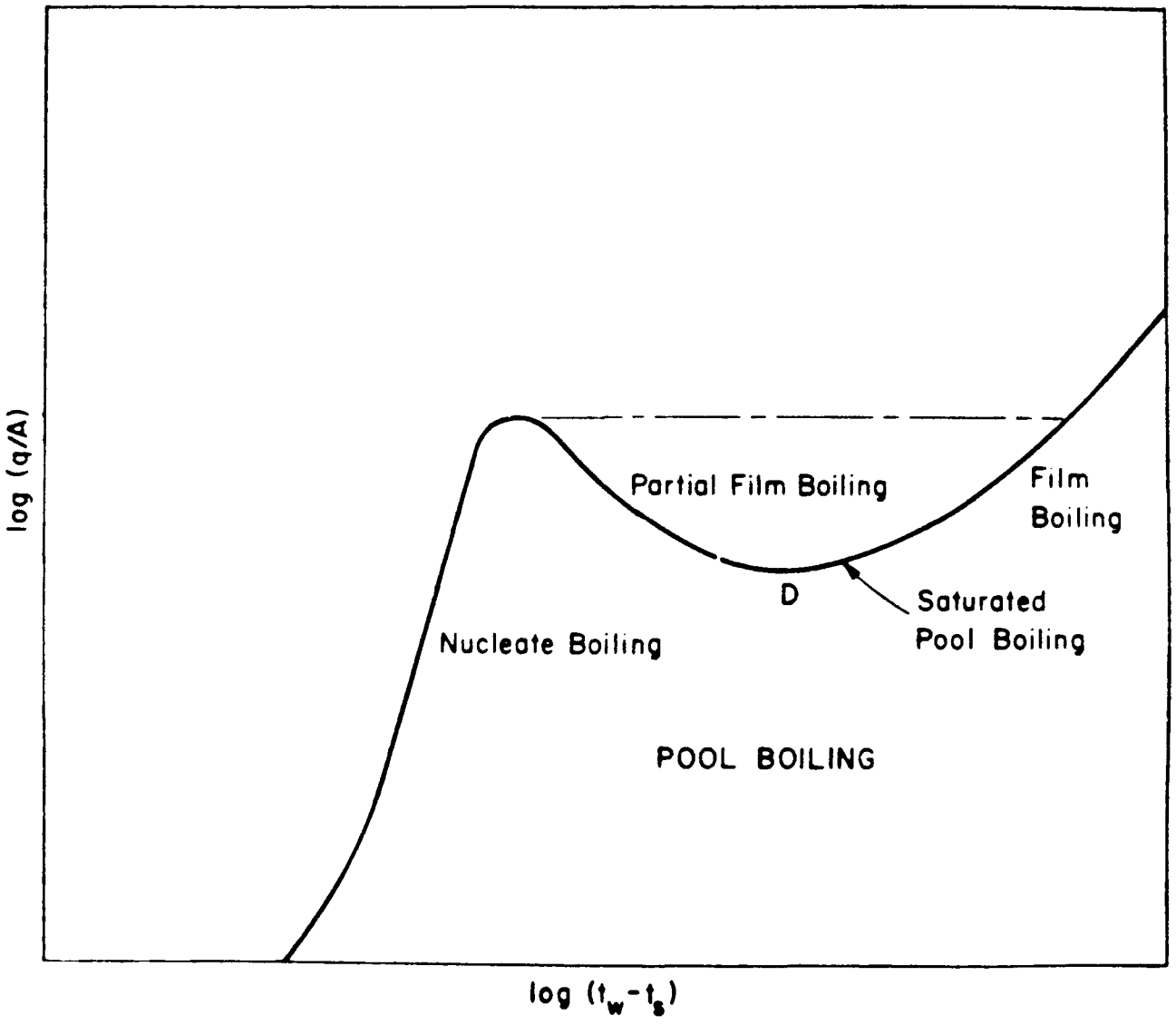

Figure 4.1 : REGIMES IN BOILING HEAT TRANSFER

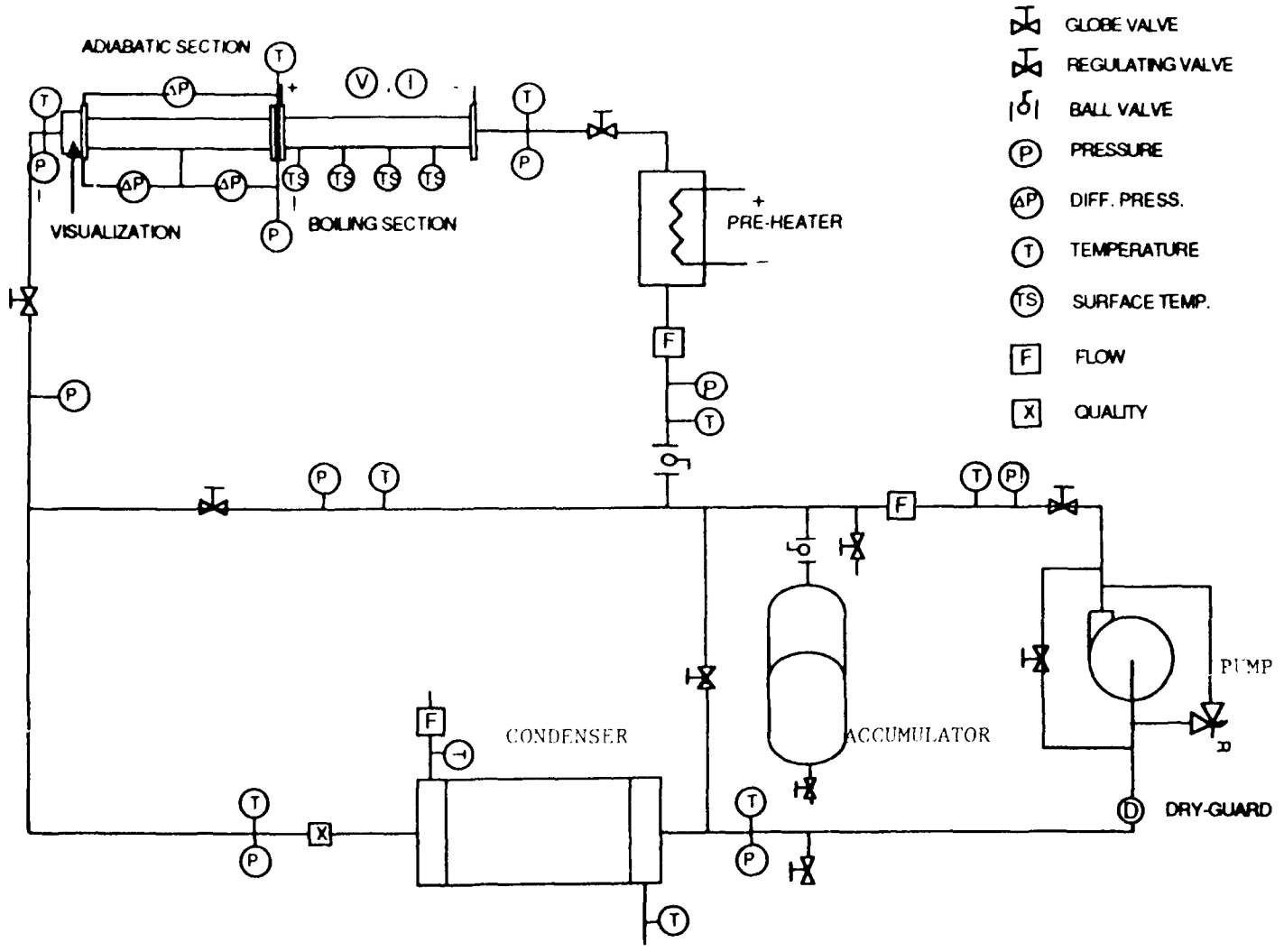

Figure 4.2 - Schematic of the Modular Two-Phase Loop

Section 5

BASELINE DESIGN

As mentioned earlier, the preliminary and final design of the system should be performed considering the host environment. This would dictate the power and size limitations as well as the accommodation requirements. A baseline configuration is designed here to perform the experiments defined above at earth gravity and aboard an airplane in Keplerian trajectory. In addition to providing the two-phase flow data for reduced gravity conditions, the baseline design will provide a proof of concept for the modular system. In this section, preliminary design including fluid selection, design analysis, and specification of the test matrix are covered. The schematic for the baseline configuration is the same as the modular system, Figure 4-2. However, a first attempt at selection of components and instrumentation is made. The heated section will be 2 foot long which is sufficient to avoid overheating when Departure from Nucleate Boiling occurs. The adiabatic section will also be 2 foot long to provide a measurable pressure drop. Exact components and complete layout of the test bed will be specified in the final design process.

5.1 Test Procedure

The major test parameters in the present study are the critical heat flux and onset of hydrodynamic instability. Therefore, the test procedure is developed to generate data for these parameters.

A great deal of information on the limit of stable two-phase flow operation at reduced gravities can be obtained by performing experiments at earth gravity. This is due to the fact that a limit rather than the exact quantitative phenomenon is desired. Tests with vertical up (+1 g) and vertical downflow (-1 g) will provide data for the effect of gravity on the onset of stability and an envelope of conditions around 0 g. Airplane trajectory testing will provide true low and high gravity conditions and confirm the conclusions of earth gravity tests.

As mentioned earlier, testing with a centrifuge to provide high g conditions was initially considered. However, due to the size limitations, adapting the set-up to centrifuge testing would be quite complex. The reason is that the available centrifuge systems do not have a large enough volume to fit the entire test set-up. The loop should be modified to have a smaller heated section which is connected to the rest of the system with flexible tubing. Another alternative is to build a large centrifuge, which is not feasible for the present program. It was therefore decided to generate the high acceleration data during the airplane trajectory tests which can provide up to 20 seconds of 2 to 4 g conditions. Due to short duration and varying gravity levels, only qualitative high g information is expected from this procedure.

Two sets of tests are planned in this program. In the first series of tests the effect of gravity on pressure drop-flow characteristics of a boiling section will be determined. For a given heat flux, tests start with a flow rate high enough that no nucleation takes place within the heated section and single-phase liquid flow exists within the entire section. Method of determination of this flow is covered in the design analysis.

Tests start by pumping the liquid through the loop at the desired flow rate. With no heat input to the test section, the preheater is adjusted to develop the required inlet subcooling. The power to the test section is then set and the test section exit pressure is adjusted. Data point is recorded after the steady state is reached.

The flow rate is then reduced gradually and a data point is recorded for every flow rate. The objective is to develop the system pressure drop-flow rate curve, but heat transfer as well as adiabatic section pressure drop data is also obtained for every flow rate. As the flow rate is reduced, pressure drop decreases until a flow rate is reached when further decrease results in an increase in pressure drop (negative slope).

A second series of tests are performed to determine the effect of gravity on the critical heat flux. For a given flow rate the power to the test

section will be gradually increased until a sudden surge in temperature occurs. These tests will be carried out by throttling the flow at the test section inlet in order to stabilize the system and avoid hydrodynamic instability induced burnout. In order to reduce the critical heat flux and the maximum wall temperature, the tests will be performed with saturated liquid at the inlet. The data acquisition system will be scanning the wall temperature measurements and voltage/current setting of the heated tube. The power will be automatically shut off when a sudden rise in temperature is sensed. For several heat inputs, pressure drop and heat transfer data will be recorded at steady state condition.

5.2 Fluid Selection

For a boiling system, the heat balance on a fixed control volume with liquid entering and two-phase mixture with quality x leaving is given by

$$\dot{q} = \dot{W} \Delta h_{in} + \dot{W} x h_{LG} \tag{5.1}$$

where Δh_{in} is the inlet subcooling and $\dot{q}$ is the heat input rate to the control volume. For a given total mass flow rate, $\dot{W}$, and quality x, the vapor and liquid superficial velocities are given by

$$J_L = \frac{W (1 - x)}{A \rho_L} \tag{5.2}$$

$$J_G = \frac{\dot{W} x}{A \rho_G} \tag{5.3}$$

where J is the superficial velocity and A is the cross-sectional area.

The type of fluid is dependent on the particular requirements of the system or experiment. For example, to remove a fixed amount of heat from a boiling system, a fluid with a larger heat of vaporization is preferred since it will require a smaller flow and pumping power. On the other hand, if an

experiment is to be performed where a range of superficial velocities should be simulated with a given power, a fluid with smaller heat of vaporization results in a wider range of J_G and J_L. The following criteria were considered in the selection of the fluid to be used in the baseline design:

1. Since the boiling section will pass the critical heat flux and may experience film boiling conditions, the working fluid should be a refrigerant to avoid overheating and possible melt down of the test section.

2. The operating conditions are selected so that the fluid temperature in most of the system is close to the highest expected ambient temperature. A fluid inlet temperature of 90°F and boiling section operating temperature of 100°F are selected for all the experiments. This would reduce the amount of heat loss to the environment and eliminate the need for extensive insulation of the system. Under most conditions, the system will be losing heat to the outside environment and a minimal amount of heat added from the pre-heater will be necessary to adjust the inlet temperature to 90°F at inlet. The refrigerant operating pressure at this temperature is a criterion in selection of the fluid. The properties of several refrigerants at 100°F are given in Table 5-1.

   Design of the system for operation under pressures close to ambient pressure is less complicated than pressures considerably different. Therefore, for 100°F operating pressure, R-11, R-12, and R-114 are preferred.

3. For the instability tests the flow rate will be gradually decreased and a wider range of flow variation would mean a better controlled system. For a given range of void fraction variation, a fluid with a larger ρ_L/ρ_G would require a wider range of flow variation.

4. The tests for the onset of instability should start with a flow rate large enough that Net Vapor Generation (NVG) does not occur within the length of the heated section. For given heat input, a fluid with a smaller Cp would require a higher flow rate for the NVG to occur at the exit. This would mean that a larger flow variation should be covered.

5. The fluid should be selected to provide a measurable pressure drop in the adiabatic section.

For different combinations of flow rates and input powers, the superficial velocities and equilibrium quality at the exit of a one foot long heated

section were determined for R-11, R-12, and R114. In addition, homogeneous equilibrium void fraction corresponding to the equilibrium quality was calculated. Possible two-phase flow regimes at reduced gravities were also obtained from Sunstrand flow regime map, Figure 5.1. It should be noted that, based on Dukler's model (6), bubble to slug transition does not depend on the fluid properties while slug to annular flow transition depends on ρ_L/ρ_G. For the present test conditions, slug to annular transition is expected to occur within the range shown in Figure 5.1. Tables 5-2 to 5-4 show these parameters for the three refrigerants under consideration.

5.2.1 Net Vapor Generation Point

Subcooled void generation along the length of a heated channel is qualitatively shown in Figure 5.2. As the wall temperature increases along the length of the heated section, a point is reached where the liquid temperature close to the wall is high enough to permit nucleation. However, this bubble layer cannot grow significantly due to high subcooling in the liquid. Further downstream, a point is reached where rapid increase in void fraction is initiated while the liquid temperature is still below the corresponding saturation temperature (Net Vapor Generation). As shown in Figure 5.2, a significant amount of void can be generated between NVG and the point where liquid reaches saturation. This void generation will have a considerable effect on pressure drop and two-phase instability.

As mentioned earlier, the tests for determining onset of instability should start with a flow rate high enough that single-phase flow exists through the entire heated section. For a given heat flux, this will be achieved by providing a flow rate larger than required to have NVG at the exit of the heated section.

Several empirical models for the onset of net vapor generation have been developed for earth gravity conditions. Among them, the model developed by Saha-Zuber (30) has used data from different fluids including Freon 22 and Freon 114. It is believed that the gravity level will have a small effect

on NVG and the Saha-Zuber model can be used to predict the point of significant voiding. In this model the liquid enthalpy at NVG is given by the following relations

$$(h_L)_{NVG} = (h_L)_{sat} - \frac{154\ \dot{q}''}{G} \qquad \text{for Pe} > 70{,}000$$

$$(h_L)_{NVG} = (h_L)_{sat} - 0.0022\ \frac{\dot{q}''\ D C_L}{K_L} \qquad \text{for Pe} < 70{,}000 \tag{5.4}$$

Where $\dot{q}''$ is the wall heat flux and G is the mass flux. Peclet number, Pe, is defined as

$$\text{Pe} = \frac{G\ D\ C_{PL}}{K_L} \tag{5.5}$$

For 500 and 1000 Watts heat input, the flow rates at which the NVG point would occur at the exit of a one foot long heated section were determined. Calculations were performed for R-11, R-12, and R-114 at 100°F and an inlet subcooling of 10°F. The following table shows that R-11 would result in the largest mass flow rate requirement.

T=100°F, ΔTin=10°F

Heat Input (Watts)	R-11	R-12	R-114
500.	0.400	0.356	0.495
1000.	0.799	0.712	0.686

Under most conditions, a fluid which will require the least pumping power is desirable. However, for the experiments designed here, a fluid which

would have a larger flow requirement for a given power is preferred. Since the flow will be gradually reduced, a better flow control can be achieved if the fluid results in a wider range of flow variation.

In order to determine the pumping power requirements, the two-phase pressure drop for a different range of parameters was evaluated in design analysis. For equivalent conditions, R-11 resulted in the largest pressure drop. Figure 5.3 shows a comparison of two-phase pressure drops for R-11 and R-114 in a one foot long section at a gravity level of 0.01 g. For the purpose of this experiment a larger pressure drop is preferred since it would result in measurable values for a given length of test section.

R-11 is selected as the working fluid due to the higher flow at NVG, wider flow range which also provides more points for a given flow regime, the larger pressure losses, and the operating pressure which is closer to the ambient pressure.

5.3 Test Matrix

The experimental program with the baseline design will consist of a series of tests at earth gravity with vertical up and downflow configurations and a set of airplane trajectory tests with a horizontal test section but different orientations. With each configuration, the tests will include evaluation of the onset of instability and critical heat flux. All the tests will be performed with a test section outlet pressure of 23 psi. The inlet temperature for the instability tests will be 90°F (10°F subcooling) while critical heat flux tests will be performed with saturated liquid at the inlet. The test matrix for instability experiments at earth gravity is shown in Table 5-5.

The critical heat flux tests will be carried out at two flow rates. The heat input to the test section will be gradually increased until a surge in wall temperature is observed. At several heat input settings, the system will be brought to steady state to generate heat transfer and pressure drop data. One of the most important design issues for a critical heat flux experiment is burnout or physical failure of the wall material. The test

section, working fluid, and test matrix should be selected to avoid overheating of the heated section. As will be discussed in the design analysis section, the critical heat flux increases with increasing flow rate and inlet subcooling. Therefore, saturated inlet conditions with the lowest set of flow rates will be used for CHF analysis.

The test matrix for the power settings of the steady-state conditions is shown in Table 5-6.

The test matrix for the airplane trajectory experiments to determine the onset of instability is shown in Table 5-7. These tests will be carried out with the flow in the direction and opposite to the direction of acceleration.

The critical heat flux tests will be carried out at the same flow rates as the earth gravity tests, 0.01 and 0.02 lbm/s. However, no steady state tests will be performed and only the critical heat flux will be recorded.

5.4 Design Analysis

Detailed design analysis was performed to evaluate the thermal performance and pressure drop characteristics of the components within the system. These calculations dictate the limits of the test parameters and were used to specify the power input and size of the condenser and heated section.

Test Section Thermal Performance

Two-phase convective boiling heat transfer coefficient depends on fluid properties, flow rate, quality, and wall temperature. Experimental efforts have shown that the nucleate pool boiling heat transfer coefficient is not affected by the gravity level. The reason is that the mechanism of heat transfer is not sensitive to gravity. Under equal conditions, the forced convective boiling heat transfer coefficient should be the same regardless of the gravity level. However, definition of equal conditions is not trivial. Equal mass flow rate and heat input combination will not result in equal conditions. The reason is that for a given quality, void

distribution is expected to be different at varying gravities. Therefore, applicability of the earth gravity heat transfer coefficients without any modifications is questionable. In addition, there is practically no reduced gravity convective boiling heat transfer data presently available.

Considering the above arguments, the test section should be designed using the earth gravity heat transfer correlations and be able to perform under anticipated worst case zero g conditions.

Since the test loop has no compressible volume upstream of the heated section, oscillatory instability is not expected to occur during the planned tests. Even if oscillations occur, the amplitude will not be so large as to cause Departure form Nucleate Boiling (DNB). However, the test section should be designed to handle such conditions. The maximum wall temperature will be calculated for nucleate boiling operation, DNB during instability testing, and DNB during the critical heat flux testing.

Nucleate Boiling Operation:

The heated section is expected to be under nucleate boiling mode of heat transfer during most conditions except when critical heat flux is reached. It is possible, although unlikely, that oscillations with large enough amplitude occur such that instability induced burnout results.

The most successful convective boiling heat transfer correlation, Ref. (31), consists of a single-phase and a two-phase heat transfer component.

$$h = h_{NB} + h_{SP} \tag{5.6}$$

The Dittus-Boelter (32) correlation modified by a Reynolds number factor, F, is used for the single-phase component

$$h_{SP} = 0.023\ F\ \left(\frac{K_L}{D}\right)\ Re^{0.8}\ Pr^{0.4}$$

$$Re = \frac{G\ (1-x)\ D}{\mu_L} \tag{5.7}$$

where K is the thermal conductivity, μ the viscosity, Pr the Prandtl number, and Re the Reynolds number. The Forster and Zuber correlation, Ref. (33), modified with a boiling suppression factor, S, is used for the boiling component of the heat transfer coefficient.

$$h_{NB} = 0.00122 \left[\frac{K_L^{0.79} C_{PL}^{0.45} \rho_L^{0.49} g_0^{0.25}}{\sigma^{0.5} \mu_L^{0.29} h_{LG}^{0.24} \rho_L^{0.24}} \right] (T_W-T)^{0.24} (P_W-P)^{0.75} \quad (5.8)$$

P_W is the saturation pressure corresponding to T_W, σ is the surface tension, and C_p is the specific heat. The factors F and S were empirically determined and are graphically presented as Figure 5.4.

The heat transfer coefficients and wall temperature for the test conditions given in Tables 5-6 to 5-8 were evaluated. For a constant wall heat flux, the heat transfer coefficient from Chen's correlation is a weak function of the mass flux. For the wall heat input of 500 Watts, the heat transfer coefficients and wall temperature for two limiting mass fluxes are given below.

W (Lbm/s)	X	hc	h_{NB} (BTU/hr/ft^2/F)	h_{TP}	T_W °F
0.02	0.287	63.6	392.5	677.7	119.2
0.20	0.003	524.5	399.9	734.2	117.8

Post CHF Heat Transfer:

Since Departure from Nucleate Boiling may occur during the experiments planned for the test loop, the heated section should be able to handle the low heat transfer coefficients typical of the post CHF regimes. These modes of heat transfer include inverted annular and dispersed flow film boiling regimes. Inverted annular film boiling will exist for low flow and low void

fraction and dispersed flow film boiling exists for high flow rate and/or high void conditions.

Inverted annular flow regime is the small region above the CHF point and usually occurs when a hot wall (in liquid deficient regime) is flooded with liquid. Calculation of the exact heat transfer in this regime is quite difficult since it requires the precise knowledge of the local flow and fluid conditions. Generally pool boiling relations are used to conservatively predict the heat transfer. These relations are based on flow of a smooth laminar film adjacent to the wall and have the following form.

$$h = K_1 \left[\frac{K_G^3 \rho_G (\rho_L - \rho_G) h_{LG} g}{\mu_G (T_W - T_{sat}) L} \right]^{1/4} \tag{5.9}$$

Where L is the characteristic dimension. The constant K_1 depends on the assumption made for the vapor-liquid interface velocity and two of the commonly use values are

$K_1 = 0.62$ [Bromley, Ref. (34)]
$K_1 = 0.714$ [Ellion, Ref. (35)]

Photographic studies of film boiling have shown a wavy interface with a wavelength close to the classical Taylor instability wavelength.

$$L_T = 2\pi \left[\frac{\sigma g_c}{g(\rho_L - \rho_G)} \right]^{1/2} \tag{5.10}$$

The most commonly used heat transfer coefficient for the inverted annular regime (modified Bromley, Ref. 36), uses the Bromley pool boiling heat transfer coefficient with Equation 5.10 for the characteristic length.

Dispersed flow film boiling regime is associated with higher flow rates (void fraction) and exists above the CHF point under most practical conditions. The most widely used heat transfer correlations for this regime

are based on the Dittus-Boelter single-phase correlation, Equation 5.7, and are modified for two-phase flow. Among them, Dougal-Rohsenow (37) has been shown to conservatively predict a wide range of data. This correlation is given by

$$h = 0.023 \frac{K_G}{D} \left(\frac{GDX}{\mu_G}\right)^{0.8} \left(\frac{C_{PG}\,\mu_G}{K_G}\right)^{0.4} \tag{5.11}$$

A qualitative comparison of predictions by modified Bromley and Dougal-Rohsenow correlations are shown in Figure 5.5. Generally, modified Bromley is applicable to low void fractions typical of inverted annular regimes and Dougal-Rohsenow to higher voids typical of dispersed flow film boiling regime. The cut-off void fraction is not known and one way to incorporate both regimes is to use a void averaged value of these models given by

$$h = (1 - \alpha)\, h_{MB} + \alpha\, h_{DR} \tag{5.12}$$

h_{MB} = Modified Bromley Heat Transfer Coefficient

H_{DR} = Dougal-Rohsenow Heat Transfer Coefficient

and shown in Figure 5.5.

A correlation for the pool boiling heat transfer coefficient which includes the effect of gravity has been proposed in Ref. (38). This correlation is based on the idea that boiling depends on the characteristic dimension of

$$D^* = D \left[\frac{g\,(\rho_L - \rho_G)}{\sigma}\right]^{1/2} \tag{5.13}$$

and that the reduced gravity conditions were simulated by using small diameter wires at 1 g. The resulting correlation for film boiling is similar to Bromley correlation and is given by

$$h = \frac{0.7}{D^{*1/3}} \left[\frac{v_G^3 \rho_G (\rho_L - \rho_G) h_{LG}^* g}{\mu_G (T_W - T_{sat}) D} \right] \quad (5.14)$$

$$h_{LG}^* = h_{LG} \left[1 + \frac{0.34 C_{PG} (T_W - T_{sat})}{h_{LG}} \right] \quad (5.15)$$

Since this model is based on pool boiling over wires, it results in unreasonable heat transfer coefficients for film boiling inside tubes. With an approach similar to modified Bromley, the Taylor instability wavelength can be used as the characteristic length in the above relation for the case of flow inside tubes.

As discussed earlier, post-CHF regime is expected to occur during the critical heat flux tests. However, maximum temperature based on post-CHF heat transfer mode was calculated for all the conditions in the test matrix.

For critical heat flux tests, where the quality and void fractions are high, Dougal-Rohsenow correlation is applicable. The predicted maximum temperatures at the exit of the heated section are listed in Table 5-8 which shows the highest calculated wall temperature to be 647°F. Similar to the nucleate boiling case, the heat transfer coefficient from the Dougal-Rohsenow correlation is a weak function of the mass flux.

For the instability tests, the maximum wall temperature was calculated from Dougal-Rohsenow for void fractions larger than 0.8 and modified Bromley for smaller void fractions. The maximum wall temperature is 871° F as shown in Table 5-9. It should be noted that the high wall temperatures are calculated due to the extremely conservative approacn used here. These values are obtained for low void fractions where departure from nucleate boiling is highly improbable.

For reduced gravity tests, the correlation of Ref. (38) with the Taylor instability wavelength as the characteristic length was used. The predicted maximum wall temperature was 734°F for a gravity level of 0.01 g.

Although the maximum wall temperature of 871°F is well below failure temperature for stainless steel, the design should allow for expansion of the test section to avoid buckling.

System Pressure Drop

Evaluation of the two-phase pressure drop is needed to determine the pumping requirements of the system. Two-phase pressure drop models were discussed in Section 3.2 and a comparison with limited reduced gravity data was presented. Based on the available data, it can be concluded that for the same system pressure and flow rate, two-phase pressure drop at reduced gravities can be significantly higher than earth gravity conditions. In addition, both frictional and acceleration pressure drops increase with quality which would mean that the highest losses will be obtained in the annular flow regime. Therefore, to estimate the largest two-phase head loss for pump design, an annular flow model under reduced gravity conditions should be used.

The triangular approach was used here to estimate the two-phase pressure drop for the range flow rates expected in the experimental program. The empirical fit obtained in Ref. (1), based on the Sunstrand experiments (7) was employed and a computer program was used to predict the pressure drops. The pressure drops across a one foot long 0.25 inch diameter tube with a flow rate of 0.02 lbm/s are shown in Figure 5.6. It can be seen that as the gravity level is reduced from 1 g to 0.01 g, the pressure drop increases significantly. Figure 5.7 shows the head loss across a foot long section at a gravity level of 0.01 g for three flow rates of 0.02, 0.1, and 0.2 lbm/s.

As shown in Tables 5-6 and 5-8, the highest quality at the exit of the heated section is less than 0.01 for the flow rate of 0.2 lbm/s and less than 0.04 for 0.1 lbm/s. Therefore, the highest expected pressure drop, from Figure 5.7, is approximately 4 psi per foot of tube. Considering a

maximum of 10 ft. length (including the adiabatic section and the lines to condenser) in two-phase flow, the maximum head loss would be 40 psi. As will be shown later, the pressure drop in the condenser is negligible compared to the overall two-phase loss and the pump should be selected to handle 40 psi of total head.

Condenser Thermal Performance

The condenser in the baseline design consists of a tube-in-tube shear flow condenser with two-phase fluid in the center and water as the secondary fluid flowing in the annulus.

In order to determine the condenser thermal performance, the overall heat transfer coefficient, U, should be determined.

$$\frac{1}{U} = \frac{1}{h_c} + \frac{\delta}{K_L} + \frac{1}{h_o} \tag{5.16}$$

h_c in the above equation is the condensation heat transfer coefficient, δ is the condensate film thickness, and h_o is the heat transfer coefficient to the secondary fluid. For low thermal conductivity liquids, the overall heat transfer coefficient is mainly controlled by the condensate film thickness.

In the present analysis a calculational method proposed in Ref. (39) is used to evaluate the condenser thermal performance and to determine the required length and pressure drop. A sightly different approach has been outlined in Ref. (40).

The local condensation heat transfer coefficient can be determined from the following relations.

$$h_c = Nu \frac{K_L}{D}$$

$$\frac{Nu\ F_2}{Pr_L\ Re_L} = F\ (X_{tt}) \qquad 0.1 < F\ (X_{tt}) < 1.0$$

$$\frac{Nu\ F_2}{Pr_L\ Re_L} = [F\ (X_{tt})]^{1.15} \qquad 1.0 < F\ (X_{tt}) < 20 \qquad (5.17)$$

$$F\ (X_{tt}) = 0.15\ [X_{tt}^{-1.0} + 2.85\ X_{tt}^{-0.476}]$$

$$F_2 = 0.707\ Pr_L\ Re_L^{0.5} \qquad Re < 50$$

$$F_2 = 5\ Pr_L + 5\ \ell n\ [1 + Pr_L\ (0.09636\ Re_L^{0.585} - 1] \qquad 50 < Re_L < 1125$$

$$F_2 = 5\ Pr_L + 5\ \ell n\ (1 + 5\ Pr_L) + 2.5\ \ell n\ (0.0031\ Re_L^{0.812}) \quad Re_L > 1125$$

where X_{tt} is the Martinelli parameter and Re_L is the Liquid Reynolds number

$$X_{tt} = \left(\frac{\mu_L}{\mu_G}\right)^{0.1} \left(\frac{1-x}{x}\right)^{0.9} \left(\frac{\rho_G}{\rho_L}\right)^{0.5} \qquad (5.18)$$

$$Re_L = \frac{(1-x)\ GD}{\mu_L} \qquad (5.19)$$

In order to calculate the condensate film thickness the overall pressure drop in the tube is calculated from

$$\frac{dP}{dZ} = \left(\frac{dP}{dZ}\right)_f + \left(\frac{dP}{dZ}\right)_m \qquad (5.20)$$

The Lockhart-Martinelli method is used to calculate the frictional pressure gradient

$$\left(\frac{dP}{dZ}\right)_f \frac{g_o D}{G^2/\rho_g} = -0.09 \left(\frac{GD}{\mu_G}\right)^{-0.2} \Big[x^{1.8} +$$

$$5.7 \left(\frac{\mu_L}{\mu_G}\right)^{0.0523} (1-x)^{0.47} \times 1.33 \left(\frac{\rho_G}{\rho_L}\right)^{0.261} + \qquad (5.21)$$

$$8.11 \left(\frac{\mu_L}{\mu_G}\right)^{0.105} (1-x)^{0.94} \times 0.86 \left(\frac{\rho_G}{\rho_L}\right)^{0.522} \Big]$$

The momentum pressure drop is evaluated by using the Zivi model for void-quality relation which results in

$$\left(\frac{dP}{dZ}\right)_m \frac{g_o D}{G^2/\rho_G} = -D \frac{dx}{dZ} \Big[2x + (1-2x) \left(\frac{\rho_G}{\rho_L}\right)^{1/3} + (1-2x) \left(\frac{\rho_G}{\rho_L}\right)^{2/3}$$

$$- 2 (1-x) \left(\frac{\rho_G}{\rho_L}\right) \Big] \qquad (5.22)$$

The film thickness can be related to the pressure drop by

$$\delta^2 = \frac{2 (1-x) G \mu_L}{\rho_L g_o \frac{dP}{dZ}} \qquad (5.23)$$

The heat transfer coefficient for the secondary side was calculated using the Dittus-Boelter heat transfer coefficient.

In order to determine the maximum length required to condense the two-phase mixture with different quality and flow rate combinations, a computer program was written using the above relations. The condenser is divided into ten sections, each with a quality change of 1/10 of entrance quality. The length and pressure drop in each section is determined by an iterative

approach. For every section, a condensate film thickness is assumed and equations 5.20 to 5.23 are used to iterate on the film thickness. The overall heat transfer coefficient is obtained from Equation 5.16 and the length required to provide the quality change in that section is calculated from

$$\Delta Z = \frac{G\, h_{LG}\, D\, \Delta x}{4U\,(T_{sat} - T_o)}$$

This program was used to evaluate different combinations of diameters and secondary side flow rates. Calculations were performed for the combinations of flow and quality expected in the test matrix (Tables 5-5 and 5-6) and with water entering the secondary side at 50°F.

Figure 5.8 shows the length of the condenser required to change the two-phase flow from the quality at inlet to quality of zero. Figure 5.9 shows the total pressure drop across that length of the condenser. For these calculations a diameter combination of 0.25 inch for inside and 0.50 inch for the outside annulus was used. The plots are shown for secondary side flow rates of 0.3 lbm/s and 0.5 lbm/s. Figures 5.10 and 5.11 show the length and pressure drop for two different diameter combinations with a secondary flow rate of 0.3 lbm/s. For a given flow rate and inlet quality, the smaller diameter combination (D_i=0.25 inch, D_o=0.5 inch) results in larger pressure drop but smaller condenser length requirement.

The condenser should be designed for the largest quality at the entrance (X=1.0). The main criterion is the condenser length since the largest pressure drop for the inlet quality of 1.0 is 0.66 psi which is small compared to the overall system head loss requirements. Therefore, the small diameter combination, D_i=0.25 inch and D_o=0.5 inch, is selected. The change in the secondary side flow rate from 0.5 to 0 3 lbm/s results in only a 3 inch increase in condenser length. Considering the pumping power requirement for the water, the lower flow rate will be used in the experiments.

The condenser length needed to subcool R-11 by 10°F was calculated to be less than 5 inch for the highest flow rate. Therefore a tube-in-tube condenser with following specifications will be more than sufficient for the purpose of this experiment.

D_i=0.25 inch

D_o=0.50 inch

L= 40. inch

Water inlet Temp.= 50°F

Water flow rate=0.3 lbm/s (2.15 GPM)

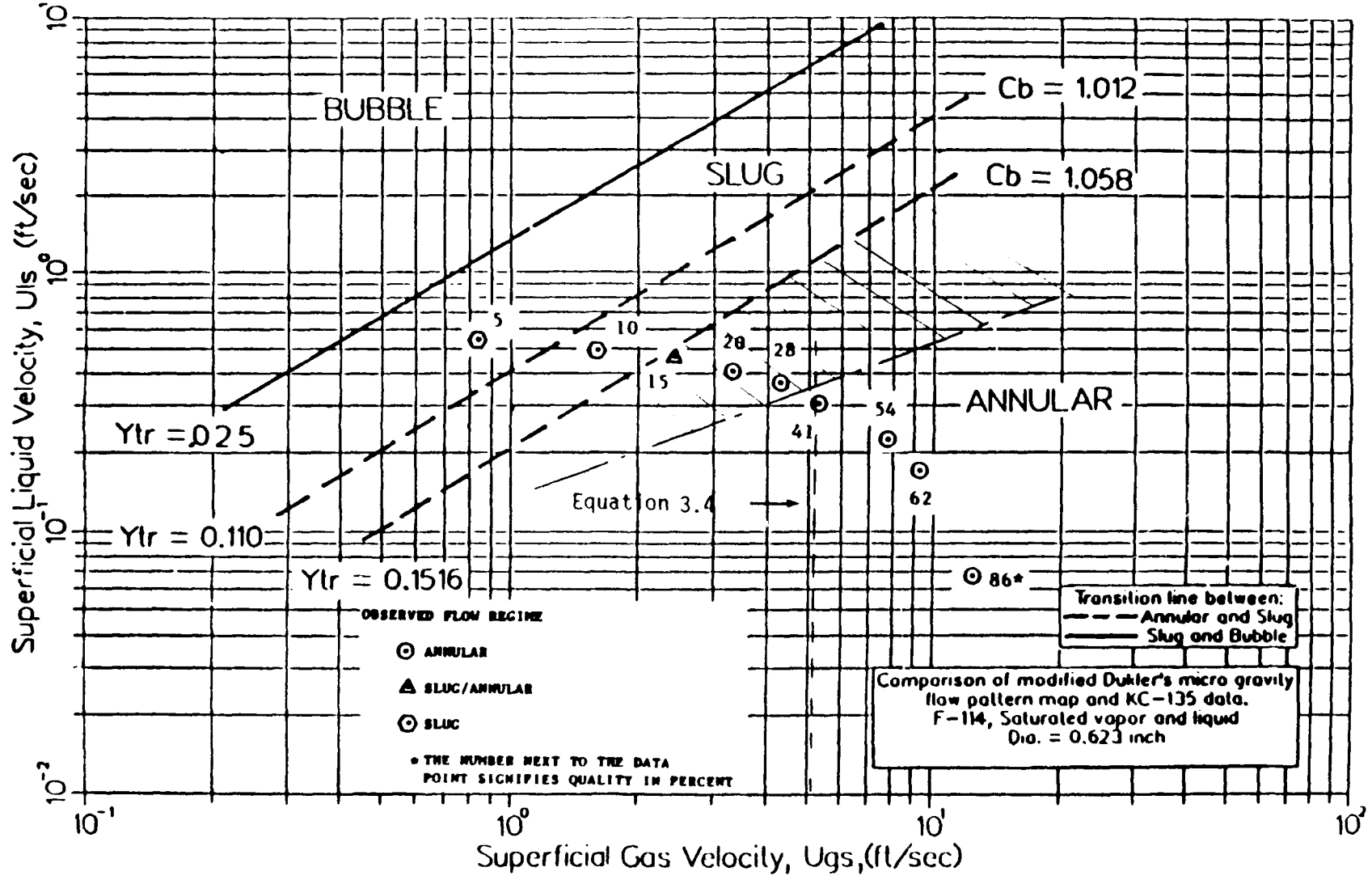

Figure 5.1 - Comparison of Flow Regime Map of Ref. (6) with Data of Ref. (7) Reproduced from Ref. (7)

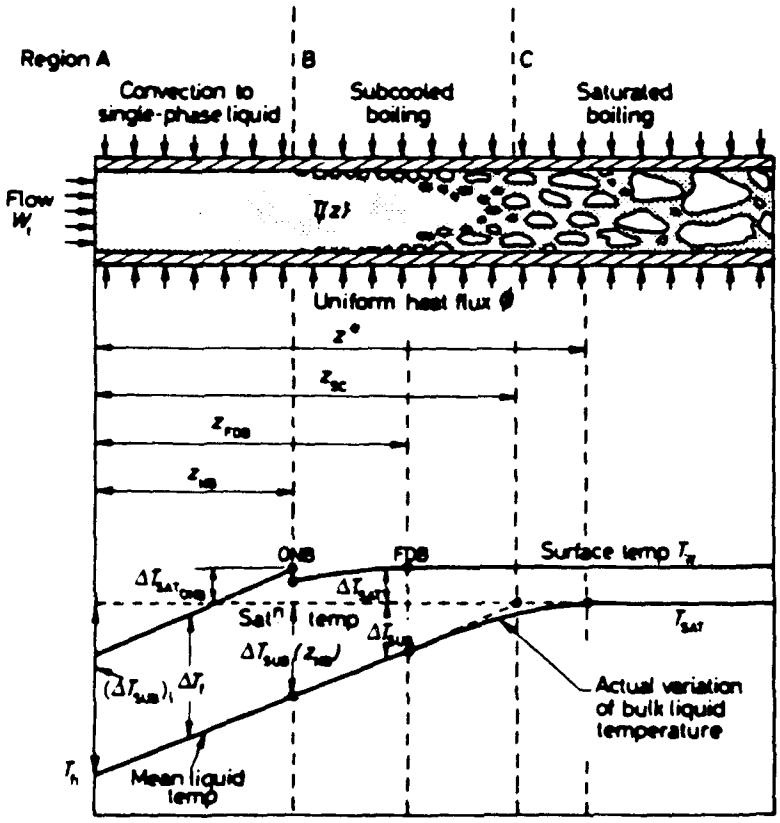

. Surface and Liquid Temperature Distributions in Subcooled Boiling

Figure 5.2

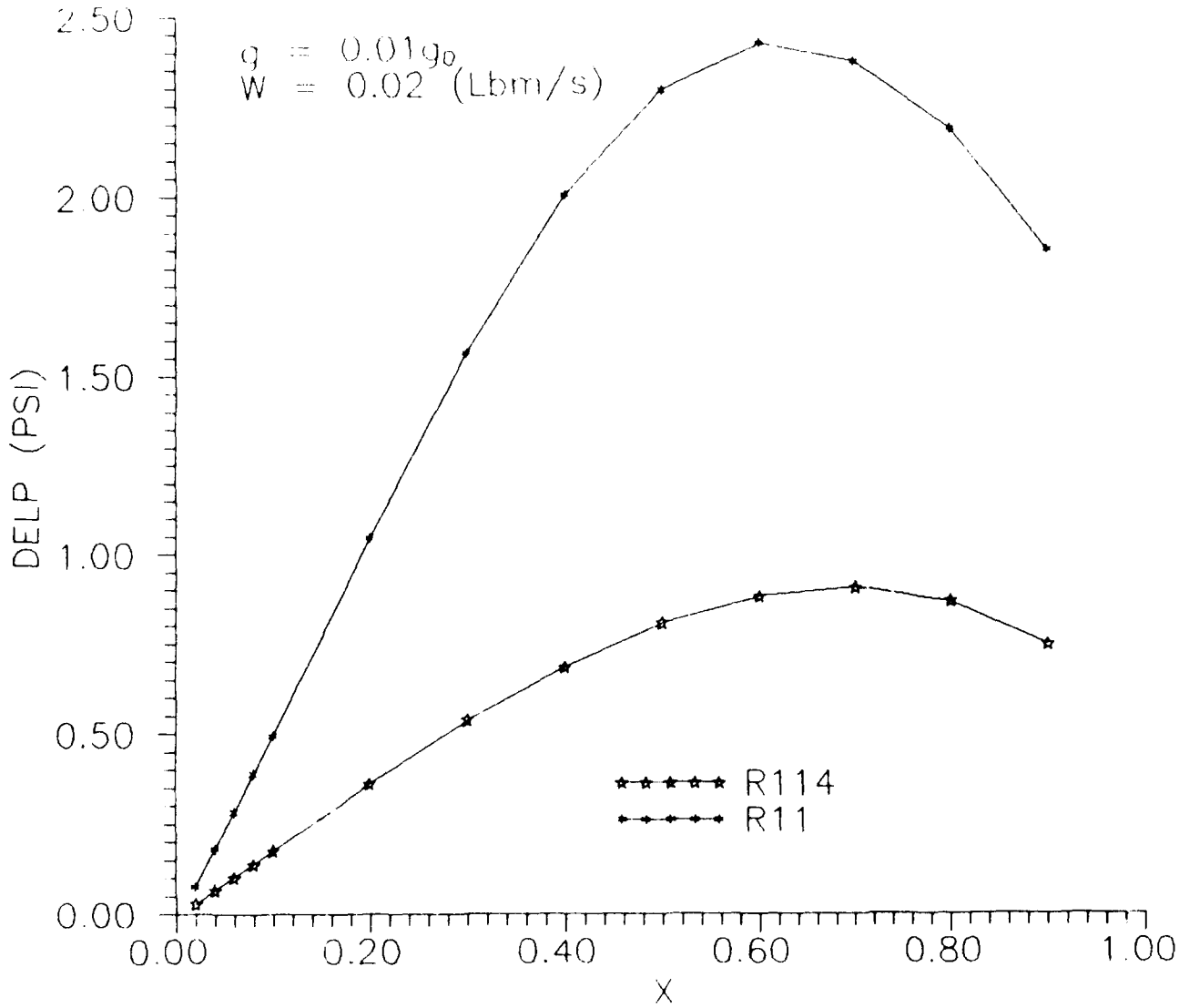

Figure 5.3 . Comparison of Two-Phase Pressure Drops for R-11 and R-114 (1 ft. Line)

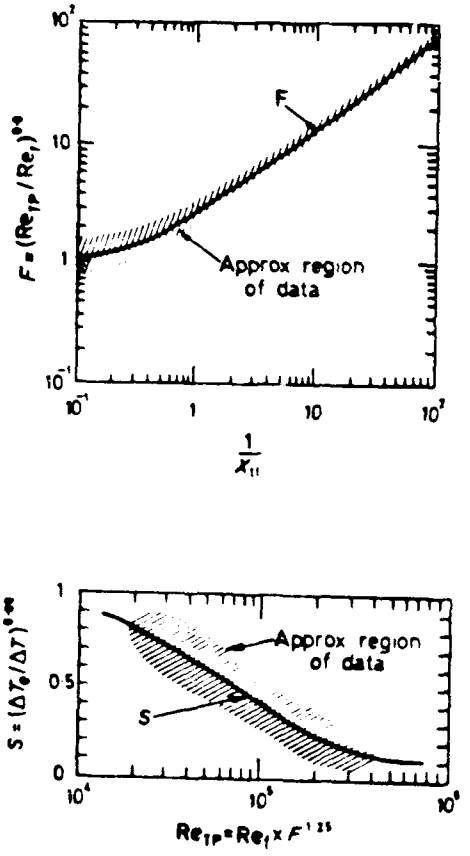

Figure 5.4 - Reynolds Number and Suppression Factors for Chen Heat Transfer Model.

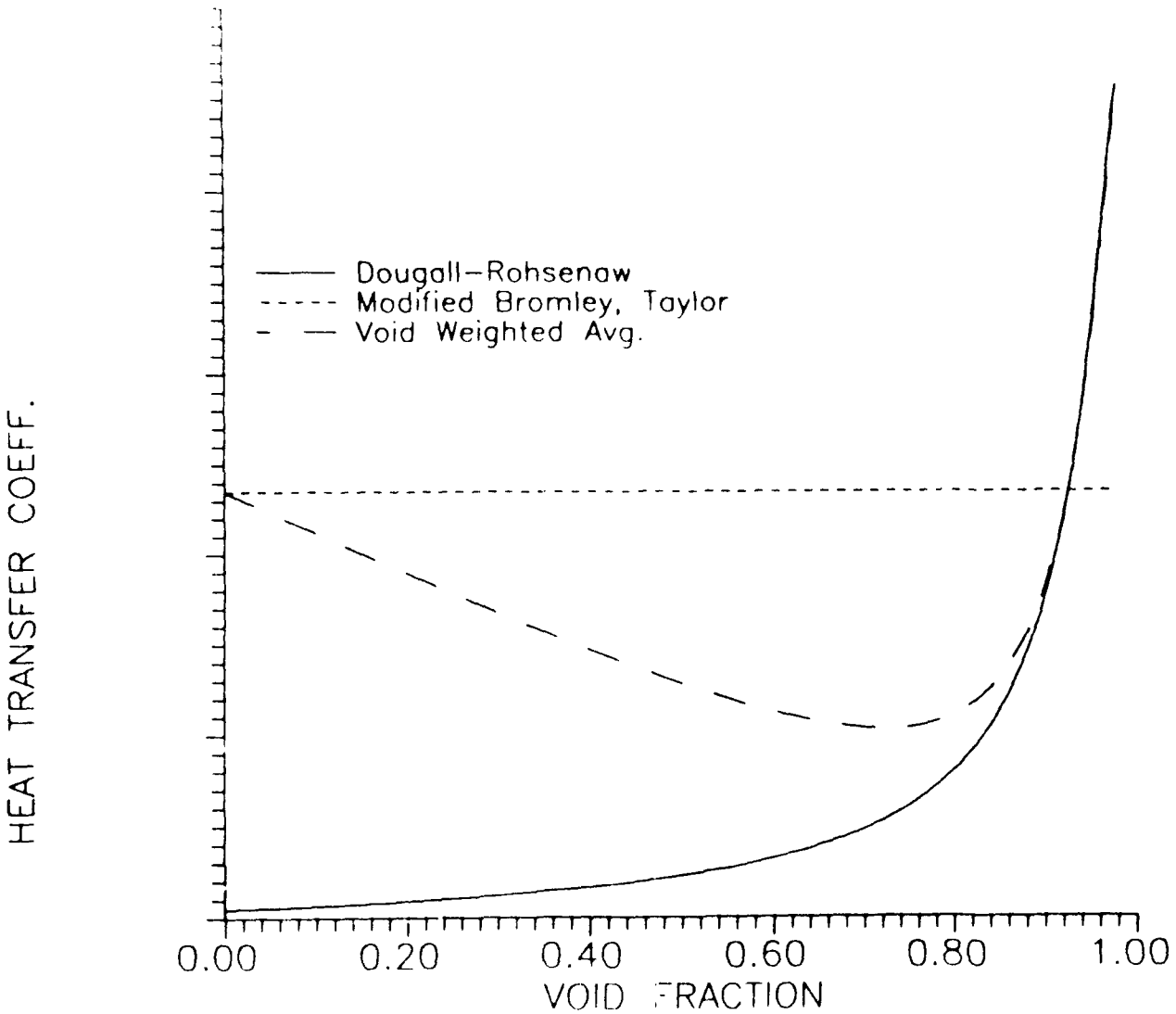

Figure 5.5 - Qualitative Presentation of Predictions by Dougal-Rohsenow, Modified Bromley, Void-Averaged Models.

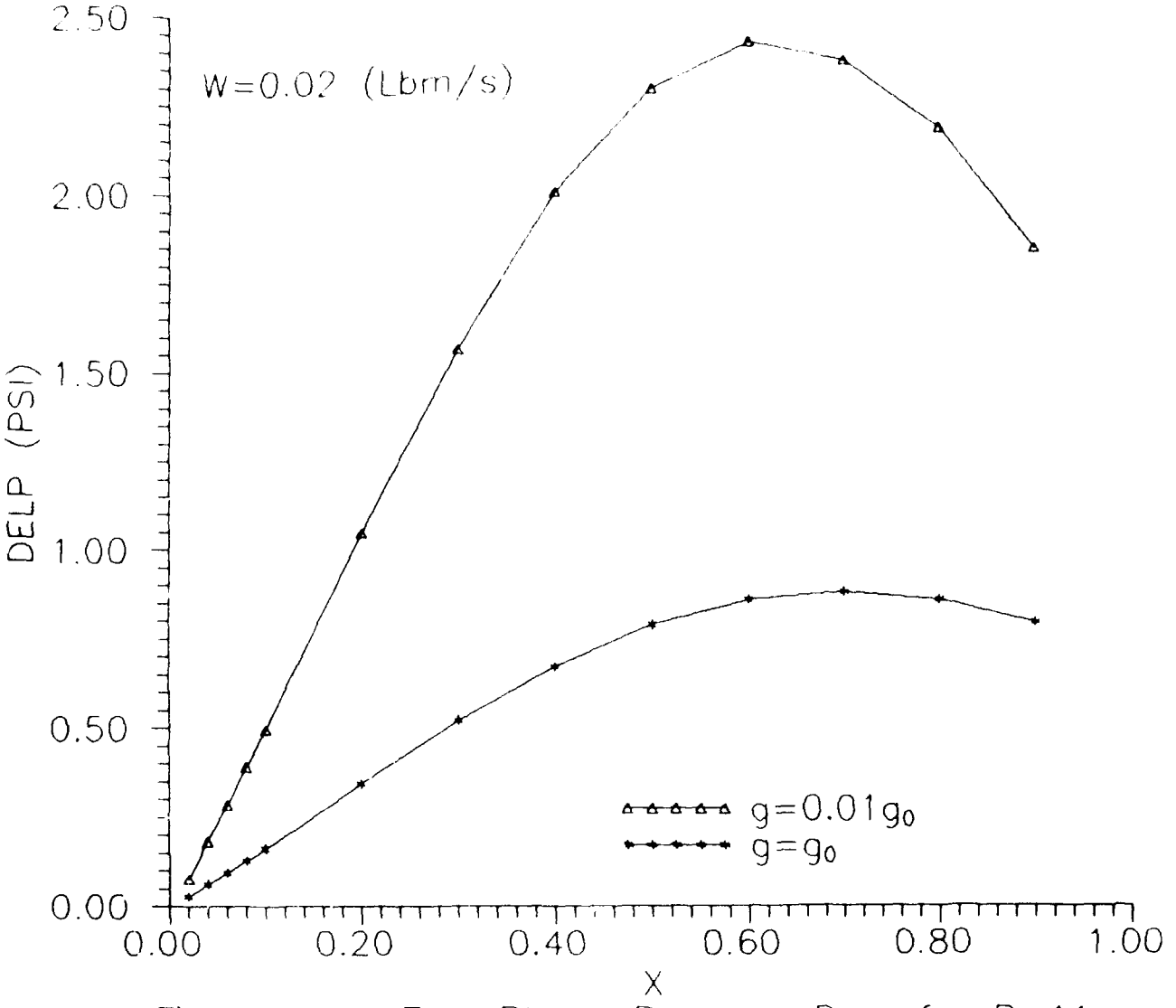

Figure 5.6 . Two-Phase Pressure Drop for R-11 (1 ft. Line)

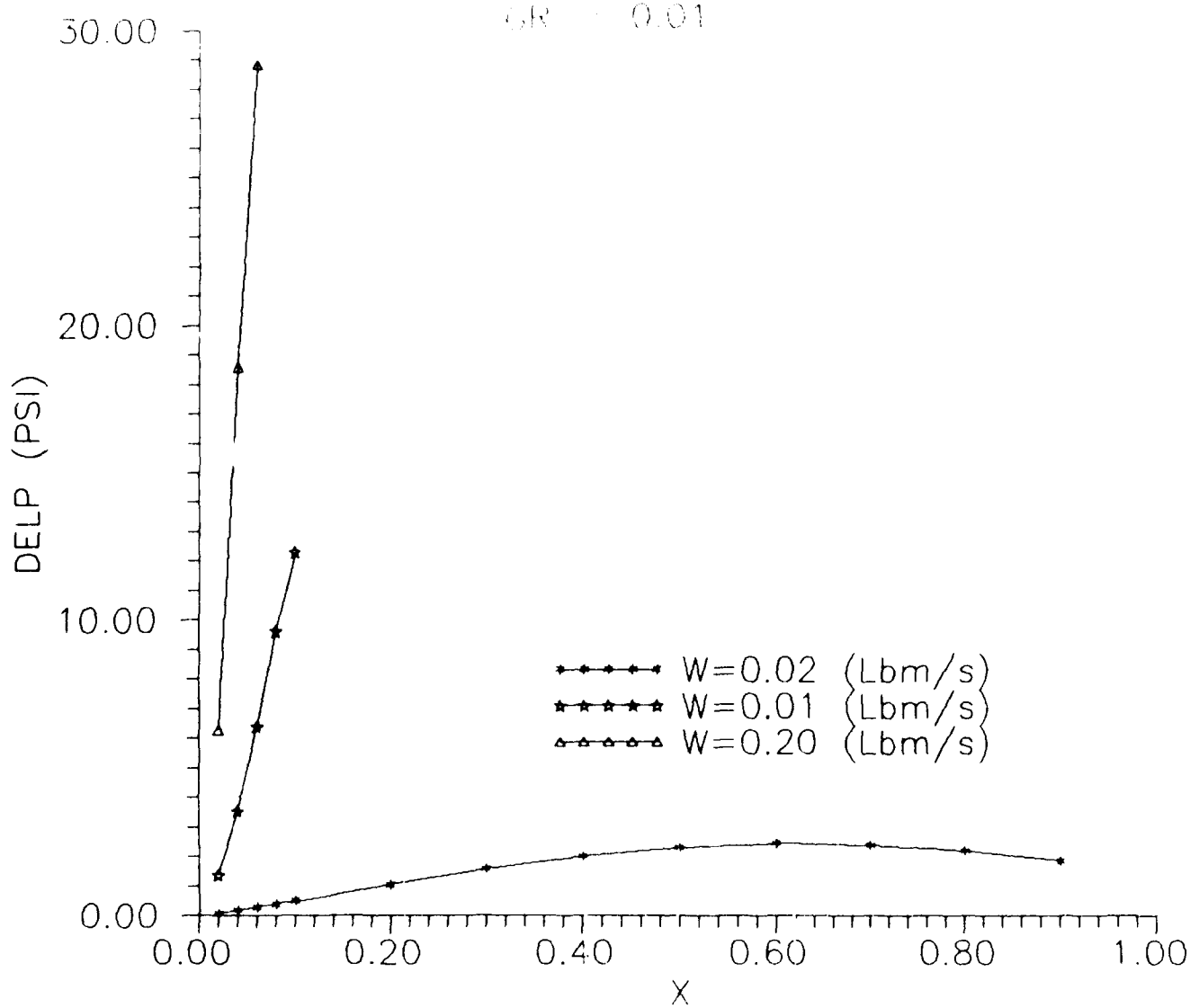

Figure 5.7 . Two-Phase Pressure Drop for R-11 (1 ft. Line)

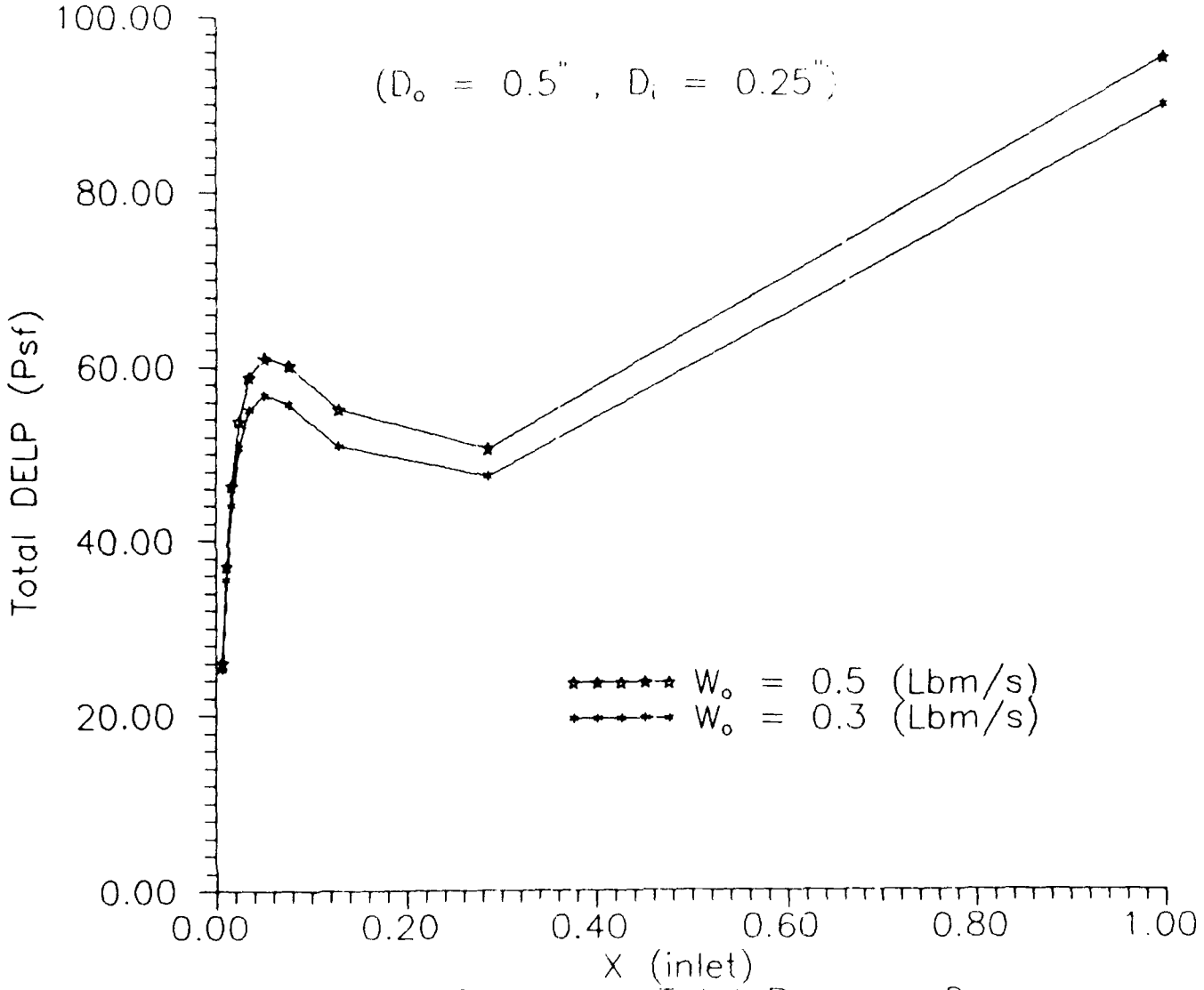

Figure 5.8 . Condenser Total Pressure Drop vs. Inlet Quality

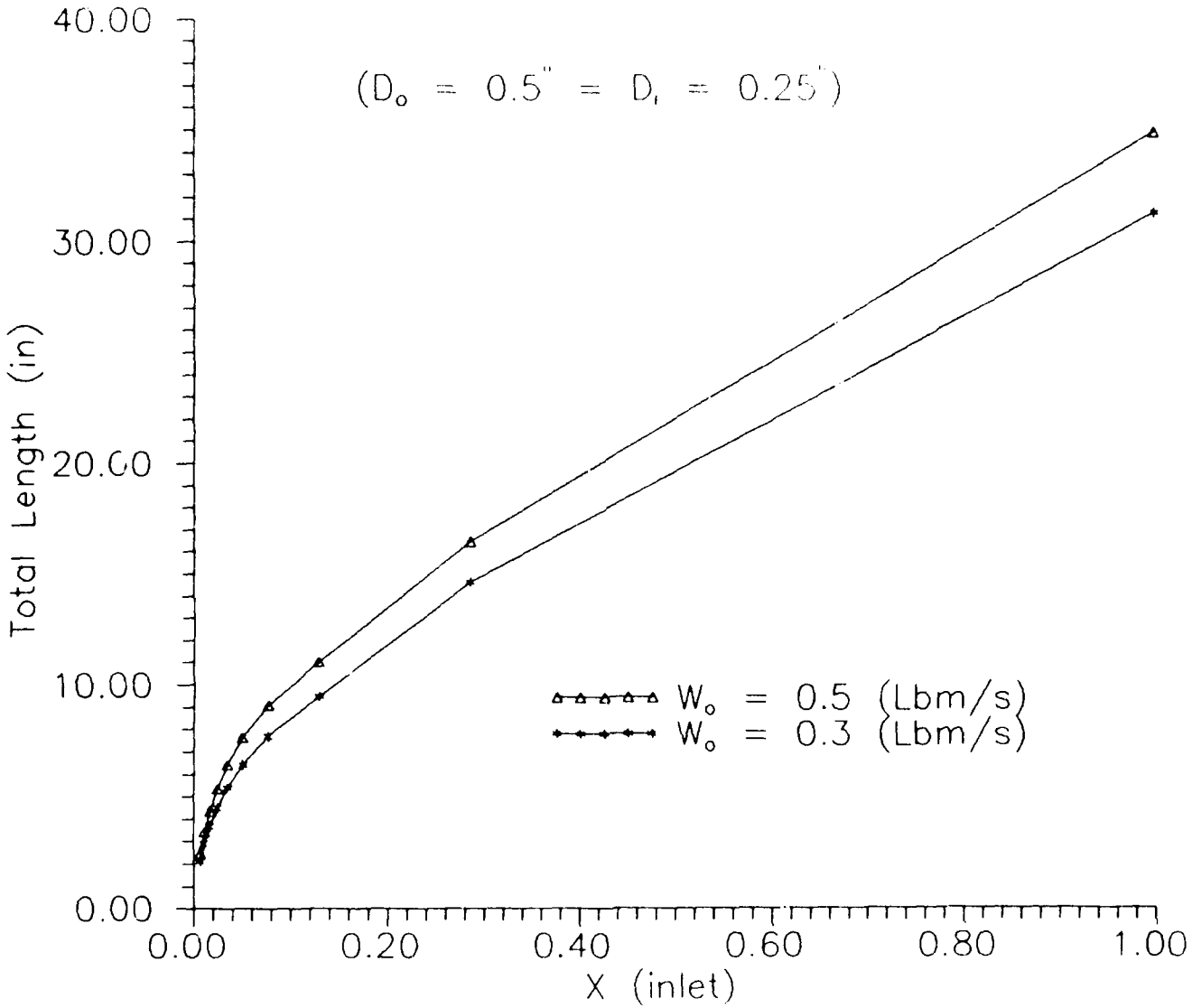

Figure 5.9 . Condenser Length vs. Inlet Quality

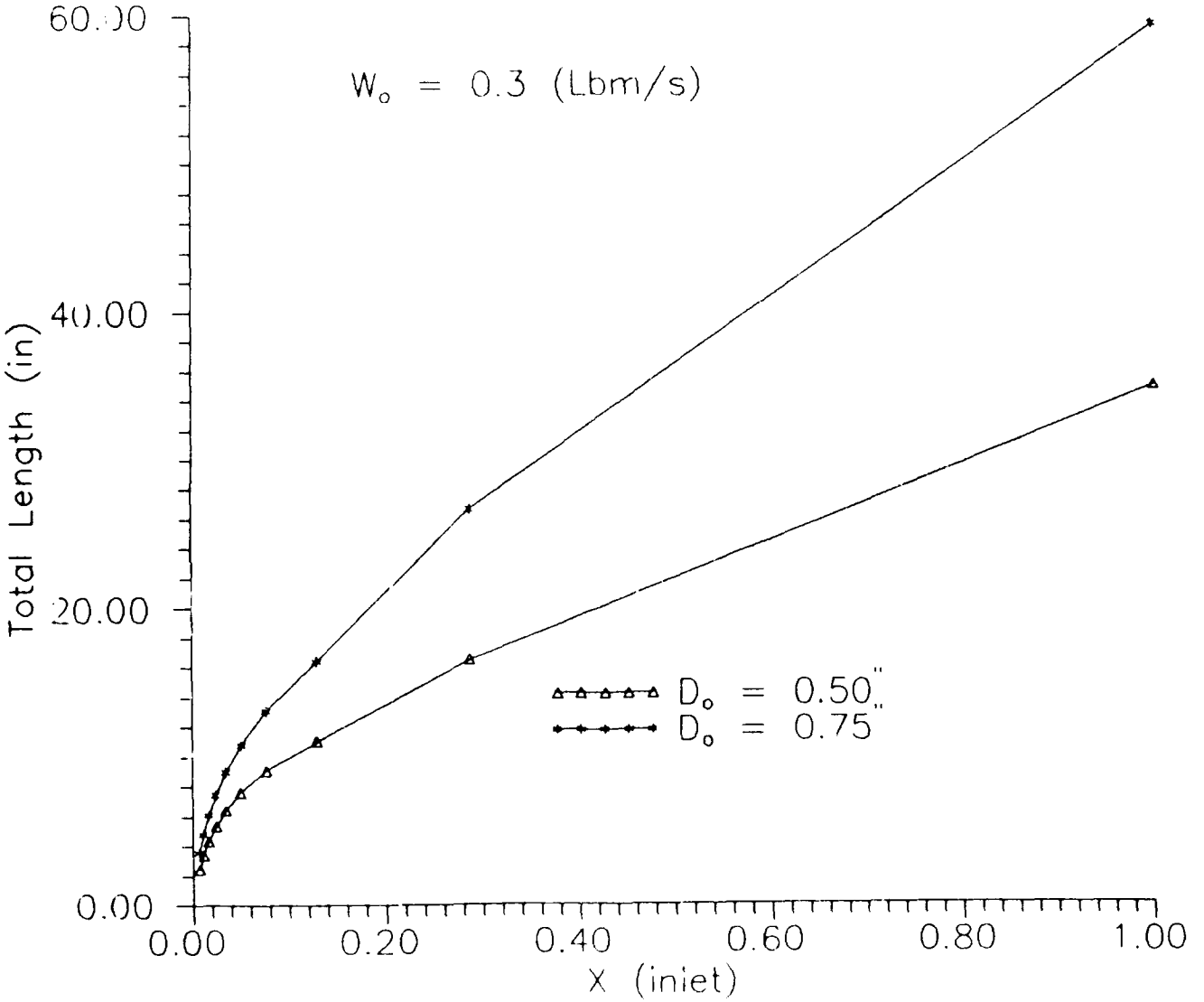

Figure 5.10 . Condenser Length vs. Inlet Quality

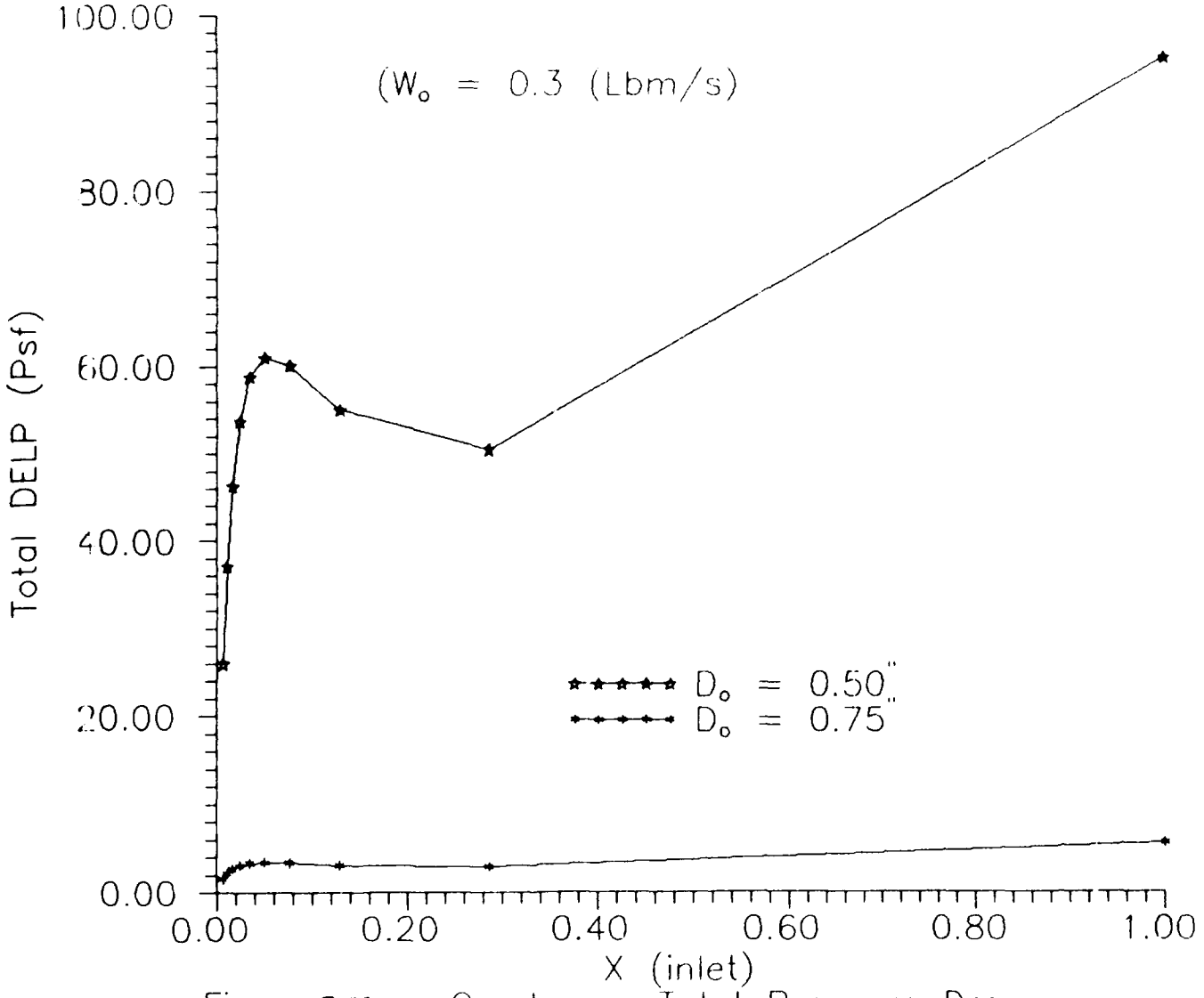

Figure 5.11 . Condenser Total Pressure Drop vs. Inlet Quality

TABLE 5-1

Thermodynamic Properties of Refrigerants

PROPERTIES AT 100°F

		R-11	R-12	R-22	R-113	R-114
P	(psi)	23.46	131.86	210.60	10.48	45.85
	(lbm/ft)	90.21	78.79	71.24	95.79	88.40
	(lbm/ft)	0.567	3.247	3.891	0.336	1.437
h	(Btu/lbm)	28.70	31.10	39.27	28.99	31.80
h	(Btu/lbm)	103.94	87.03	112.11	93.45	84.71
h	(Btu/lbm)	75.24	55.93	72.84	64.46	52.91
C	(Btu/lbm-F)	0.214	0.240	0.313	0.232	0.249
K	(Btu/hr-ft-F)	0.048	0.037	0.047	0.042	0.035

TABLE 5-2

Flow Variables for R-12 at 100°F (P=131.86 psi)

Flow Rate (lbm/s)	Input Power (Watts)	Quality	J_G (ft/s)	J_L (ft/s)	α HEM	Flow Regime
0.01	300	0.466	4.208	0.199	0.955	Annular
0.01	500	0.805	7.272	0.037	0.990	Annular
0.01	1000	1.000	9.034	0.000	1.000	Steam
0.02	300	0.212	3.821	0.587	0.867	Ann./Slug
0.02	500	0.381	6.885	0.461	0.937	Annular
0.02	1000	0.805	14.545	0.145	0.990	Annular
0.04	300	0.084	3.045	1.364	0.691	Slug
0.04	500	0.169	6.109	1.237	0.832	Slug
0.04	1000	0.381	13.769	0.922	0.937	Annular
0.06	300	0.042	2.270	2.140	0.515	Slug
0.06	500	0.098	5.334	2.014	0.726	Slug
0.06	1000	0.240	12.994	1.698	0.884	Slug
0.08	300	0.021	1.495	2.917	0.339	Bubble
0.08	500	0.063	4.559	2.854	0.620	Slug
0.08	1000	0.169	12.219	2.475	0.832	Slug
0.10	300	0.008	0.719	3.693	0.163	Bubble
0.10	500	0.042	3.783	3.567	0.515	Slug

TABLE 5-2 (Continued)

Flow Variables for R-12 at 100°F (P=131.86 psi)

Flow Rate (lbm/s)	Input Power (Watts)	Quality	J_G (ft/s)	J_L (ft/s)	α HEM	Flow Regime
0.10	1000	0.127	11.443	3.251	0.779	Slug
0.14	300	0.000	0.000	5.212	0.000	Liquid
0.14	500	0.018	2.233	5.120	0.304	Bubble
0.14	1000	0.078	9.893	4.805	0.673	Slug
0.18	300	0.000	0.000	6.702	0.000	Liquid
0.18	500	0.004	0.682	6.673	0.093	Bubble
0.18	1000	0.051	8.342	6.358	0.567	Slug
0.22	300	0.000	0.000	8.191	0.000	Liquid
0.22	500	0.000	0.000	8.191	0.000	Liquid
0.22	1000	0.034	6.791	7.911	0.462	Bubble

TABLE 5-3

Flow Variables for R-11 at 100°F (P=23.41 psi)

Flow Rate (lbm/s)	Input Power (Watts)	Quality	J_G (ft/s)	J_L (ft/s)	α HEM	Flow Regime
0.01	300	0.350	18.103	0.211	0.988	Annular
0.01	500	0.602	31.153	0.129	0.996	Annular
0.01	1000	1.000	51.763	0.000	1.000	Steam
0.02	300	0.161	16.631	0.546	0.968	Annular
0.02	500	0.287	29.681	0.464	0.985	Annular
0.02	1000	0.602	62.306	0.259	0.996	Annular
0.04	300	0.066	13.686	1.215	0.918	Slug
0.04	500	0.129	26.736	1.133	0.959	Annular
0.04	1000	0.287	59.362	0.928	0.985	Annular
0.06	300	0.035	10.742	1.884	0.851	Slug
0.06	500	0.077	23.792	1.802	0.930	Annular
0.06	1000	0.182	56.417	1.597	0.972	Annular
0.08	300	0.019	7.797	2.552	0.753	Slug
0.08	500	0.050	20.847	2.470	0.894	Slug
0.08	1000	0.129	53.473	2.265	0.959	Annular
0.10	300	0.009	4.853	3.221	0.601	Slug
0.10	500	0.035	17.903	3.139	0.851	Slug

TABLE 5-3 (Continued)

Flow Variables for R-11 at 100°F (P=23.41 psi)

Flow Rate (lbm/s)	Input Power (Watts)	Quality	J_G (ft/s)	J_L (ft/s)	α HEM	Flow Regime
0.10	1000	0.097	50.528	2.934	0.945	Annular
0.14	300	0.000	0.000	4.559	0.000	Liquid
0.14	500	0.017	12.014	4.477	0.729	Slug
0.14	1000	0.062	44.639	4.272	0.913	Slug
0.18	300	0.000	0.000	5.897	6.732	Liquid
0.18	500	0.007	6.125	5.815	0.513	Bub./Slug
0.18	1000	0.042	38.750	5.610	0.874	Slug
0.22	300	0.000	0.000	7.234	2.296	Liquid
0.22	500	0.0002	0.236	7.152	0.032	Bubble
0.22	1000	0.029	32.861	6.947	0.825	Slug

TABLE 5-4

Flow Variables for R-114 at 100°F (P=45.85 psi)

Flow Rate (lbm/s)	Input Power (Watts)	Quality	J_G (ft/s)	J_L (ft/s)	α HEM	Flow Regime
0.01	300	0.491	10.091	0.169	0.983	Annular
0.01	500	0.850	17.332	0.050	0.997	Annular
0.01	1000	1.000	20.413	0.000	1.000	Steam
0.02	300	0.222	9.058	0.516	0.946	Ann./Slug
0.02	500	0.401	16.378	0.397	0.976	Annular
0.02	1000	0.850	34.678	0.100	0.997	Annular
0.04	300	0.087	7.136	1.211	0.855	Slug
0.04	500	0.177	14.456	1.092	0.930	Slug
0.04	1000	0.401	32.756	0.795	0.976	Annular
0.06	300	0.043	5.215	1.906	0.732	Slug
0.06	500	0.102	12.535	1.787	0.875	Slug
0.06	1000	0.252	30.834	1.490	0.954	Annular
0.08	300	0.021	3.293	2.601	0.559	Slug
0.08	500	0.065	10.613	2.482	0.810	Slug
0.08	1000	0.177	28.913	2.185	0.930	Ann./Slug
0.10	300	0.007	1.371	3.296	0.294	Bubble
0.10	500	0.043	8.691	3.177	0.732	Slug
0.10	1000	0.132	26.991	2.880	0.904	Slug

TABLE 5-4 (Continued)

Flow Variables for R-114 at 100°F (P=45.85 psi)

Flow Rate (lbm/s)	Input Power (Watts)	Quality	J_G (ft/s)	J_L (ft/s)	α HEM	Flow Regime
0.14	300	0.000	0.000	4.686	0.000	Liquid
0.14	500	0.017	4.848	4.567	0.515	Slug
0.14	1000	0.081	23.148	4.269	0.844	Slug
0.18	300	0.000	0.000	6.076	0.000	Liquid
0.18	500	0.003	1.004	5.957	0.144	Bubble
0.18	1000	0.053	19.304	5.659	0.773	Slug
0.22	300	0.000	0.000	7.465	3.772	Liquid
0.22	500	0.000	0.000	7.346	0.000	Liquid
0.22	1000	0.034	15.461	7.049	0.687	Slug

TABLE 5-5

Test Matrix for Earth Gravity Instabilty Experiments

Configuration	Heat Input (Watts)	Flow Rate (lbm/s)	Equilibrium Exit Quality
Vertical Up	300	0.26	0.00
Vertical Up	300	0.25	0.00
Vertical Up	300	0.24	0.00
Vertical Up	300	0.23	0.00
Vertical Up	300	0.22	0.00
Vertical Up	300	0.20	0.00
Vertical Up	300	0.18	0.00
Vertical Up	300	0.16	0.00
Vertical Up	300	0.14	0.00
Vertical Up	300	0.12	0.003
Vertical Up	300	0.10	0.009
Vertical Up	300	0.08	0.019
Vertical Up	300	0.06	0.035
Vertical Up	300	0.04	0.066
Vertical Down	300	0.27	0.00
Vertical Down	300	0.26	0.00
Vertical Down	300	0.25	0.00
Vertical Down	300	0.24	0.00
Vertical Down	300	0.23	0.00
Vertical Down	300	0.22	0.00

TABLE 5-5 (Continued)

Test Matrix for Earth Gravity Instabilty Experiments

Configuration	Heat Input (Watts)	Flow Rate (lbm/s)	Equilibrium Exit Quality
Vertical Down	300	0.20	0.00
Vertical Down	300	0.18	0.00
Vertical Down	300	0.16	0.00
Vertical Down	300	0.14	0.00
Vertical Down	300	0.12	0.003
Vertical Down	300	0.10	0.009
Vertical Up	500	0.45	0.00
Vertical Up	500	0.44	0.00
Vertical Up	500	0.43	0.00
Vertical Up	500	0.42	0.00
Vertical Up	500	0.40	0.00
Vertical Up	500	0.38	0.00
Vertical Up	500	0.36	0.00
Vertical Up	500	0.34	0.00
Vertical Up	500	0.32	0.00
Vertical Up	500	0.30	0.00
Vertical Up	500	0.28	0.00
Vertical Up	500	0.26	0.00
Vertical Up	500	0.24	0.00
Vertical Up	500	0.22	0.00

TABLE 5-5 (Continued)

Test Matrix for Earth Gravity Instabilty Experiments

Configuration	Heat Input (Watts)	Flow Rate (lbm/s)	Equilibrium Exit Quality
Vertical Up	500	0.20	0.003
Vertical Up	500	0.18	0.007
Vertical Up	500	0.16	0.011
Vertical Up	500	0.14	0.017
Vertical Up	500	0.12	0.024
Vertical Up	500	0.10	0.035
Vertical Up	500	0.08	0.050
Vertical Up	500	0.06	0.077
Vertical Up	500	0.04	0.129
Vertical Up	500	0.02	0.287
Vertical Down	500	0.46	0.00
Vertical Down	500	0.45	0.00
Vertical Down	500	0.44	0.00
Vertical Down	500	0.43	0.00
Vertical Down	500	0.42	0.00
Vertical Down	500	0.40	0.00
Vertical Down	500	0.38	0.00
Vertical Down	500	0.36	0.00
Vertical Down	500	0.34	0.00
Vertical Down	500	0.32	0.00

TABLE 5-5 (Continued)

Test Matrix for Earth Gravity Instabilty Experiments

Configuration	Heat Input (Watts)	Flow Rate (lbm/s)	Equilibrium Exit Quality
Vertical Down	500	0.30	0.00
Vertical Down	500	0.28	0.00
Vertical Down	500	0.26	0.00
Vertical Down	500	0.24	0.00
Vertical Down	500	0.22	0.00
Vertical Down	500	0.20	0.003
Vertical Down	500	0.18	0.007
Vertical Down	500	0.16	0.011
Vertical Down	500	0.14	0.017
Vertical Down	500	0.12	0.024
Vertical Down	500	0.10	0.035

TABLE 5-6

Test Matrix for Earth Gravity Critical Heat Flux Experiments

Configuration	Flow Rate (lbm/s)	Heat Input (Watts)	Equilibrium Exit Quality
Vertical Up	0.01	200	0.252
Vertical Up	0.01	300	0.378
Vertical Up	0.01	500	0.630
Vertical Up	0.01	700	0.882
Vertical Down	0.01	200	0.252
Vertical Down	0.01	300	0.224
Vertical Down	0.01	400	0.504
Vertical Down	0.01	500	0.630
Vertical Up	0.02	200	0.126
Vertical Up	0.02	400	0.252
Vertical Up	0.02	600	0.378
Vertical Up	0.02	800	0.504
Vertical Up	0.02	1000	0.630
Vertical Up	0.02	1200	0.756
Vertical Down	0.02	200	0.126
Vertical Down	0.02	300	0.189
Vertical Down	0.02	400	0.252
Vertical Down	0.02	500	0.315
Vertical Down	0.02	600	0.378
Vertical Down	0.02	800	0.504
Vertical Down	0.02	1000	0.630

TABLE 5-7

Test Matrix for the Airplane Trajectory Experiments

Heat Input (Watts)	Flow Rate (lbm/s)
300	0.26
300	0.25
300	0.24
300	0.23
300	0.22
300	0.20
300	0.16
300	0.12
300	0.08
500	0.45
500	0.44
500	0.43
500	0.42
500	0.40
500	0.38
500	0.36
500	0.34
500	0.32
500	0.28
500	0.24
500	0.20
500	0.16
500	0.12
500	0.08

TABLE 5-8

Maximum Wall Temperatures for Critical Heat Flux Experiments at 1 g

W (lbm/s)	$\dot{q}$ (Watts)	X_e	α	Tmax (°F)
0.01	200	0.252	0.982	482.2
0.01	300	0.378	0.990	514.4
0.01	400	0.504	0.994	539.0
0.01	500	0.630	0.996	559.0
0.01	600	0.756	0.998	576.1
0.01	700	0.882	0.999	591.0
0.02	200	0.126	0.958	482.0
0.02	300	0.189	0.974	514.4
0.02	400	0.252	0.982	539.0
0.02	500	0.315	0.987	559.1
0.02	600	0.378	0.990	576.1
0.02	700	0.441	0.992	591.0
0.02	800	0.504	0.994	604.3
0.02	1000	0.630	0.996	627.3
0.02	1200	0.756	0.998	646.9

TABLE 5-9

Maximum Wall Temperatures for Instability Experiments at 1 g

W (lbm/s)	$\dot{q}$ (Watts)	X_e	α	Tmax (°F)
.020	300.0	.1606	.968	572.2
.040	300.0	.0661	.918	651.9
.060	300.0	.0346	.851	769.9
.080	300.0	.0188	.753	513.0
.100	300.0	.0094	.601	513.0
.120	300.0	.0031	.329	513.0
.020	500.0	.2867	.985	595.1
.040	500.0	.1291	.959	638.3
.060	500.0	.0766	.930	691.0
.080	500.0	.0503	.894	756.9
.100	500.0	.0346	.851	841.9
.120	500.0	.0241	.797	871.0
.140	500.0	.0166	.729	871.0
.160	500.0	.0110	.638	871.0
.180	500.0	.0066	.513	871.0
.200	500.0	.0031	.329	871.0

Section 6

INSTRUMENTATION AND COMPONENT DESCRIPTION

6.1 Instrumentation

The instrumentation was briefly discussed for the conceptual design. Following is some specific instruments which have been tentatively selected for the baseline configuration.

Pressure

The pressure measurements for the baseline system consist of three differential pressures along the two foot long adiabatic section. Two pressure transducers measure ΔP over one foot long sections between the middle and the two ends, and one measures the total ΔP. Validyne ultra low range differential pressure transducer model DP103 can be used for this purpose. This transducer can handle up to 100 psi line pressure and has a measurement range of 0.008 to 12.5 psid. A miniature carrier/demodulator will be needed for every transducer.

As shown in the schematic of the test loop, a total of nine absolute pressures will be measured. Validyne P300A transducer/demodulator is an all welded rugged unit which, based on the diaphragm selected, handles up to 3200 psi. The signal from the transducers located downstream of the pump and downstream of the adiabatic section will be used by the control system to stop the system operation when overpressure is detected. This will be accomplished by shutting the power to the test section heater and the pump.

Temperature

The test section wall surface temperature will be measured by six thermocouples and six RTD's alternately placed 2 inches apart. Omega thin film RTD series F elements are as small as 2 mm by 2 mm and have a temperature rating of -50 to 600°C. These units can be cemented to the outside wall of the test section. Unsheeted fine gage type E thermocouples

will also be welded to the outside wall. A thermocouple measurement closest to the exit of the heated section will be used by the control system to stop the power input when accidental overheating of the test section is detected. Ten insertion thermocouples will be used for fluid temperature measurement. Flush mounted insulated units will be used for this purpose.

Flow Rate

Three turbine meters will be used for measurement of flow rate downstream of the pump and in the test section leg of the test loop. The flow in the main loop will have a range of 1 to 15 GPM and a Sponsler precision turbine meter with a nominal meter size of 5/8 inch will provide accurate flow measurement. The test section leg has a flow range of 0.05 to 4 GPM and may need a combination of LO-FLO MF-125 with a range of 0.05 to 2.0 GPM and a 3/8 inch meter with a range of 0.75 to 5 GPM. Water flow rate on the secondary side of the condenser will be measured with a Sponsler LO-FLO MF-125 turbine meter.

A calibrated signal conditioner (model SP 711) will be needed for every unit to linearize and amplify the sine wave form signal. All turbine meters require at least 10 diameters of undisturbed line upstream and 5 diameters downstream of the measurement point.

Phase Content

A full flow drag disk will be used to calibrate the known flow rate at the entrance of the condenser for flow quality. These drag disks are commercially available but some development effort will be needed for calibration of quality.

6.2 Components

In selection of the components of the baseline design, special attention should be given to using materials compatible with R-11. Among the commonly used elastometers, Viton A results in smaller linear swell. In addition,

TFE fluorocarbons are compatible with all Freons. Following is a tentative list of components selected:

Pump

The head requirement for the Freon pump was determined for the maximum two-phase pressure drop in 10 ft. of piping which would result in 40 psi pressure drop. The flow requirement was set at three times the highest flow in the test section leg, 10 GPM. A magnetically coupled gear pump with a flow rating of 21 GPM and maximum outlet pressure of 100 psi (Cole-Palmer unit T7011) can be used for this purpose. This pump has Ryton gears and no seals. A stainless steel pressure relief valve (Cole-Palmer T-3245) is bypassed across the pump for overpressure protection. A dryguard switch (Cole-Palmer T-7382) is used upstream of the pump to protect the pump in case a line gets plugged.

Accumulator

A bladder type accumulator with a wet volume of approximately three times the loop volume should be used. An Oil-Air Industries accumulator model 1-100-1 with a volume of 1 gallon and gas volume of 235 in^3 will provide sufficient volume for this system. This accumulator has a pressure rating of up to 3000 psi and can be supplied with Viton bladder.

Valves

Other than the ball valve used to isolate the accumulator, the rest of the valves in the system will be globe type regulating valves. NUPRO NB series Severe Service valves will be used for all the lines except upstream of the heated section where a fine metering valve (NUPRO series S) will be required.

Data Acquisition Unit

Data from 40 channels will be read by the acquisition and control system. Among these signals, five readings are needed for the system control and all readings will be retained and recorded. The signals used for system

control are heater voltage and current, the pressures downstream of pump and the adiabatic section, and the last surface temperature of the heated section.

One alternative for the data acquisition and control system will consist of:

(1) an STD Buss with a Z80-C processor and 4 MHz clock

(2) a 16 K CMOS RAM on-board memory unit with 200 nanosecond access time

(3) a 16 K EPROM to store the control package

(4) an RS/232 serial port

(5) three 16 channel (differential) A/D converters

(6) power supply with battery backup

Analog signals from the experiment will be converted to 4 byte digital values by the A/D converter and stored on the memory unit. Static RAM memory could be used for this purpose and the data channels will be scanned in one second intervals.

Another alternative is to use commercially available CPU modules and stand-alone interface systems. Omega CPU module OM-992 contains an 8088 processor and an RS 232C port. Five OM-912 analog input modules wil be required for the 40 input data channels. In addition, a data storage device should interface with an OM-992 unit.

Section 7

REFERENCES

1. D. Abdollahian, "Study of Two-Phase Flow and Heat Transfer in Microgravity," Final Phase I Report, SLI-8802, January 1988.

2. Z. I. Anotoniak, "Two Phase Alkali - Metal Experiments in Reduced Gravity," Battelle Pacific Northwest Laboratory, PNL-5906, June 1986.

3. D. B. Heppner, et al., "Zero-G Experiments in Two-Phase Fluid Flow Regimes," ASME Paper 75-ENAS-24, 1975.

4. O. Baker, "Simultaneous Flow of Oil and Gas," The Oil and Gas J., Vol. 53, July 1954.

5. E. Quandt, "Analysis of Gas-Liquid Flow Patterns," Chem. Eng. Progress Symp. Series, Vol. 61, No. 57, 1965.

6. A. E. Dukler, et al., "Gas Liquid Flow at Microgravity Conditions: Flow Patterns and Their Transitions," ASME Winter Annual Meeting, Boston, December 13-18, 1987.

7. D. Hill and R. S. Downing, "A Study of Two-Phase Flow in a Reduced Gravity Environment - Final Report," Sunstrand Energy Systems Report, Contract NASA-17195, October 1987.

8. Y. Taitel and A. E. Dukler, "A Model for Predicting Flow Regime Transitions in Horizontal and Near Horizontal Gas-Liquid Flow," AIChE J., 26, 47-55, 1976.

9. D. Abdollahian, R. Grief, V. P. Carey and W. L. Ping, "Experimental and Analytical Study of Two-Phase Flow in Zero Gravity, Final Report," AFWAL Report No. AFWAL-TR-87-3102, March 1988.

10. T. W. Lovell, "Liquid Vapor Flow Regime Transitions for Use in Design of Heat Transfer Loops in Spacecraft - An Investigation of Two-Phase Flow in Zero Gravity," AFWAL Report No. AFWAL-TR-85-3021, 1985.

11. A. E. Bergles and H. L. Morton, "Survey and Evaluation of Techniques to Augment Convective Heat Transfer," MIT Department of Mechanical Engineering, Report No. 5382-34, February 1965.

12. R. F. Lopina, et al., "Heat Transfer and Pressure Drop in Tape Generated Swirl Flow," MIT Report 70281-47, 1967.

13. W. R. Gambill, R. D. Bundy, and R. W. Wansbrough, "Heat Transfer, Burnout, and Pressure Drop for Water in Swirl Flow Through Tubes With Internal Twisted Tapes," ORNL-2911, March 1960.

14. F. A. Blatt and R. R. Adt, Jr., "The Effects of Twisted Tape Swirl Generators on the Heat Transfer Rate and Pressure Drop of Boiling Freon II and Water," ASME Paper No. 63-WA-42, 1963.

15. J. H. Lienhard, "Interacting Effects of Gravity and Size Upon the Peak and Minimum Pool Boiling Heat Fluxes," NASA/CR-1551, 1970.

16. W. S. Hill and F. R. Best, "Definition of Two-Phase Flow Behavior for Spacecraft Design," 7th Symposium on Space Nuclear Power Systems, Albuquerque, NM, January 1990.

17. C. Crowley, Creare Inc., Personal Communication, January 4, 1990.

18. M. Schuller, Kirtland AFB, Personal Communication, January 17, 1990.

19. T. Swanson, NASA GSFC, Personal Communication, January 11, 1990.

20. Y. Taitel, D. Bornea and A. E. Dukler, "Modeling Flow Pattern Transitions for Steady Upwards Gas-Liquid Flow in Vertical Tubes," AIChE J., 26, 345-354, 1980.

21. K. Mishima and M. Ishii, "Flow Regime Transition Criteria for Upward Two-Phase Flow in Vertical Tubes," Int. J. Heat Mass Transfer, 27, 723-737, 1984.

22. R. C. Lockhard and R. C. Martinelli, "Proposed Correlation of Data for Isothermal Two-Phase Two-Component Flow in Pipes," Chem. Eng. Prog., 45, 39, 1949.

23. R. C. Martinelli and D. B. Nelson, "Prediction of Pressure Drop During Forced Circulation Boiling of Water," Trans. ASME, 7, 695, 1948.

24. J. R. S. Thom, W. M. Walker, T. A. Fallon, and G. F. S. Reising, "Boiling in Subcooled Water During Flow in Tubes and Annuli," Proc. Inst. Mech. Eng., 3C180, 1966.

25. C. J. Baroczy, "A Systematic Correlation for Two-Phase Pressure Drop," AIChE reprint No. 37, paper presented at 8th National Heat Transfer Conference, Los Angeles, August 1965.

26. D. Chisholm, "Pressure Gradients Due to Friction During the Flow of Evaporating Two-Phase Mixtures in Smooth Tubes and Channels," Int. J. Heat Mass Transfer, 16(2), 347-358, 1973.

27. L. Friedel, "Improved Pressure Drop Correlations for Horizontal and Vertical Two-Phase Pipe Flow," 3R International, 18(7), 485-492, 1979.

28. G. F. Hewitt and N. Hall-Taylor, Annular Two-Phase Flow, Pergamon Press, 1970.

29. M. Ishii and K. Mishima, "Liquid Transfer and Entrainment Correlation for Droplet-Annular Flow," 8th Int. Heat Transfer Conf., San Francisco, 1986.

30. P. Saha and N. Zuber, "Point of Net Vapor Generation and Vapor Void Fraction in Subcooled Boiling," Proc. Fifth Int. Heat Transfer Conf., Vol. IV, 1974.

31. J. C. Chen, "A Correlation for Boiling Heat Transfer to Saturated Fluids in Convective Flow," ASME Paper 63-HT-34.

32. F. W. Dittus and L. M. k. Boelter, University of California Engineering Publications, Vol. 2, 443, 1930.

33. H. K. Forster and N. Zuber, "Dynamics of Vapor Bubbles and Boiling Heat Transfer, AIChE Journal, 1(4), 531-535, 1955.

34. L. A. Bromley, "Heat Transfer in Stable Film Boiling," Chem. Eng. Progr., B46, 221-227, 1950.

35. M. E. Ellion, "A Study of the Mechanism of Boiling Heat Transfer," Jet Propulsion Laboratory, Memo 20-88, C. I. T., 1954.

36. J. E. Leonard, et al., "Calculation of Low Flow Film Boiling Heat Transfer for BWR LOCA Analysis," General Electric Licensing Topical Report, NEDO-20566-1-A, 1982.

37. R. S. Dougall and W. M. Rohsenow, "Flow Boiling on the Inside of Vertical Tubes with Upward Flow of the Fluid at Low Qualities," MIT Report No. 9079-26, 1963.

38. N. Bakhru and J. H. Lienhard, "Boiling From Small Cylinders," Int. J. Heat Mass Transfer, Vol. 15, 1972.

39. W. M. Rohsenow and J. P. Hartnett, Handbook of Heat Transfer, McGraw-Hill Book Company, New York, 1973.

40. R. E. Eastman, et al., "Two-Phase Fluid Thermal Transport for Spacecraft," AFWAL Report No. AFWAL-TR-84-3028, October 1984.